Università degli Studi di Palermo

AREA QUALITÀ, PROGRAMMAZIONE E SUPPORTO STRATEGICO
SETTORE STRATEGIA PER LA RICERCA
U. O. DOTTORATI

Dottorato di ricerca in Energia e Tecnologie dell'Informazione
Dipartimento di Ingegneria
Settore Scientifico Disciplinare ING-IND/11 - Fisica Tecnica Ambientale

Energy evaluation and life cycle assessment of an innovative building integrated technology: the smart window-luminescent solar concentrator

IL DOTTORE
Vincenzo Muteri

IL COORDINATORE
Prof. Ing. Maurizio Cellura

IL TUTOR
Prof. Ing. Maurizio Cellura

CO TUTOR
Prof.ssa Sonia longo
Dott.ssa Letizia Bua
Prof.ssa Marzia Traverso

CICLO XXXIII
ANNO CONSEGUIMENTO TITOLO 2021

Abstract

Luminescent Solar Concentrators (LSC) represent one of the innovative and potentially most versatile technologies related to Building Integrated Photovoltaics (BIPV). The peculiarity of these devices lies in the fact that they can be integrated into the surface of the building to replace openings such as skylights or windows, thanks to their characteristic of being semi-transparent and of functioning both with direct and diffused radiation. Eni developed the own technology Eni Ray Plus® based on LSC and integrated it in a multifunctional smart window-LSC (SW-LSC) prototype. The device uses the energy produced by LSC modules to power an autonomous and passive shading system, exploiting irradiation sensors, motors and batteries. It independently regulates the movement of the shading system and allows energy surplus, through the electricity generated by modules.

The final aim of this thesis is to explore the energy performances of the SW-LSC prototype into the building and to determinate the life cycle environmental impacts of the device through the application of the Life Cycle Assessment methodology. In addition, the focus is to highlight the impacts of the LSC modules only, assuming that they can be applied into glazed buildings, and to compare them with those of other PV technologies on the market.

The first part of the work is focused on SW-LSC optical, thermal and electrical performances, comparing them with those of a traditional window. The analysis followed an experimental approach that involved lighting and electrical monitoring studies in a real test room, in order to create validated models for conducting simulations in larger buildings. The results were expressed through the study of illuminance maps, electricity generation obtainable from the integrated photovoltaic technology and in terms of energy savings. In conclusion, the models created allowed to evaluate the performances of the new technology, providing useful information for energy saving strategies in buildings.

The second part of the work regarded the evaluation of the life cycle impacts. The functional unit (FU) chosen was the whole SW-LSC (5,27 m^2) considering its thermal and optical characteristics (Uw = 1,6 -1,8 W/m^2K, tvis = 77% and g = 85% of LSC modules) and the possibility to produce about 1.5 kWh/year. The system boundary was from cradle to gate considering the assembly and maintenance phase, while the end of life (EOL) was considered separately through a recycling/landfill scenario. Results showed that global warming potential (100 years) for SW-LSC was 5.91E+03 kg CO_{2eq} and the production phase had the greatest impact (about 96%). The EOL recycling/landfill scenario results showed the possibility to reduce impacts by an average of 45%. The dominance analysis of SW-LSC components showed that the aluminum frame was the main hotspot (about 60% contribution) in all categories (except in abiotic depletion potential, 16% contribution), followed by the light-shelf (about 19% contribution). The batteries and motors for the shading system were the biggest contributors in the abiotic depletion potential category (36% and 30%, respectively). Since the materials of the SW-LSC prototype are not yet optimized in an eco-design context, it is important to underline that other alternative materials will be taken into consideration during the marketing phase (such as the use of wood or a wood-aluminum combination for the frame). The alternative scenario, which involved the use of 75% recycled aluminum for the window frame, showed that it is possible to reduce environmental impacts from 3% to 46% (with a mean value of 33.6%). Finally, the results for the SW-LSC were compared with those of the EPDs of some traditional windows (the functional unit for the comparison was the m^2). A further comparative study was carried out between the LSC modules and some building integrated photovoltaic technologies, using 1 kWh of electricity generation as a functional unit. LSC modules impacts were on average 870% lower than that of various PV technologies when compared on the basis of m^2; the only exception concerned the comparison with CIS and a-Si technologies, where LSC modules impacts were about 150% higher in some categories (global warming potential, ozone layer depletion potential and photochemical oxidation potential). LSC modules had highest impacts in all categories (from 200% to 1900%) if compared with other PV

technologies on the basis 1 kWh of energy generated. The results based on energy generation are easily interpretable considering the lower performance of LSC modules compared to other technologies; however, LSC modules show greater versatility and different possible applications due to the their transparency.

The SW-LSC could represent an option for the future efficiency of the built environment: in this sense, even if the power output from LSC modules integrated into the window is limited, it is sufficient to cover the energy demand of an efficient system of Venetian blinds that allow regulating the internal loads autonomously and independently, with a consequent energy saving. Furthermore, thanks to the thermal characteristics of the frame and the regulation of the light inside the environment, the SW-LSC represents an element designed to improve thermal and lighting comfort inside buildings.

TABLE OF CONTENTS

List of figures

List of tables

1 – Introduction

The building sector has a key role to achieve the objectives recommended by the European Union to reduce greenhouse gas emissions and to increase the use of technologies powered by renewable sources by 2030 [1]. The building sector is responsible for almost 40% of global CO_2 emissions and energy consumption, considering both commercial and residential buildings [2]. In the residential sector, the use of energy is related to heating and cooling of indoor environments, lighting, and other household needs. All these aspects are influenced by factors such as building location and envelope features, weather conditions, type and efficiency of equipment, access to energy, availability of energy sources, energy policies and the lifestyle of the occupants. In the commercial sector, the energy use is mainly related to heating and water heating systems, cooling, lights and other equipment strictly connected to the activity that is carried out inside the building [3]. Consequently, it is important to evaluate different strategies that could allow energy savings and better management of the thermal loads inside the buildings, both in commercial and residential ones.

The future of this sector involves an evolution towards buildings that are more efficient, “intelligent” and self-regulating, allowing to reach maximum energy saving and greater comfort for inhabits. [4] In this field, the concept of nearly zero-energy buildings (nZEBs) has become an obligation providing energy independence and synergy with the grid [5]. A successful design and construction of nZEB includes energy-efficient measures and the adoption of renewable energy sources (RES), targeting the minimization of the energy needs, to obtain the right balance between consumption and generation [6]. Other significant aspects of nZEBs are the integrated design [7] and the use of smart technologies: smart technologies and controls facilitate the operational phase of buildings based on the energy control and storage strategy; the integrated design ensures the exploitation of space, opening to new design and construction scenarios. [8].

Excluding the new third photovoltaics technology which promises innovative types of installation, the actual trend of photovoltaics installation in the urban context is the building roof. Even if this solution is always to be considered, sometimes there are problems connected with the spaces available and possible shadows around the building, which could compromise or reduce the potential of the devices. Furthermore, in the perspective of nZEBs, the energy provided by the roof-photovoltaic is sufficient only for small building, which does not exceed a certain height [9], and this complicates the achievement of the energy balance; consequently, it is required the use of other solutions and additional renewable technologies.

In addition to the self-energy production, another aspect to consider for buildings is the increase in efficiency of the whole structure and the comfort for the inhabits. In this sense, the envelope must be efficient also from a thermal and lighting point of view. If this is possible, especially in new buildings, thanks to measures such as external insulation or choice of efficient building materials, the problem of transmittance of glazed elements always remains. These elements are responsible for problems connected to the thermo-balance of the structure and this leads to worse performance of the building itself since the energy loss connected to the transparent surfaces of a building (skylight, windows, etc.) causes more energy consumption related to the use of heating or cooling devices. Furthermore, the control of solar radiation and light inside the rooms is, in most cases, entrusted to manual shading systems that do not allow the regulation of loads and internal lighting passively and efficiently.

Considering these aspects (increases in energy generation from renewable sources and the problems connected to glazed elements), the technology of Luminescent Solar Concentrator (LSC) has suitable features for buildings integration, especially in the urban context. LSC modules consist of a coloured plastic/glass panel, impregnated or coated with luminescent species such as organic and inorganic dyes and quantum dots [10]. LSC modules are able to capture sunlight and to concentrate it to photovoltaic cells located to the panel edges, where it is converted into electricity. The main advantage of LSC lies in being able to produce electricity even

in low light conditions and to be integrated as transparent element of architectural structures.

The technology of LSC was originally introduced more than three decades ago. During the energy crisis in the 1970s, Weber and Lambe [11] proposed a technique to concentrate sunlight employing LSC technology. A few years later, Batchelder et al. [12, 13] provided a detailed theory and experimental analysis of LSC technology, as well as characterization techniques of the LSC [14]. Until nowadays, the large-scale diffusion of these solar devices has been inhibited by the low conversion efficiency, caused by several loss mechanisms mainly due to dyes properties, which showed low absorption or excessive self-absorption of solar radiation. Thanks to the research and development of new dyes, this problem has been largely solved, even if the efficiency of LSC modules is still lower if compared to traditional photovoltaics. Initially, the main attraction of this technology was its low manufacturing cost that represented a possibility to compete with the more expensive silicon technologies. Today, one of the more interesting aspects regards the possibility of integrating LSC modules in replacements of transparent surfaces where, therefore, it would be impossible to exploit traditional silicon modules; considering the different types of applications, the most efficient solution would be for the two technologies to operate in parallel. Furthermore, it must be considered that LSCs have a lower production cost (about 1/3) [15] than traditional photovoltaics and, thanks to the concentration factor, they also allow the use of a lower quantity of silicon for the same area (Si cell area is only 3 - 4% of LSC module area while, for traditional PV, cell area is 90% of module area).

Thanks to its characteristics and adaptability, LSC technology is suitable for building integration. The concept of integrating LSC modules into a window led to the design of a multifunctional smart window-LSC (SW-LSC) prototype.

The SW-LSC device could be used to increase the energy saving of buildings and comfort of the inhabitants, both for new buildings or for replacing the old windows. In fact, by adjusting properly solar radiation availability inside the rooms, it is possible to reduce the energy consumption for lighting, cooling and heating and, at the same time, maximize the comfort for the occupants. Generally, windows are a

critical element in the envelope: their sizing is one of the most critical issues within building energy performances, can cause high thermal losses, overheating and glare problems. [16] However, if designed correctly, they play an important role in improving indoor thermal comfort [17] [18] and can also become active elements, being able to contribute to the on-site energy generation.

Since the SW-LSC represents a novelty from a technological point of view, it is important to analyse the aspects related to product development and eco-design that could lead to the evaluation of new opportunities and improvements for the subsequent phase of marketization. In this contest, the application of Life Cycle Assessment (LCA) is nowadays an effective and recognized method to evaluate the sustainability of a new product and to try to predict the possible burdens connected with its life cycle. This analysis would allow to justify the more complex design (compared to traditional windows) of the SW-LSC, in order to obtain a more efficient, but also sustainable product. In addition, in the eco-design context, it is possible to identify the best options to minimize the levels of the negative impacts of the product.

Through this work, author want to explore and analyse the potential and limitations of the SW-LSC prototype. For this reason, the main goal is to evaluate the environmental impacts of the SW-LSC prototype and LSC technology, and compare the impacts with that of similar technologies on the market. The results could also help for future analyses, especially when the device will be commercialized and more information on both the final product and the large-scale production process will become available. The analysis is also expanded in order to consider the daylight, thermal and electrical performances of the device; in this sense, the comparison of the results with those of a traditional window in the same conditions (room size and structural characteristics, measurement period, etc.) will help to evaluate the potential of SW-LSC as an integrated building element.

2 - State of the art

The smart window-luminescent solar concentrator (SW-LSC) device incorporates the advantages of the production of electricity from photovoltaic modules, the luminescent solar concentrators, with the functionality of a smart window, which manages heat loads through a shading system managed autonomously and passively (motorized venetian blind). Considering the innovative nature of the coupling between LSC modules and smart window, the state-of-the-art research has focused on related technologies or technologies that have similar operational and structural characteristics. First, a brief introduction of LSC technology and its operation is made. Then, since the main purpose of this work is the life cycle assessment of the smart window-LSC system, a literature review of LCA of photovoltaic systems, from first to third generation, was provided. This will allow a comparison between the results of the analysis carried out in this work and those present in the literature, taking into account the different assumptions and methodologies used in the various studies (functional unit, system boundaries, etc.). Part of the work described in this section was also previously published in "*Review on Life Cycle Assessment of Solar Photovoltaic Panels*" [19]. Then, the focus passes to BIPV systems and LCA of BIPV system, in which LSC modules belong due to their operational characteristics; moreover, a part of this section was dedicated to semi-transparent PV, integrated into buildings. Finally, author focused on the state of art of smart-windows, including the main categories as electrochromic, photochromic and thermochromic, in order to consider the window application of LSC modules in this research work. It is important to underline that LCA studies of smart windows are lacking in the literature; consequently, the analysis of the state of the art of these technologies takes on a more general character and should be considered as an overview of technologies potentially similar to the one considered. At the end of this section, a brief description of Venetian blinds is provided and some articles concerning this screening system are analyzed. In summary, the state of art consists of four main sections:

- LSC technology;

- LCA of PV technologies;

- LCA of BIPV and BIPV technologies;

- Smart-Windows.

2.1 LSC technology

LSC technology consist of a transparent matrix of polymeric material doped with a luminescent dye (fluorophore). The transparent matrix acts as a waveguide and it is made in form of slab. The fluorophore allows absorbing and re-emitting the incident solar radiation, while the waveguide concentrates it towards the edges of the slab; here, small photovoltaic solar cells convert solar radiation into electrical energy (Fig.1).

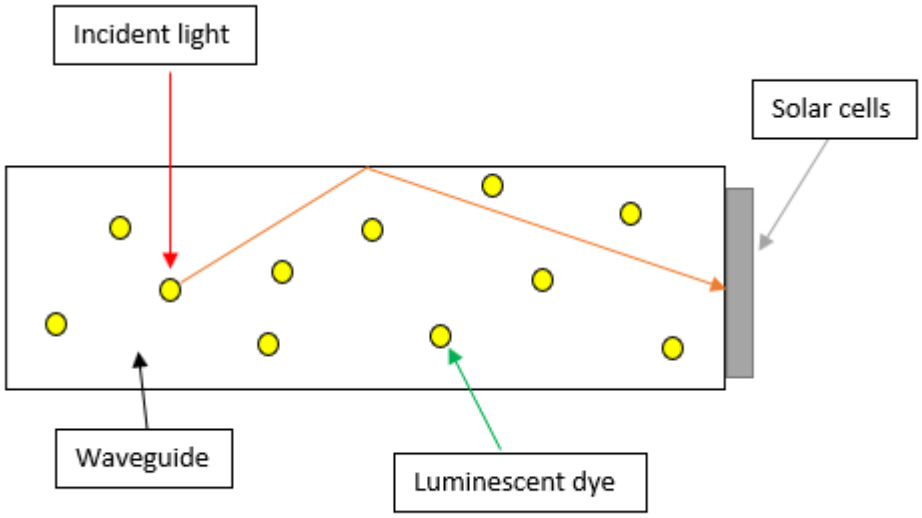

Figure 1 - Operating principle of the LSC technology: Red arrow represent the incoming solar radiation; orange arrow shows the internal reflection through the waveguide towards the solar cell.

LSCs were initially developed in order to reduce PV technology cost. First, since these devices work both with direct and diffuse light (which is concentrated by a factor of 5-10) small solar cells can be used instead of large solar active area. Then, the transparent plastic was expected to be lower than the area cost of planar silicon solar cell. The optical efficiency of LCS modules is closely linked to the internal reflection mechanisms of light and to its interaction with the luminescent molecules inside the matrix. Generally, the nature of this interaction leads to a series of losses

that are defined within the formula that expresses the optical efficiency of the LSC (Equation 1) [125]

$$\eta_{opt} = (1 - R)P_{TIR} \times \eta_{abs} \times \eta_{PLQY} \times \eta_{Stokes} \times \eta_{host} \times \eta_{TIR} \times \eta_{self} \quad (1)$$

where R is the reflection of solar light from the waveguide surface, P_{TIR} is the total internal reflection efficiency, η_{abs} is the fraction of solar light that is absorbed by the dye, η_{PLQY} is the photoluminescent quantum yield of the used luminophore(s), η_{Stokes} is the energy lost due to the heat generation during the absorption and emission event, η_{host} is the transport efficiency of the waveguided photons through the waveguide, η_{TIR} is the reflection efficiency of the waveguide determined by the smoothness of the waveguide surface, and η_{self} is the transport efficiency of the waveguided photons related to re-absorption of the emitted photons by another luminophore [10]. All these terms are connected to a specific event/problem: R is related to surface losses, P_{TIR} to internal reflection, η_{self} to re-absorption events, η_{abs} and η_{self} to the luminophores used, η_{PLQY} and η_{STokes} to the luminophores yield, η_{host} and η_{TIR} to the waveguide. The development of the LSC was initially limited by the performance of the luminescent dyes, which suffered of stability problems under solar radiation and re-absorption losses. Today, these problems have been solved thanks to the synthesis of more performing dyes and the development of different luminescent species (quantum dots, organic dyes, etc).

2.2 LCA of PV technologies

PV systems can be distinguished based on the solar cell technology and materials and they are generally classified according three generations (Tables 1 – 3):

- The first generation (Fig. 2) includes the traditional panels with a crystalline silicon (c-Si) base structure, as single-crystalline silicon (sc-Si) and multi-crystalline silicon (mc-Si) cells;

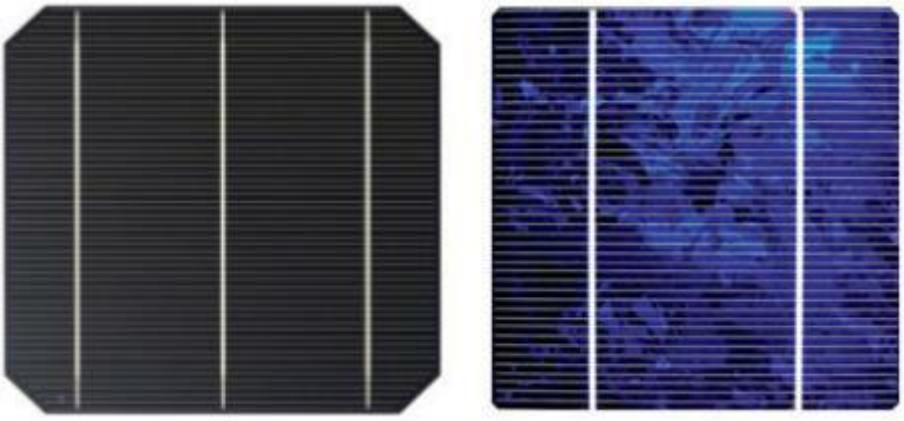

Figure 2 *- Single and multicrystalline silicon solar cells (first generation PV)*

- The second generation (Fig. 3) is based on the thin-film solar cells, which include amorphous silicon (a-Si), cadmium telluride (CdTe) and cadmium sulfide (CdS), copper indium gallium selenide (CIGS)/copper indium selenide (CIS), gallium arsenide (GaAs) and tandem/multi-junctions modules based on Si;

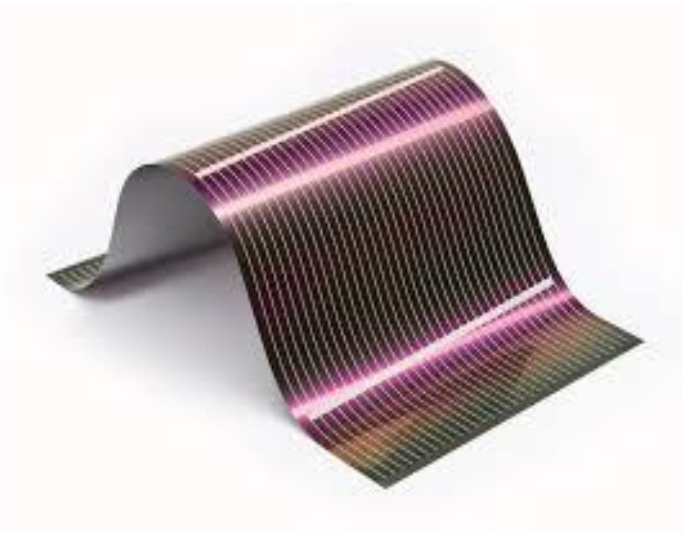

Figure 3 *- An example of thin-film solar cell (second generation PV)*

- The third generation encloses the innovative non-silicon based technologies and new concept devices as organic/semi-organic PV panels (OPV), perovskite solar cells (PSC), dye-sensitized solar cell (DSSC), and quantum dot (QD) cells.

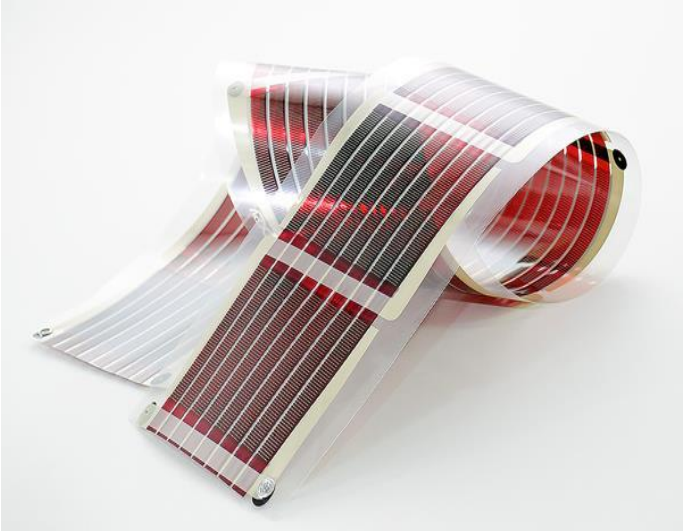

Figure 4 *- An example of Organic Solar Cell (OPV) (third generation PV)*

Table 1 *- 1st generation PV cells*

1st generation PV cells: Silicon based solar cells (-Si)	
Type	Description
sc-Si	Silicon is of the most common material used in PV modules, thanks to its excellent electronic, chemical and mechanical properties [20]. Solar technologies based on this semiconductor are considered the most mature. In general, the fabrication of silicon wafers is made through CZ process, which is a both material and energy intensive process. This type of solar panel is the purest one and has a high efficiency (16 – 22% commercial, 25 – 27% laboratory)
mc-Si	This type of silicon solar cell are a suitable alternative to reduce PV module cost, but it is less efficient if compared with sc-Si cells (15 – 18%).

Table 2 *- 2nd generation PV cells*

2nd generation PV cells: Thin Film Solar Cells (TFSC)	
Type	Description
a-Si	a-Si solar cells are the cheapest on the market, thanks to the limited amount of semiconductor material required for each cell. On contrary, since the layers are much thinner, there is less material to absorb solar radiation compared to

	sc-Si and mc-Si and the efficiencies of this solar modules are lower than crystalline ones (4 – 8% commercial, 12% laboratory [21]). In addition, these cells these cells are subject to power output degradation when exposed to the sun. [22]
GaAs	GaAs cells show a high efficiency (29% laboratory) and less thickness than silicon ones, but also higher cost. Furthermore, the materials used are not abundant in nature.
CdTe	CdTe cells can exploit a broader wavelength spectrum than Si cells, close to the natural one and have an efficiency of 10-15% (21% laboratory) [23]. Regarding the materials, cadmium is abundant and generated as a by-product of important industrial materials like zinc, but it is one of the most toxic materials known, also if combined with telluride.
CIGS	CIGS cells are characterized by a good resistance to heat and by a manufacturing process that is less energy intensive than manufacturing of the crystalline silicon solar cell. Anyway, they are less efficiency than Si solar cells (20% maximum) and very expensive to produce.
CIS	Similarly to CIGS technology, CIS cells show a good resistance to heat if compared to silicon based modules [23], but they are less efficient (10- 13%) and relatively expansive due to the material used. Manufacturing processes are less energy intensive than manufacturing of crystalline technology.

***Table 3** - 3rd generation PV cells*

3rd generation solar cells	
Type	Description
PSC	Perovskite is one of the most promising material for PV technology, since perovskite solar cells have a good efficiency (19-22%) [23] and possibilities for improvement are still possible. In addition, perovskite is cheaper to produce than silicon. The disadvantage is that perovskite breaks down quick when exposed to external condition (heat, snow, moisture, etc).
OPV and polymer solar cells	These cells are characterized by lightweight, mechanical flexibility, disposability and large-scale roll-to-roll production capability. Unfortunately, they also have low efficiency (4-5%, up to 9%) [23], low durability and low stability.

DSSC	DSSC, like perovskite, is one of the most promising PV technology. The solar cells are flexible, not pollutant and easily recyclability. DSSC cells have a good efficiency (around 10%) also at high temperature and work even in low-light conditions. Some of the technology problems are that the electrolyte can freeze at low temperatures and contains volatile organic solvents.
QDs	QD solar cells are easy to synthesis and manufacture, but actually, the efficiency is low (around 1.9%).

Fukurozaki et al. [24] examined a 1.2 kWp sc-Si PV (efficiency of the cell of 15.3%) mounted on a rooftop, in Brazil. The authors considered separately all processes from metallurgical silicon grade (MG-Si) production to panel fabrication, including transportation, installation and operation. BOS (including supporting structure, inverter and cabling) was considered too. They excluded the decommissioning stage. The lifetime (LT) of the panel, structure and cabling was 30 years, while the inverter LT was 15 years. The main results regarded Cumulative Energy Demand (CED), Energy Pay Back Time (EPBT), Global Warming Potential (GWP) and CO_2 emission rate. CO_2 emission rate was calculated by dividing the life cycle $CO_{2equivalent}$ emissions by the PV lifetime (year) and the annual energy output in their primary energy equivalent. CED was 1619 MJ/m^2 of panel area. The most energy intensive processes were the purification of MG-Si (3133 MJ), the mounting construction (2632 MJ) and the panel assembling (2468 MJ). GWP for the entire PV system life cycle was 843 kg CO_{2eq}; the main hotspots were the panel production phase (159 kg CO_{2eq}) and the construction phase (151 kg CO_{2eq}). The EPBT and CO_2 emission rate were calculated for different Brazilian locations, characterized by different latitudes and irradiations (from 1506 to 1935 kWh/m^2/year). The highest EPBT value was about 3.13 years while the lowest was 2.47 years; CO_2 emissions rate ranged from 14.54 kg/kWh to 18.68 kg/kWh.

Kim et al. [25] evaluated the environmental performance of sc-Si and mc-Si panels with power conditioning system (PCS) and BOS, in Korea. The system boundaries were defined as pre-manufacturing, manufacturing, use and disposal stages. The authors considered two scenarios for the PV efficiency: a base scenario (efficiency: sc-Si 15.95%; mc-Si 14.91%) and a best scenario (efficiency: sc-Si 27.60%; mc-Si

20.40%). The results related to GWP in the base scenario showed that sc-Si and mc-Si systems emit 41.8 g CO_{2eq} and 31.5 g CO_{2eq}, respectively. The best efficiency case could reduce the GWP of the sc-Si and mc-Si systems by 34.3% and 20%. The major contributors in terms of CO_{2eq} (concerning only silicon module manufacturing phase) were the mc-Si and ingot manufacturing processes, due to the electricity required for the purification of mc-Si and for the crystallization process of the ingot. The EPBT of the sc-Si and mc-Si PV systems in the base efficiency case were 4.65 years and 3.68 years, while in the best efficiency case were 3.11 years and 2.97 years. Authors calculated fossil-fuel consumption and CO_2 payback time (CO_2PBT). The sc-Si and mc-Si PV systems in the base case consumed 0.56 MJ and 0.44 MJ of fossil fuels per kWh, while in the best case there was a reduction of 33% and 19.3%, respectively. CO_2PBT values for the base scenario were 2.53 years (sc-Si) and 1.91 (mc-Si), while for the best case were 1.66 years and 1.53 years, respectively. A sensitivity analysis regarding GWP was performed with different irradiations (1301.35-1700 kWh/m^2/years); the results showed that the increase of irradiation allowed a GWP reduction of 26% and 22% for base case, and a reduction of 22% and 24 % for best case (for sc-Si and mc-Si, respectively).

Stylos & Koroneos [26] estimated the GHG emissions caused during the life cycle of a large-scale grid connected PV system (PV modules, inverters, batteries and steel foundation), using a cradle to use approach (from raw material extraction to module fabrication and use). They analyzed four different scenarios of manufacturing a mc-Si panel, with cell efficiency variable from 14% to 20%. The emissions obtained ranged from 12.28 to 58.81 g CO_{2eq}/kWhe. In the end, a comparison with CO_{2eq} emissions of a diesel power station was made, showing that carbon footprints of PV systems were lower than diesel power station in every scenario.

Fu et al. [27] performed a LCA for a PV system with mc-Si modules in China. They calculated EPBT and environmental impacts as GWP, acidification potential (AP), eutrophication potential (EP), ozone layer depletion potential (ODP), photochemical ozone creation potential (POCP) and human toxicity potential (HTP), from materials extraction to cell and module fabrication. The authors did

not take into account the end-of-life (EoL), due to lack of accurate data in China about the disposal phase, and BOS. The total primary energy demand (PED) from renewable and non-renewable energy was calculated as 0.517 MJ/kWh (48.5% due to mc-Si production stage), while the worst EPBT was 6 years, considering different areas of China. The mean value was approximately 2 years. As concern environmental impacts, AP was 4.27E-04 kg SO_{2eq}/kWh (73.4% due to sulfur dioxide caused by electricity consumption) and EP was 4.23E-05 kg $PO_4^{3-}{}_{eq}$/kWh (mainly due to emissions of nitrogen oxides and phosphate). The calculated GWP of the PV system was 5.09E-02 kg CO_{2eq}/kWh; the main contributor to GWP was the carbon dioxide (83.6%). HTP index was 17.76E-02 kg DCB_{eq}/kWh (dominated by the emissions on air and freshwater (FW)); ODP was 3.02-09 kg R_{11eq}/kWh (dominated by Halon 1301/1211 and carbon tetrachloride) while POCP was 2.69E-05 kg C_2H_{4eq}/kWh (mostly caused by inorganic and organic emissions to air). Comparing the environmental impacts of each process, the authors found that the production of solar grade mc-Si contributed the most, accounting for about 52.4% of the total impacts. The next were the manufacturing processes of cells and modules, accounting for 20.1% and 18.6%, respectively. Moreover, a sensitivity analysis was conducted to find out the effects on the energy demand and environmental impacts of different factors (electricity and steam consumption during the production of solar grade mc-Si, glass consumption and disposal during the process of wafer slicing, electricity consumption during the process of cells, aluminum and glass consumption during the modules assembly). It emerged that a 10% decrease in electricity consumption during solar grade mc-Si production would lead to a 3.37% drop in PED, 3.97% in AP, 3.81% in EP, 3.56% in GWP and 3.21% in POCP; a 10% reduction of aluminum consumption, during the module assembly phase, would lead to a 7.01% drop in ODP. A 10% decrease in glass consumption and disposal during wafer slicing process would lead to a decrease of 2.11% on HTP while a 10% decrease in steam consumption would lead to a decrease that range from 0.46% (EP) to 1.06% (AP).

Yang et al. [28] analyzed a mc-Si PV module in China focusing on international trade, which played a significant role in the development of the Chinese PV industry, and distinguished domestic and imported raw materials. The authors

underlined the importance of international trade because it causes the separation of consumption and production of PV products, which are two important phases with different environmental impacts. They considered three scenarios: scenario 1 (baseline) in which all materials were assumed to be produced in China and international trades were ignored; scenario 2 in which mc-silicon was imported as raw material; scenario 3 that accounted for the market share of all raw materials from various sources. For better comparison with other previous reported study, only the manufacturing phase was considered. The following impacts were calculated: GWP_{100}, abiotic depletion potential (ADP), AP, EP, HTP, freshwater aquatic eco-toxicity potential (FAEP), marine aquatic eco-toxicity potential (MAEP), terrestrial eco-toxicity potential (TETP), ODP and POCP. GWP was 2.91E+03 kg CO_{2eq} for scenario 1 and around 2.22E+03 kg CO_{2eq} for scenarios 2 and 3; the difference lie in the fact that imported mc-Si manufacturing requires less energy than local production. Mc-Si production was the GWP "hotspot" of the entire process. However, PV module packaging was also a major contributor to GWP. These processes accounted for 52% and 29% of GWP in scenario 1, 38% and 38% in scenario 2, and 39% and 38% in scenario 3. Other results of first scenario are shown on Table 4.

Table 4 *- Environmental impacts of mc-Si PV in scenario 1 [28]*

Environmental impacts	Results
ADP	3.40E+00 kg SB_{eq}
AP	1.76E+01 kg SO_{2eq}
EP	1.80E+00 kg PO_{4eq}
HTP	6.25E+01 kg $1.4DB_{eq}$
FAEP	1.52E+01 kg $1.4DB_{eq}$
MAEP	2.69E+02 kg $1.4DB_{eq}$
TEPT	7.10E-02 kg $1.4DB_{eq}$
ODP	4.51E-04 kg $CFC\text{-}11_{eq}$
POCP	6.07E-01 kg C_2H_{4eq}

The manufacturing of PV modules in scenarios 2 and 3 allowed reducing impacts for 8 of 10 factors considered; in particular, scenario 2 was similar but never better than scenario 3. Scenario 1 was a better option for ADP and ODP, but the worst option for all other impacts compared to scenarios 2 and 3. Similar to GWP, the processes of mc-Si production and PV module packaging were the major hotspots for all impacts, except for MAEP and FAEP, in which heavy metals were also significant.

Hong et al. [29] evaluated the life cycle environmental effects associated with PV cell (mc-Si) in China. System boundary was set by using a cradle to gate approach. The method used (IMPACT2002+) considered 15 mid-points impact categories, which are resumed in Tab. 5.

***Table 5** - Mid-points categories results of mc-Si PV in China (IMPACT2002+) [29]*

Mid-points categories	**Results**
GWP	1.84E+03 kg CO_{2eq}
non-renewable energy	2.41E+04 MJ primary
carcinogens (CNG)	12.45 kg $C_2H_3Cl_{eq}$
non-carcinogens (NCG)	48.96 kg $C_2H_3Cl_{eq}$
ionizing radiation (IR)	4.83E+03 Bq C-14_{eq}
ODP	3.22E-05 kg CFC-11_{eq}
respiratory inorganics (RI)	2.09 kg PM 2.5_{eq}
respiratory organics (RO)	0.51kg C_2H_{4eq}
FAEP	1.11E+05 kg TEG water
TETP	1.87E+04 kg TETP soil
terrestrial acidification/nitrification (TA)	71.92 kg SO_{2eq}
land occupation (LO)	4.22 m^2org. arable
aquatic acidification (AA)	11.80 kg SO_{2eq}
aquatic eutrophication (AE)	0.08 kg PO_4 P-lim
mineral extraction (Mex)	104.16 MJ plus

The production of mc-Si PV cell had a significant contribution to the impact scores in RI, GWP and non-renewable energy but represented a small role to the impact scores in CNG, NCG, and TETP. The contribution of mc-Si PV cell production in the remaining categories was negligible. The results of a sensitivity analysis showed that more than 25% of overall environmental burden could be reduced by improving energy efficiency, choosing secondary aluminum for mc-Si production, and reducing mc-Si wafer consumption for PV cell production.

Latunussa et al. [30] analyzed an innovative process for the recycling of silicon PV panel, considering that this phase is generally neglected and that disposal phase will became a relevant environmental issue in the future. The analysis followed a "gate to gate" approach, considering all the impacts from the delivery of the waste to the recycling plant, up to the sorting of the different recyclable materials and the disposal of residues. The impacts of the recycling process of 1000 kg of silicon PV waste are shown in Table 6.

Table 6 *- Impact indices of the recycling process of 1000 kg of silicon PV [30]*

Impact indices	Results
ADP mineral	4.36E-03 kg SB_{eq}
CED	3.15E+03 MJ
FAEP	3.15E+03 CTUe
marine eutrophication (ME)	1.09E+00 kg N_{eq}
AE	5.58E-02 kg P_{eq}
terrestrial eutrophication (TE)	1.21E+01 molc N_{eq}
AP	2.68E+00 molc $H+_{eq}$
POCP	3E+00 kg $NMVOC_{eq}$
IR (ecosystems)	9.42E-05 CTUe
IR human health (HH)	3.05E+01 kg U_{235eq}
particulate matter (PM)	9.81E-02 kg PM 2.5_{eq}
HTP (non-cancer effects)	1.95E-06 CTUh
HTP (cancer effects)	2.95E-05 CTUh

ODP	3.21E-05 kg $CFC\text{-}11_{eq}$
climate change (CC)	4.46E+02 kg CO_{2eq}

All these impacts were calculated excluding the credits derived from the energy recovery. The credits related to this energy recovery were significant (around 30%) for impact categories as ODP, IR (ecosystems), IR (HH), CC, AE and PM; CED could also be reduced from 3150 MJ to 2780 MJ. The results also highlighted that most of the impacts for the recycling process are due to the transport of the PV waste to the site, the plastic incineration and the further treatment for the recovery of metals from the bottom ash.

Hou et al. [31] investigated the environmental impacts of grid connected power generation from c-Si PVs. The authors included BOS and the fossil fuel burned in transportation and assembly. The results were expressed in terms of EPBT and GHG. EPBT ranged from 1.6 and 2.3 years while GHG ranged from 60.1 to 87.3 g CO_{2eq}/kWh; about 84% or even more of the energy consumption and total GHG emission derived from the PV manufacturing process. Also, authors underlined that an improvement in efficiency (from actual 16-18% to 22% or higher in future) could be obtained for the examined c-Si by applying Passivated Emitter Rear Locally-diffused (PERL) or Heterojunction with Intrinsic Thin layer (HIT) cell, and this could lead to a GHG emission of 47.5 g CO_{2eq}/kWh.

Akinyele et al. [32] evaluated the life cycle impacts of a 1.5 kW solar PV system. In particular, they examined the life cycle emission rate (LCER), GWP, CED, EPBT and net energy ratio (NER) of six different locations in Nigeria, one for each of the geo-political zones. The different results were dependent from the different radiations of the zones. LCER ranged from 37.3 to 72.2 g CO_2/kWh and CED from 380 to 8700 MJ_{eq}, GWP ranged from 1907 to 5819 kg CO_{2eq}, EPBT from 0.82 to 2.3 years and NER from 7.08 to 30.17.

Huang et al. [33] considered the life cycle environmental impacts of mc-PV system in China, with a particular focus on decommissioning and recycling phases. Recycling phase included the dismantling of the modules and the processes

connected to main elements like glass (re-melting of glass), ethylene vinyl acetate (EVA) (thermal treatment of EVA) and the chemical treatment of aluminum, argentum and silicon. The functional unit (FU) was a mc-Si PV module with a capacity of 1 kW, containing five 200 Wp modules. The authors calculated 14 midpoint environmental impacts, considering production and recycling phase; they only excluded transportation and use phases from the analysis. The 14 environmental impacts were normalized for each process and a comparison of two different scenarios (landfill and recycling) was made. Mc-Si production, cell processing and module assembling were the phases with the highest environmental impacts. Focusing on the EoL, the recycling scenario showed less environmental impacts than the landfill scenario: even if dismantling of the modules and the treatment of the main elements in the recycling process had a certain environmental burden, their contribution was still lower than the landfill scenario.

Luo et al. [34] made a comparative LCA of PV electricity generation in Singapore by three different mc-Si PV configurations. The FU was one 60-cell silicon PV module and the system boundary was from the mining of silica to the PV system installation. The indicators for evaluating the environmental impacts were EPBT and GHG emissions. The three different roof-integrated PVs consisted in:

- an aluminum back surface field (Al-BSF) solar cells with a conventional module structure (i.e. glass/encapsulant/cell/encapsulant/back-sheet);

- a passivated emitter and rear cell (PERC) device with a conventional module structure;

- a PERC solar cell with a frameless double-glass module structure (i.e. glass/encapsulant/cell/encapsulant/glass).

For the examined scenarios the EPBTs were 1.11, 1.08 and 1.01, respectively, while the GHG emissions were 30.2, 29.2 and 20.9 g CO_{2eq}/kWhe, respectively.

Mohr et al. [35] studied the environmental effects of substitution of fossil electricity with solar electricity from PVs installed in Western Europe into the life cycle of two types of PV modules: a thin film GaInP/GaAs tandem module (efficiency 28.5%) and a classic mc-Si module (efficiency 14.4%). The study considered two

scenarios: scenario 0, in which the environmental impacts of each module were calculated using electricity generated by fossil fuel (hard and brown coal, industrial and natural gas, oil and peat) and scenario S, based on the assumption that the amount of fossil electricity needed in the life cycle of each modules was replaced with the electricity generated by the corresponding module. The authors found that, for both modules, the impact categories that had greater benefit from the substitution of fossil electricity with PV electricity were ADP, AP, GWP, MAEP and POCP. For the GaInP/GaAs module, the impact scores decrease up to a factor of 4.9 (GWP), while for the mc-Si module the impact scores decreased up to a factor of 2.5 (ADP and GWP). The impact categories connected with toxicity were smaller or negligible, comparing the two scenarios. In fact, there is the overlap of a benefit due to the reduction in the use of fossil fuels and of a negative aspect related to the increase in materials (chromium steel for GaInP / GaAs and aluminum for mc-Si module, in particular) for the production of additional PV modules to generate the necessary electricity.

Van der Meulen & Alsema [36] focused on novel applications of nano-crystalline silicon (nc-Si) materials combined with a-Si devices. In this case, PV module operated in a grid-connected system and it was installed on a rooftop in Southern Europe. Authors examined the life cycle of a-Si and the environmental effects of adding nc-Si layer (this approach it is called “micromorph” technology); they also considered two different clean-processes (with SF_6 and NF_3) during the module manufacturing phase and two different efficiency values: micromorph module efficiency was 8.5%, while the best amorphous efficiency was 6.7%. Despite this high efficiency, the use of the new technology resulted in higher material (17-20 times higher) and higher total energy requirements (45% higher). GHG emissions for a-Si cells were lower than 40 g CO_{2eq}/kWh, while they were more than 70 g CO_{2eq}/kWh for nc-Si/a-Si cells (micromorph technology). Authors also considered improvement scenarios (most likely, optimistic and Oerlikon Solar process) that included an increase of process yield factor from 70% to 93%, a reduction of thickness bottom layer (from 2000 to 1300 nm) and an improvement in NF_3-gas utilization. In all scenarios, a-Si technology showed GHG lower than 30 g CO_{2eq}/kWh, while for the combination of nc-Si/a-Si cells, GHG emissions were

always higher than 40 g CO_{2eq}/kWh except for optimistic and Oerlikon process with SF_6 clean processing. In conclusion, GHG emissions for the micromorph technology resulted in a 60-85% increase for NF_3 clean processing and 15-90% in SF_3 clean processing, compared to a-Si technology. In addition, authors found that the use of NF_3 lead to higher GHG emissions in comparison with SF_6, in particular when production of NF_3 and cleaning process are applied to micromorph technology.

A study of environmental indicators and EPBT of CdTe PV systems was made by Held & Ilg [37]. They considered a ground-mounted power plant in Europe, with an efficiency of 10.9%. The authors calculated GHG emissions and EPBT index. EPBT was from 0.7 to 1.1 years while GHG emissions ranged from 19 to 30 g CO_{2eq}, depending on the location site. Through CML2001 method, other five impacts indices were evaluated in this study: Primary Energy from resources (PE), AP, EP, GWP and POCP. The results are showed in Table 7.

***Table 7** - Environmental impacts of the ground mounted CdTe power plant [37]*

Impact	**Production phase**	**End of Life (without recycling credits)**	**Life cycle (BOS included, transportation and maintenance excluded)**
PE [MJ]	750	81	1270
AP [kg SO_{2eq}]	0.21	9.10E-03	0.36
EP [kg $PO_4^{3-}{}_{eq}$]	0.018	8.03E-04	0.029
GWP_{100} [kg CO_{2eq}]	45.3	6.0	86.1
POCP [kg C_2H_{4eq}]	0.015	6.63E-04	0.032

Kim & Fthenakis [38] made a comparative LCA about energy payback of two different technologies (multi-junction a-Si and nc-Si/a-Si modules). The authors used a cradle-to-gate approach, considering only the production phase (no recycling or disposal); they adopted an efficiency of 6.3% for present and 8% for future applications. Nc-Si/a-Si modules required an amount of energy between 750 to

1270 MJ/m^2, while triple-junction module required 860 MJ/m^2. EPBT (nc-Si and a-Si) was 0.7-0.9 years while triple junction EPBT was 0.8 years.

Mohr et al. [39] made a LCA study of tandem flexible solar cells composed of a-Si/nc-Si (10% efficiency). The authors also made a comparison between the a-Si/nc-Si PV system roof-integrated and the roof-mounted mc-Si PV system (14.4% efficiency), both in the Netherlands with an annual insulation of 1000 kWh/m^2. EPBT for a-Si/nc-Si PV system was 2.3 years and 3.4 for mc-Si system, while CED was 1.4 MJ/kWh for both systems. The authors calculated 18 midpoint indices and assessed endpoint level considering the damage to human health, to ecosystem and to resources depletion. The overall damage scores of the a-Si/nc-Si PV system and the mc-Si PV system were 0.012 and 0.010 Ecopoints/kWh, respectively; CC, HTP, PM formation, and FD contributed to 96% of the overall damage scores for both PV systems.

Kreiger et al. [40] examined a process to reduce the consumption of silane during the manufacturing of two types of PV: a hydrogenated amorphous silicon (a-Si:H) based PV and a tandem (a-Si:H/µc-Si:H) with a thin film technology based PV. The inventory data were based on US and European input data while the approach used was "cradle to gate". Then, a comparison between recycling and no recycling was made. By using a recycling process, the energy consumption decreased (per kg of silane used) from 1146 to 409 MJ for a-Si:H and to 397 MJ for the tandem module a-Si:H/µc-Si:H. The GHG emissions decreased (per kg raw silane) from 61.3 kg CO_2 to 22 kg CO_2 for a-Si:H and to 21.2 kg CO_2 for the tandem module a-Si:H/µc-Si:H.

Collier et al. [41] examined two new promising thin-film technologies: copper zinc tin sulphide (CZTS or $CuZnSnS_4$) and zinc phosphide (Zn_3P_2). The authors assumed an electricity mix from United States and an efficiency of 10% for both panels. The approach used was a "cradle to gate" and the impact assessment method was TRACI 2.1. For all four impacts studied (PED, GWP, FW use and eco-toxicity (Ex)), a comparison between the new thin-film PVs (Zn_3P_2 and CZTS), the "old" thin film PVs (a-Si, CdTe, CIGS) and the c-Si PVs (sc-Si and mc-Si) was made. The results are showed in Table 8.

Table 8 - Comparison between new thin films and Si-based technologies [41]

	Zn_3P_2	CZTS	CdTe	CIGS	sc-Si	mc-Si	a-Si
PED [MJ]	2.7E-01	6.4E-01	2.9E-01	6.0E-01	7.0E-01	5.7E-01	3.5E-01
GWP [kg CO_{2eq}]	3.0E-02	3.8E-02	1.8E-02	3.6E-02	3.5E-02	2.9E-02	1.9E-02
FW use [kg]	4.3E-02	1.3E-01	4.5E-02	1.3E-01	6.2E-01	1.4E-01	6.9E-02
Ex [CTUeco]	9.1E-06	2.0E-05	8.8E-06	8.4E-05	8.9E-04	3.6E-04	1.95E-05

CdTe and Zn_3P_2 had similar impacts and outperformed CIGS and CZTS. The impacts from CdTe were slightly higher than that of Zn_3P_2, except for GWP. When compared with Si-based PV, all the four thin film technologies outperformed sc-Si and mc-Si on impacts as Ex and FW use. CdTe and Zn_3P_2 performed better for GWP and PED and had impacts similar to a-Si cell. Regarding the dominance analysis, the manufacturing phase was the biggest contributor for all the technologies.

Bergensen et al. [42] performed a hybrid LCA to compare environmental, HH and natural resource consequences of electricity generated by CIGS and CdTe technologies, in the United States. The authors developed two life cycle inventories for ground-mounted utility scales and roof-mounted distributed-scales PV systems. It was considered a present efficiency (2010) of 12% for CIGS and 11.6% for CdTe and a future improvement (for 2030) to 20.8% and 19%, respectively. In addition, a reduction of thickness was considered for the future scenario. The results showed that the impact categories were similar for both ground-mounted alternative, except LO (since roof-mounted PV use no land directly). The environmental impacts of U.S. thin-film PV technology was at least 90% lower than those of the U.S. grid mix in 7 of 12 categories (AP, GHG, FD, respiratory effects, photochemical oxidation (POx), Ex and EP). In particular, CdTe and CIGS were estimated to emit 20 and 22 g of CO_{2eq}/kWh in the present scenario. Considering future scenario, life cycle GHG emissions from CdTe and CIGS were reduced by 69% compared to their 2010 estimates, to 6 and 7 g of CO_{2eq}/kWh, respectively.

Lunardi et al. [43] made a comparative LCA of chalcogenide/Si tandem solar modules and they investigated the environmental performances of CIGS/Si, CZTS/Si and AZTS/Si tandem solar cells, compared with Si solar modules. The efficiency of these modules was 22% and a complete cradle to grave approach was used. The results are showed in Table 9. Si and CIGS/Si presented the worse impacts for most of the examined categories.

***Table 9** - Environmental impact results for chalcogenide/Si solar modules [43]*

	AZTS/Si	**CZTS/Si**	**CIGS/Si**
GWP [g CO_{2eq}]	25	27	29
EPBT [years]	1.3	1.3	1.4
HTP (cancer effect) [CTUh/kWh]	3.4E-11	4.6E-11	4.9E-11
HTP (non-cancer effect) [CTUh/kWh]	6.9E-10	8.6E-10	1E-09
AE [kg Peq/kWh]	8.8E-07	1.08E-06	1.8E-06
FAEP [CTUe/kWh]	0.059	0.081	0.095
ADP [kg Sb_{eq}/kWh]	2.0E-08	2.1E-08	2.3E-08

In a recent study, Rajput et al. [44] evaluated EPBT, energy production factor (EPF) and life cycle conversion factor (LCCE) of a 3.2 kW CdTe PV system, in India. The efficiency of the cell was 11%. Results showed that EPBT was 3.6 years, EPF was 0.27 and LCCE was 0.0018.

Regarded organic solar cell, authors made an [45] LCA of a typical heterojunction organic cell (LT 15 years) on laboratory scale manufacturing. The analysis was quite complex, due to the fact that authors analyzed in-depth every fabrication step and the life cycle of all different materials used in the various layers. The results were shown for module efficiency of 5% (efficiency for laboratory cells) and 10% (expected industrial efficiency in 2020). Calculated EPBT were 4 and 2 years, CO_2 emission factors were 109.94 g CO_{2eq}/kWh_e and 54.92 g CO_{2eq}/kWh_e, and ERF were 3.75 and 7.49, respectively for the two efficiency values. The PE consumption for 1 m^2 of this organic solar module (90% active area) was 2800 MJ; more than 70% referred to direct process energy (in particular the energy for N_2 atmosphere

maintenance) while 25% was attributable to embodied energy cell input materials (indium tin oxide (ITO) and nitrogen were the two main hotspots).

In a second study [46] authors studied a single junction organic solar cell, using different active layers and various combinations of typical donor/acceptor materials, focusing in particular on the role of polymer (the donor material) and fullerene (electron acceptor molecule). The results showed that EPBT ranged from 0.3 to 0.7 while PE from 4 to 7 MJ/W_p, depending on the active materials required. BOS was not considered in the calculations and no device degradation was assumed. Degradation factor is an important aspect of OPV studies, so this might cause an increasing of the calculated EPBT. ITO coated/PET showed a relative high embodied energy (63.45 MJ/m^2) compared to the other components (aluminum contacts and encapsulation, 0.048 MJ/m^2 and 43.5 MJ/m^2 respectively), while the embodied energy of fullerenes was strongly variable (from 65 to 495 GJ/kg depending on the production method and on fullerenes structure). The main difference between fullerenes production techniques (pyrolysis and plasma) is attributable to electricity and inert gas (argon and helium) required for plasma technique; for this reason, authors suggested the use of this technique in low-cost electricity areas or where there are limitations connected to the combustion by-products from pyrolysis technique.

Sengul & Theis [47] evaluated the environmental impacts of QD-PV considering raw materials acquisition, manufacturing and use phases. The results of this analysis were compared with literature data of different types of PVs (ribbon mc-Si, mc-Si, sc-Si, CdTe, CIS, DSSC) and with other energy sources like coil, oil, lignite, natural gas, diesel, nuclear, wind and hydropower. The authors calculated for QD-PV an EBPT (1.5 years), GWP (5 g CO_{2eq}/kWh) and CED (286 kWh_{eq}/m^2). EBPT of QD-PV was shorter than the other PV types except for CdTe, while it was of the same order of EPBT of coal, natural gas and nuclear, lower than EPBT of lignite and higher than EPBT of wind and hydropower. Regarding the GWP, considering an estimated efficiency of 14%, QD-PV modules had lower GWP than all PV types, coil, oil, lignite, natural gas and diesel, but higher than nuclear, wind and hydropower energy sources. In addition, QD-PV showed the lowest SO_x (≈ 25mg SO_x/kWh) and NO_x emissions (≈ 12 mg NO_x/kWh), except than nuclear, wind and

hydropower, while heavy metal emissions were the highest compared to all other types of PV modules and the lowest compared to the others energy sources. The main contributors to the energy requirement of QD-PV modules (including PV frame and BOS) were the encapsulation and protection of solar cells (42%), production of QD solar cells (33%) and BOS (21%). At last, hazardous waste disposal, ITO and aluminum foil production were the processes that highly contributed to heavy metal emissions for QD cells production.

Espinosa et al. [48,49], in two different works, made a LCA of flexible polymer solar cells prepared using roll-to-roll method. Both assessments were based on a cradle to gate approach and the same functional unit (1 m^2 of processed surface). In the first work [48] the analysis regarded a full roll-to-roll process for the fabrication of flexible polymer solar cell modules. Authors considered an organic solar module efficiency of 2% and 3%. Results were expressed in terms of EPBT that was 2.02 and 1.35 years, respectively; CO_2 emissions were 56.65 g CO_{2eq}/kWh_e and 37.77 g CO_{2eq}/kWh_e, while embodied CO_2 was 15.49 kg CO_{2eq}. PE consumption of 1 m^2 of processed surface (active area 67%) was 379 MJ, distributed to direct process energy (77 MJ) and embodied energy of input materials (302 MJ); the main contributor to this value was ITO on PET substrate (87%). Authors also showed how EPBT and ERF changed with efficiency (from 1.25% to 10%) and active area (50%, 67%, 85%). When efficiency was increased from 1.25 to 10, EPBT decreased from 4.34 to 0.54 years (active area 50%), from 3.24 to 0.4 years (active area 67%) and from 2.55 to 0.32 years (active area 85%). In the same way, ERF increased from 3.36 to 27.66 (active area 50%), from 4.63 to 37.07 (active area 67%) and from 5.88 to 47.03 (active area 85%). EPBT of the organic cell produced with this roll-to-roll process was in line with the EPBT of dye sensitized modules (0.74-2.1 years, 10% efficiency) but higher than flexible OPV (0.19 years, 5% efficiency). In the second work [49], authors analyzed a new process allowing to replace the ITO electrode in organic modules. The main problem of ITO electrode is indium, a material that could represent a point of congestion for the future of OPV large-scale production. Recycling and EoL scenarios were excluded due to lack of data; BOS was not considered. The results showed an EPBT of 9.45 years (1% efficiency; active area 36.7%) but through efficiency optimization it was evaluated that EPBT

could fall to 0.94 years (10% efficiency and 36.7% active area). Total equivalent PE consumption per FU (1 m^2 of processed surface) was 486 MJ, where only 55.6MJ was due to direct process energy (silver electrode printed and drying during deposition were the main hotspot); the embedded energy in materials was ten times higher than direct process energy (430.37 MJ). Again, authors showed how EPBT and ERF changed with two parameters (efficiency and active area): when efficiency changed from 1% to 10% ERF increased from 1.59 to 15.88 (active area 36.7 %), from 2.94 to 28.24 (active area 68.1%) and from 3.67 to 36.7 (85% active area); EPBT decreased from 5.31 years to 0.53 years (active area 68.1%) and from 4.09 years to 0.41 years (active area 85%). CO_{2eq} emission factor were 137.68 g CO_{2eq}/kWh_e (1% efficiency), 91.79 g CO_{2eq}/kWh_e (3% efficiency) and 55.07 g CO_{2eq}/kWh_e (5% efficiency), while embodied CO_{2eq} was 20.66 kg CO_{2eq}.

Anctil & Fthenakis [50] made an analysis of different processes and material for OPV. The main scope of this LCA was to compare CED of different OPV technologies (single junction small molecule, multi-junction and polymer PV) and to evaluate the impact of using different processing conditions (thermal treatments, interface layers, low bandgap polymer, type of heterojunction). The functional unit chosen was the production of a power of 1 watt-peak (W_p). Authors found that fullerenes were the most energy-intensive components of OPV; for this reason, polymer solar cells, that required a high quantity of large fullerenes, had on average a high CED (4.5-5.8 MJ/W_p) compared to the other OPV technologies. Processes and materials used in small molecule PV had a very low impact on CED, compared to polymer PV; in this case, the other components of the system were a hotspot and CED strictly depended from efficiency and type of small molecule used (CED was 3.6 MJ/W_p for 5% efficiency and 5.9 MJ/W_p for 3% efficiency). Regarding multi-junction devices, the greater efficiency (6.5%) had not noticeable consequence on the CED/W_p that was higher, compared to polymer PV (5-6.1% efficiency) and slightly lower than small molecules PV with 3% efficiency; this result can be explained through the increase of complexity of the devices and the need of additional materials and processes.

Parisi et al [51] made a comparison of different DSSC configurations, focusing on manufacturing phase. The following configurations (substrate-electrolyte-counter electrode-substrate) were analyzed:

- glass – liquid electrolyte (LE) – carbon;

- glass – ionic liquid electrolyte (ILE) – cobalt sulfide (CoS) PET;

- PET - LE - Pt PET; PET - LE- Pt glass;

- steel - LE - Pt PET; steel - LE -Pt glass;

- glass - ILE - Pt glass; glass - LE - Pt glass.

Results showed that the substitution of glass with PET reduced the environmental burden in all impact categories (CC, HTP, LO, NLT, PM, FD); the use of steel (for the solar cell back contact) was a main contributor in most categories, especially FD and CC (HH). Authors also assessed that the replacement of the platinum cathode with a CoS contributed to lower environmental impacts. Finally, the authors calculated GWP_{100} and CED; these indices followed the same trend of previous results; in fact, the configuration with steel-LE-Pt glass was the worst for GWP_{100} (1.1 kg CO_{2eq}) and CED (43 GJ) while PET-LE-Pt PET had the lowest values (GWP_{100} was 0.2-0.3 kg CO_{2eq} and CED was 10 GJ).

Azzopardi and Mutale [52] applied LCA to a hybrid QD based solar cell under development. The study was based on laboratory-scale production. Authors compared this solar cell with previous thin film through sustainability criteria results (EPBT, GHG emissions and NER), assuming a 10% efficiency and a LT of 25 years. They did not consider EoL and recycling because of lack of data. The calculated EPBT was less than half than crystalline technology (1.51 years); also, the CO_{2eq}/kWh was lower (2.89 g CO_{2eq}/kWh). NER was 20.82 for hybrid QD based solar cell (blend type) and 16.66 for hybrid QD based solar cell (variant type). At the end of the work, authors conducted a sensitivity analysis regarding NER and CO_{2eq}/kWh, varying LT (from 1 to 10 years) and efficiency (from 1% to 10%). The results showed that lifetimes greater than 1 years and efficiency higher than 1% are needed for these systems to be less impacting from the energy and environmental point of view.

Espinosa and Krebs [53] assessed the impacts related to an organic tandem solar cell and compared the architecture of this system with a simpler flexible single device. They found that a tandem device performed approximately 20% better than the single one. The authors considered three different efficiencies (1%, 3%, 5%) and evaluated an EPBT from 0.24 to 0.3 years and a CED from 43.86 to 51.34 MJ_{EPE}/m^2. The mid-point categories calculated with CML2001 method were ADP, AP, EP, GWP_{100}, ODP, TETP and POx. The environmental hotspots were silver, PET and electricity. Silver was one of the major drivers of ADP, EP and TETP, followed by PET and electricity mix. CED for PET and electricity was 16.5 MJ and 14 MJ, respectively.

Parisi et al. [54] studied the evolution of the sensitized cells from Gratzel prototype to upscale solar application. The evaluated system was mounted on rooftop and the base efficiency considered was 8%. The performances of the PV system were calculated for different irradiations (corresponding to Nord, Centre and South Europe) with a cradle to gate approach, including the synthesis of main components, fabrication of module and operational phase. During the study, 17 impact indices and CED index were calculated for three different types of dyes: the porphyrin dye YD2-o-C8, the ruthenium-based dye N719 and the organic metal-free dye D5 dye. The calculated mean values of CED were 224.4 MJ (for YD2-o-C8 dye), 111.2 MJ (for D5 dye) and 61.8 MJ (for N719 dye); the single score indicators were 2.08 points (for YD2-o-C8 dye), 0.81 points (for D5 dye) and 1.07 (for N719 dye). The major impact was due to the module support materials, that could be reduced by about of 35% changing from glass to polymeric substrate.

A study about a rooftop grid connected DSSC system was conducted by Parisi & Basosi [55]. The main scope of the study was the assessment of NER, GWP_{100} and EPBT indices. The authors used a cradle to gate approach (no recycling phase) and considered an efficiency of 8%. The results showed a NER of 12.67 (considering a LT of 20 years), an EPBT of 1.58 years and a GWP_{100} of 22.29 CO_{2eq}/kWh. A sensitivity analysis was conducted for all these three parameters. EPBT ranged from 2.11 years to 0.97 years (with efficiency that ranged from 6% to 13%); NER minimum value was 7.30 (efficiency 6%; LT 15 years), while maximum value was 29.41 (efficiency 13%; LT 30 years). In the same way, the corresponding values for

GWP_{100} were 38.68 CO_{2eq}/kWh and 9.60 CO_{2eq}/kWh. The hotspots for the ten environmental indices (ADP, AP, EP, GWP_{100}, ODP, HTP, FAEP, MAEP, TE and POx) were the manufacturing of single cell (from 37% to 80%) and the electricity production (20% to 45%).

Tsang et al. [56] examined the environmental impacts of two different OPV solar modules: a default OPV technology (OPV-D) with polymer-based bulk heterojunction with a fullerene derivative and a polymer in its layer, and a second all-polymer technology (OPV-PP), polymer acceptor-polymer donor. The authors wanted to examine how different production integrations, duration use and disposal routes, influenced the environmental impacts of OPV systems. For this reason, they considered two system scenarios, a solar rooftop array (S1) and a portable solar charger (S2), and two different EoL scenarios, namely landfill and incineration. Then, they compared the results with silicon PV technologies: in particular, OPV (D and PP) with mc-Si in S1 scenario (Table 10) and OPV (D and PP) with a-Si in S2 scenario (Table 11).

Table 10 *- Comparison between OPV (D and PP) and mc-Si in scenario 1[56]*

Panel Type	**OPV-D**		**OPV-PP**		**mc-Si**
	Incineration	Landfill	Incineration	Landfill	
CED	122 MJ/m^2	125 MJ/m^2	108 MJ/m^2	112 MJ/m^2	3240 MJ/m^2
EPBT	436 days	449 days	384 days	398 days	918 days
CO_2PBT	192 days	185 days	175 days	168 days	363 days

Table 11 *- Comparison between OPV (D and PP) and a-Si in scenario 2 [56]*

Panel Type	**OPV-D**		**OPV-PP**		**a-Si**
	Incineration	Landfill	Incineration	Landfill	
CED	293 MJ/m^2	354 MJ/m^2	280 MJ/m^2	341 MJ/m^2	1100 MJ/m^2
EPBT	220 days	265 days	42 days	45 days	640 days
CO_2PBT	118 days	97 days	16 days	14 days	280 days

In S1 and S2, for both EoL scenarios, OPV-D and OPV-PP showed better results compared to mc-Si and a-Si results. Finally, a last comparison, concerning relative life cycle impacts, was made between OPV-D (S1 and S2) and m-Si. In S1, OPV-D (incineration) impacts ranged from 97% lower for TETP to 32% lower for AE; the only exception was MD that was 21% higher for OPV-D; in S2, OPV-D impacts ranged from 89% lower for urban LO to 39% lower for TETP.

Celik et al. [57] performed a cradle to gate (from laboratory to fab) LCA for different PSC structures suitable for low-cost manufacturing (solution, vacuum and HTL-free). They considered an efficiency of 15% (best efficiency of 15.6%). EPBT for this system was 1-1.5 years, while GWP ranged from 100-150 g CO_{2eq}/kWh. Moreover, nine midpoint environmental impact categories were calculated with TRACI method. The environmental impacts of manufacturing processes are showed in Figure 5 (the values expressed refer to HTL-free process).

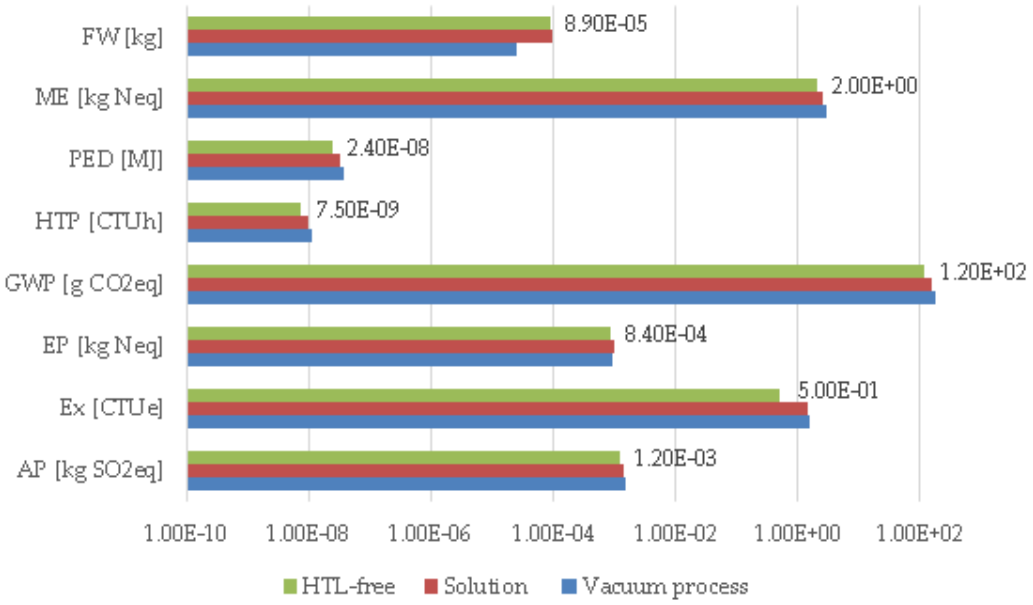

***Figure 5** - Environmental impacts of manufacturing processes (logarithmic scale 100) [57]*

For all impact categories, except Ex and ME, the electricity consumption during the manufacturing was a hotspot (50% - 90%); in particular, electricity consumption reached a contribution of 80% for GWP, HTP, PED and FW use. The results were compared with some 1st and 2nd generation devices: the total environmental impacts

(when all impact categories were normalized to sc-Si ones) of perovskite devices were higher (solution and vacuum) or similar (HTL-free) to mc-Si solar cells, lower than sc-Si solar cells and quite higher than a-Si, CdTe and CIS solar cells. Regarding electricity requirements, PSC had higher energy requirements than all other technologies. This result was probably influenced by the lack of data on the production of large-scale perovskite cells and, therefore, could be subject to change in the future (the same should happen for the corresponding environmental impacts).

The study made by Hengevoss et al. [58] described a LCA and eco-efficiency analysis of prospective tandem OPV modules (new materials such as nano-sized zinc oxide, nano-sized silver and semiconductor polymer are used; a light management and a new flexible PET based encapsulation with organic and inorganic barriers). The authors considered a power conversion efficiency of 8% with LT scenarios of 15 and 20 years. The aim of the LCA was to calculate environmental impacts of this prototype OPV, the EPBT and GWP for the generated electricity, using two different types of modules (installed on roof top) as benchmark (mc-Si and CdTe). The results for OPV showed that CED was 108-112 MJ_{eq}/m^2, GWP was 5.7-6 kg CO_{2eq}/m^2, MD was 0.046-0.056 $\$/m^2$ while Ex was 5.3-6.7 CTU/m^2. The OPV module had an EPBT of 1.6 and 2.5 months, when exposed to Southern Europe irradiation (2000-1800 kWh/m^2y) value. Finally, considering CED, Ex, MD and EPBT of CdTe and m-Si, it resulted that 1 m^2 of OPV module represented only 3%-10% of 1 m^2 of CdTe and mc-Si modules respectively; EPBT of OPV (installed at façade) was 18-55% of that of the benchmarks and GWP was 12-60% of that of the benchmarks. One of the most contributors to CED of the OPV was encapsulation (20%), followed by the PEDOT:PSS polymer (19%) and the light management (13%). Including the whole system (module and BOS), the EPBT of OPV added up to 3.4 and 4.7 months. Considering an optimistic efficiency scenario for OPV (10% power conversion efficiency), GWP decreased by 20% (15 years LT) and by 19.7% (20 years LT) for 1000-1200 kWh/m^2y irradiation, while decreased by 20% (15 years LT) and 19% (20 years LT) for 1800-2000 kWh/m^2y irradiation.

Zhang et al. [59] made a comparison of life cycle environmental impacts of different PSC systems. The study focused on cradle to grave impacts of five typical perovskite solar cells, developed with different materials and manufacturing processes: $MASnI_3$, $MAPbI_3$, $FAPbI_3$, $CsPbBr_3$ and $MAPbI_2Cl$. The results in terms of primary energy consumption to produce 1 cm^2 of active area of solar cells (process energy) and the embodied energy of materials (landfill scenario) are showed in Tab. 12.

***Table 12** - Primary energy consumption of perovskite solar cells (1 cm^2 active area) and embodied energy of materials (landfill scenario)*

Type of cells	**$MASnI_3$**	**$MAPbI_3$**	**$FAPbI_3$**	**$CsPbBr_3$**	**$MAPbI_2Cl$**
PE consumption of 1 cm^2 of cell [MJ]	9.16E-02	8.06E-02	8.88E-02	7.26E-02	9.12E-02
Embodied energy of materials [MJ]	1.5	2.01	1.96	1.28	1.49

The 95% of the embodied energy was from system manufacturing in each solar cell system. The authors selected nine different environmental categories to evaluate the performances of each PSC. Following the previous order ($MASnI_3$, $MAPbI_3$, $FAPbI_3$, $CsPbBr_3$, $MAPbI_2Cl$): ADP was 1.32E-05, 1.28E-05, 8.11E-06, 7.13E-06 and 8.72E-06 kg Sb_{eq} while GWP was 49.4, 67.2, 63.1, 41.6 and 49.5 g CO_{2eq}. Other results were not expressed in absolute value but only in normalized graphic form; anyway, it emerged that the different environmental impacts obtained may be attributable to the amounts of organic solvents used in the fabrication of the devices and to the different efficiency values. Considering the manufacturing of 1 cm^2 of cell as FU, $MAPbI_3$ and $FAPbI_3$ had the highest impacts, except than ADP; instead, considering the production of 1 kWh as FU, $MASnI_3$ and $CsPbBr_3$ had the highest impacts in all categories. This difference was attributable to the low power conversion efficiency of these cells (only 5.73% and 4.88%) compared to other cells (20% for $MAPbI_3$, 15.56% for $FAPbI_3$, 10.9% for $MAPbI_2Cl$). The production of CO_{2eq} (GWP) connected with the generation of 1 kWh (FU) of electricity was between 2.63 and 6.78 kg CO_{2eq}, following an inverse trend than that of the efficiency of each cell. In addition, gold production made the largest impact

contribution to PV systems, so the substitution of this material (with silver or aluminum) could reduce the total environmental impact score.

Lunardi et al. [60] studied different perovskite/silicon (Si) tandem structure and compared them with three different single junctunions PSC (Ag-Au-Al as back electrodes), a sc-Si and a HIT Si cells. They carried out a LCA to evaluate GWP, HTP, AE, FAEP, ADP impacts and EPBT associated with the three perovskite tandem cells. The differences between these cells were in the materials and in structures. The first two cells used the same HIT Si solar cell for the bottom subcell and the same perovskite structure for the top sub-cell (efficiency of 20%). The third tandem structure used a more common lower cost p-n junction silicon solar cell (efficiency of 16%). All the following results for tandem PSC/Si were calculated in a scenario (20 years) where perovskite solar layer became opaque after 1 year LT, making impossible for the bottom Si to generate power; so it was hypothesized the substitution of materials for perovskite layer every year. The comparison between the environmental impacts of all cells is showed in Figure 6.

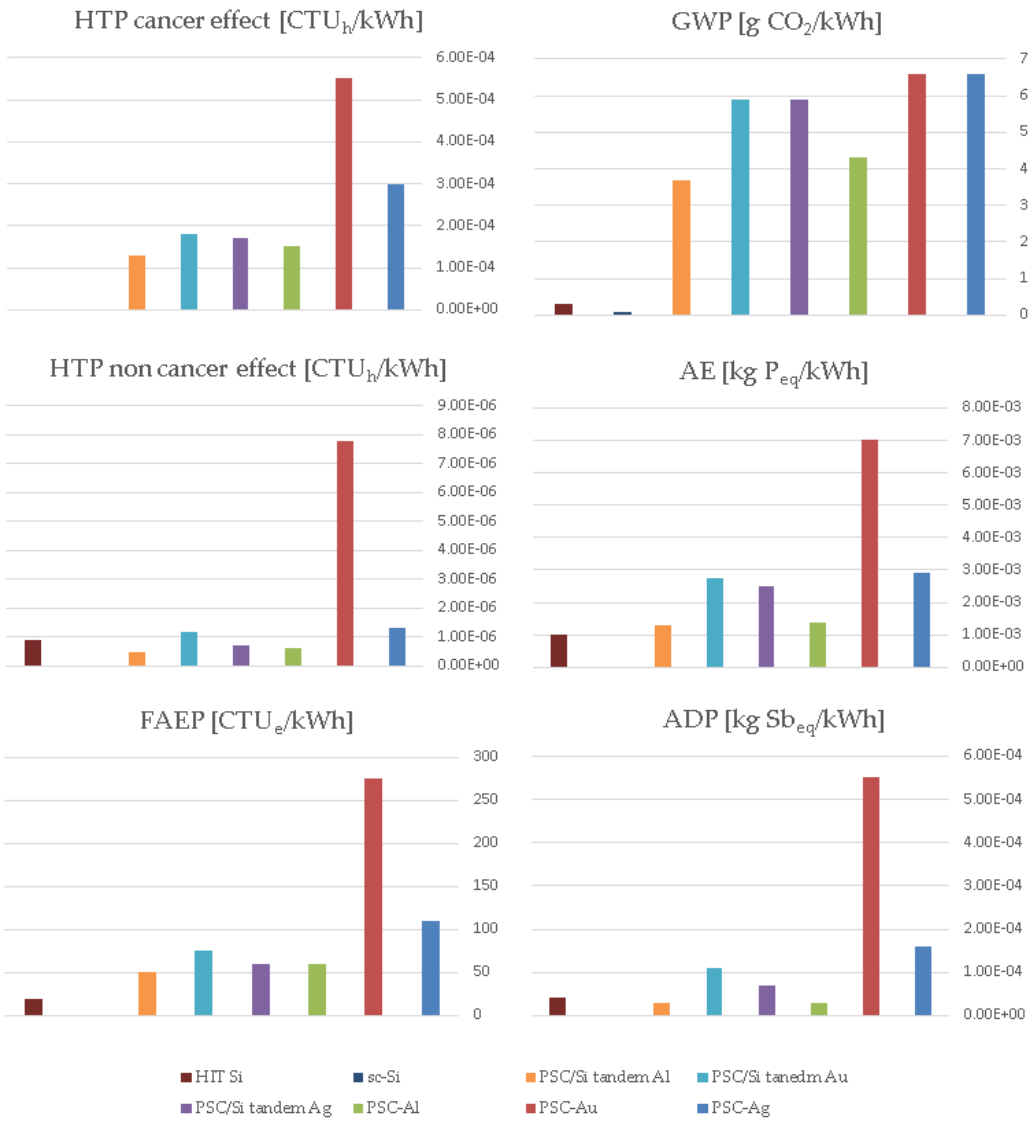

***Figure 6** - Environmental impacts of different solar cells [60]*

For a different scenario, the most optimistic for perovskite life, the layer remained electrically conductive after 1 year and no substitution was required: in this case, all impacts categories related to tandem PSC/Si, except HTP (non-cancer effect), resulted in the same order or lower than that of HIT Si. The EPBT for Si p-n junction was 1.6 years while for Si HIT was 2 years. The EPBT for perovskite and perovskite/Si tandem solar cell was lower (1.3-1.5 years), compared to both silicon cells.

Another work about PSC was performed by Maranghi et al. [61]. Authors evaluated the environmental hotspots connected with lab scale fabrication of different PSC

configurations, through the harmonization of previous LCA studies of this technology. The PSC configurations analyzed were:

•FTO glass/TiO_2/$MAPbI_3$/Spiro-OMeTAD/Au and ITO glass/ZnO/$MAPbI_3$/Spiro-OMeTAD/Ag (G1-G2);

• FTO glass/TiO_2/$MAPbI_3$/Spiro-OMeTAD/Ag (E);

• FTO glass/TiO_2/$MASnI_3$/Spiro-OMeTAD/Au (S);

• FTO glass/TiO_2 nanotube (TNT)/$MAPbI_3$/Iodine LE/Pt glass (Z);

•FTO glass/SnO_2/$MAPbI_3$/CuSCN/MoOx-Al solution and vacuum based (C1-C2);

• FTO glass/SnO_2/$MAPbI_3$/C-Paste (HTL free) (C3);

•FTO glass/TiO_2/$MAPbI_3$(Solvent)/Spiro-OMeTAD/Au with four different solvents (AB1-AB2-AB3-AB4).

Considering 1 cm^2 as FU and only the manufacturing phase, that take place in European area for all cells, it resulted that five of the above configurations (S, AB1-4) have a higher impacts (results were expressed by points in a Single Score) compared to the others. Only 6 of 12 categories showed a percentage impact higher than 1%: HTP (cancer and no cancer effects), IR, FE, Freshwater Ex, and MD. S configuration had an impact of 2.2E+01 mPt (milliPoints), while AB1-AB2-AB3-AB4 configurations impact was around 1.5E+01 mPt. For the S configuration, the hotspot was the gold in the back contact (two order of magnitude higher than other configurations) while for AB1-4 the hotspot was the direct emission of metallic zinc on water (HTP and FAEP). Then, a comparison of CED (calculated with CED-single score impact method) was made: S configuration resulted to be out of scale compared to the other configurations (CED 104 MJ); CED for Z configuration was 2.6 MJ while for E configuration was 1.2 MJ. All remaining configurations showed a CED equal or less than 1 MJ.

2.3 LCA of BIPV and BIPV technologies

Building Integrated Photovoltaics (BIPV) offers the opportunity for widespread use of photovoltaic technology for energy production, through the integration of

photovoltaic elements into building components, providing a great advantage over traditional PV systems and Building Applied Photovoltaic (BAPV), which require photovoltaic panels to be simply attached to the external parts of building envelopes (on roofs or facades). On the other hand, being considered a functional part of the building structure, they require a complex fulfillment of multiple conditions (aesthetic, economic, structural, acoustic, thermal, etc.). Different type on BIPV applications are showed in Figure 7.

Figure 7 *- Classification of BIPV product. [62]*

Hudișteanu et al. [63] analyzed a PV system integrated into buildings in different locations of a temperate zone (Romania). They chose four big cities (Bucharest, Iasi, Timisoara and Cluj-Napoca) that were characterized by different climatic conditions. The PV panels were examined for the same orientation in two different fixed positions (vertical and horizontal). They considered a 1 m^2 of PV panel and the aim of the study was to determinate the most suitable solution of integration in order to obtain the maximum efficiency. Results showed that the highest energy production was achieved for horizontal position of PV panel and it ranged from 144 to 151 kWh/m^2.year (highest value in Bucharest), while for vertical-S, vertical-SE and vertical-SW the values ranged from 107.9 to 126.4 kWh/m^2.year. Comparing the monthly efficiency with the annual one, authors proved that the efficiency of PV panels is negatively influenced by cell's operating temperature. In fact, during summer, when solar radiation reaches maximum values, the total efficiency of PV panel resulted to be lower due to the high operating temperatures.

Biyik et al. [64] collected in a review several studies regarding BIPV technologies. Among these, Omer et al. [65] reported the monitoring results of a thin film PV facade (58° tilt angle- 2% efficiency) and a monocrystalline PV roof slates (52 ° tilt angle-3,6% efficiency); author calculated the annualized energy cost of the two technology that resulted to be 34£/kWh and 3.69£/kWh, respectively. Yang et al. [66] examined the performance of a BIPV system with an air gap between PVs and wall that allow cooling and increase in efficiency. They found that the maximum power output was related to the root installation and the total annual energy output was estimated to 6878 kWh. Mallick et al. [67] compared the performances of a novel parabolic PV concentrator with those of a non-concentrating system. The results showed that the maximum power output point of the concentrating system was 62% higher than the non-concentrating one while the efficiency had an opposite trend due to the temperature of the cells (6.8% and 8.6, respectively). Urbanetz et al. [68] evaluated the yearly electricity generation amounts of two systems: a 3.072 kWp thin-film a-Si BIPV system and a curved, 12 kWp, PV thin-film a-Si laminates. The results showed that the first system had an annual energy yield of 1265 kWh/kWp, while the second system generated 1110 kWh/ kWp. They also found that, in the summer period, the yield of curved system was relatively higher. Yoon et al. [69] analyzed an experimental BIPV application of transparent thin-film a-Si cells into the windows. The system was monitored for a two-year period: the monthly electricity generation was 48.4 kWh/kWp, while the annually electricity generation was 580.5 kWh/kWp. At the end of the review, Biyik et al. [64] summarized some interesting aspects related to the collected BIPV studies: first, in recent years, PV research started to focus on novel designs to increase the efficiency both for system and PV cells, trough new system configurations, new cooling methods and new photovoltaic materials. Then, they found that a widely range of BIPV electric generation capacity ranged from a few MWhr/yr to more than 100 MWhr/yr while the efficiency values ranged from 5% to 18%. Finally, they reported that both façade and rooftop BIPV applications were equally common in the literature while, regarding the technology, DSSC seems to offer a promising solution for BIPV future applications.

Another study that underlined the importance of operating temperature for BIPV system power performance was conducted by Ritzen et al. [70]. Authors compared the performances of ventilated and non-ventilated monocrystalline BIPV systems installed on rooftops. The results showed that electricity production of the ventilated BIPV was 2.6% higher than that of a non-ventilated system.

Cerón et al. [71] made a state of the art of building integrated photovoltaic system. It emerged that most of BIPV modules were multi-crystalline silicon and that the power density ranged between 100 W/m^2 and 150 W/m^2. The main typology of BIPV modules were opaque and rectangular shape; regarding the mechanical characteristics, frameless modules represent a significant chunk of the market (48%). In addition, BIPV roofing elements were the most common while there are fewer products for BIPV façade. In terms of weight, BIPV façade system are heavier than BIPV roofing (typical values under 30 kg/m^2). A last consideration regard the guarantee power over years: BIPV products have usually 90% of power guarantee during first 10 years, and 80% of power guarantee during first 25 years.

Lamnatou et al. [72] investigated the life-cycle property of a building integrated concentrator PV (BICPV) in different cities (Barcelona, Exeter and Dublin). They chose a functional unit of 1 kWp and the phases considered in the analysis were: modules manufacturing, installation, use/maintenance, transportation and disposal. The geometrical concentrator ratio (CR) of the CPV is 2.8x and the main application of the system was a double-glazed BICPV. The results showed that PBT values for Barcelona ranged from 3.6 to 5.8 years, while for Exeter and Dublin PBTs ranged from 3.7 to 7.8 years. The environmental assessment allowed to highlight that is CPC was the component with the maximum contribution to resources consumption while PV cells were the highest contributors to ecosystems/ecosystem quality and human health.

Menoufi et al. [73] analyzed the LCA study BICPV scheme at the University of Lleida (Spain). The integrated concentrating system had a maximum achieved CR of 10x (suns). Authors also compared, through EPS 2000 methodology, the environmental impact of the actual BICPV scheme with a conventional BIPV scheme. It consists of two transparent PV modules with the same power of a CPV

installed at the south wall and supported by an aluminum framework. The results showed that CPV system represents only 10% of the total impact points of the BICPV scheme. In addition, replacing the BICPV scheme with a BIPV one caused an increment in the environmental impact by about 13.5%, while the impact of the PV system was about 2.35 times the impact of the CPV. The highest impact categories were abiotic stock resources (75% and more of the total) and human health (from 25% to 10% of the total).

Perez & Fthenakis [74] analyzed the life cycle of a PV array applied as a vertical curtainwall façade (façade-integrated BIPV systems) covering 12 floors and 150 m^2. The material inventories were collected through SimaPro v7.1 software. The results showed that the BIPV system considered has an EPBT of 3.8 years and the GWP was 60.5 g CO_2-eq/kWh.

Baumann et al. [75], in their study, compared the impacts related to a ground-based system (1 MWp, in Toledo) and a BIPV system (40kWp, in Newcastle). Both systems used silicon wafer technology; in addition, BlPV facade was studied with CdTe modules. The lifetime of all PV systems was fixed at 25 years. The results indicated that the total energy requirement for the ground-based system and for the BIPV was 6486 kWhe/kWp and 4199 kWhe/kWp, respectively, while for the BIPV with CdTe was 1323 kWhe/kWp. The EBPTs were 4.3, 6.9 and 2.3 respectively. The CO_2 emissions were 88 t/GWh for the 1 MWp plant in Toledo/Spain and 143 t/GWh for the BIPV façade; with CdTe technology, the CO_2, emissions would fall to about 50 t/GWh. The impact of PV modules resulted to be always higher (about three times) if compared with those of BOS system, except for BIPV with CdTe that resulted to be of the same order.

Hammond et al. [76] focused on LCA of a domestic BIPV in UK. The functional unit was 2.1 kWp BIPV roof tile system. The system was installed on a new building and was connected to grid. The lifetime of the system was 25 years. The system boundaries covered the whole life cycle of the system, expect disposal and recycling phases. Results showed that heavy metal emissions were the largest normalized impact. In addition, the benefits of the electricity generated during the operational lifetime of the system, allowed a reduction of impacts in all impact

categories (greenhouse, acidification eutrophication, heavy metals, carcinogens, winter smog, and energy resources) except for the creation of summer smog. These results are shown in Table 13.

Table 13 *- Environmental impacts of the production and lifetime operation of the 2.1 kWp BIPV system [76]*

Category	Unit	BIPV system production	Avoided roof tiles	Net lifetime impact (25 years): base output
Greenhouse gases	kg CO_{2eq}	4.275	-213.5	-20.733
Acidification	kg SO_2	22.4	-0.045	-73.115
Eutrophication	kg PO_4	2.55	-0.078	-3.488
Heavy metals	kg Pb	0.168	-0.0015	-0.053
Winter smog	kg SPM	16.76	-0.028	-54-811
Summer smog	kg C_2H_4	2.18	-0.033	0.479
Energy resources	MJ LHV	84.616	-1.882	-389-979

Jayathissa et al. [77] assessed the environmental impact of a dynamic, adaptive, BIPV system. The assessment focused at sex midpoint indicators: terrestrial acidification potential (TAP), freshwater eutrophication potential(FEP), human toxicity potential(HTP), metal depletion potential(MDP), and photochemical oxidant formation potential (POFP). In addition, author calculated the GWP. The FU chosen was the electrical power production of the system in kWh. The main contributors to GWP were PV panels, followed by the electronics and the supporting structure. The control and electronics systems play a large role in freshwater eutrophication, and human toxicity due to the high life cycle emissions of electronic systems. Results are shown in Table 14.

Table 14 *- Total impact of the BIPV system [77]*

Category	Total impact
Global warming	2498 kg CO_{2eq}
Terrestrial acidification	14.8 kg SO_{2eq}

Freshwater eutrophication	2.95 kg P_{eq}
HTP	4530 kg 1.4 DCB_{2eq}
Metal depletion	3527 kg Fe_{eq}
Photochemical oxidant formation	8.68 kg NMVOC

Finally, in two different studies [78,79] were estimated the Energy payback time and the environmental payback time of two BIPV systems. The first work by Tripathy et al [78], regarded BIPV thermal system that consisted of a mono-crystalline silicon based semi-transparent PV modules that cover an area of 11.376 m^2, mounted on a rooftop and inclined at an optimum tilt angle The EPBT of the system ranged between 7.30 years and 16.9 years. In the second work, a roof-mounted PV system (22 kWp) in Hog Kong was analysed by Lu et al. [79]. The orientation of all the PV modules was facing south with an inclined angle of 22.5; the system was connected to grid. Results showed that EPBT was 7.3 years and the GPBT was 5.2 years.

Keoleian et al. [80] modeled, through an LCA approach, the life cycle energy and environmental performance of an amorphous silicon BIPV installed on a roof in the US. The study focused in particular on-air emissions; the inventory models were constructed using Ecobalance software. Authors also compared the BIPV system with a conventional one. The functional unit used was a square meters (m^2) of building material and kWh of electricity for a lifetime of 20 years. The EPBTs for different cities is reported in Table 15.

Table 15 *- EPBTs of the system for different cities [80]*

City	**EPBT, years**
Atlanta	4.24
Boston	4.97
Boulder	4.24
Chicago	5.02
Detroit	5.14

Fort Worth	3.97
Los Angeles	3.93
Miami	4.02
Minneapolis	4.99
New York	4.87
Oklahoma City	4.08
Philadelphia	4.87
Phoenix	3.39
Raleigh	4.42
Portland	5.52

The electricity production efficiency (electricity output/total primary energy input excluding insolation) for the system studied ranged from 3.6 in Portland to 5.9 in Phoenix. The energy performance of this BIPV system is dramatically better than conventional electricity generation, that ranged from 0.26 to 0.36. Table 16 shows the total mass of air pollutant emissions avoided by the system during 20 years period.

Table 16 *- Total mass of air emissions avoided by the reference system over a 20 years period*

Air emission	**Mass of air pollutants avoided (g)**					
	Boston	Boulder	Detroit	Phoenix	Portland	Raleigh
Carbon dioxane (CO_2 as C)	2.42E+07	3.27E+07	6.60E+07	4.19E+07	2..44E+07	5.23E+07
Carbon monoxide (CO)	6.55E+03	7.48E+03	1.35E+04	9.99E+03	5.18E+03	1.14E+04
Lead (Pb)	1.11E+00	9.26E+00	2.83E+01	1.37E+01	5.20E+00	1.93E+01
Mercury (Hg)	3.24E-01	6.11E-01	1.31E+00	7.76E-01	4.61E-01	9.86e-01
Methane (CH_4)	6.34E+04	9.97E+04	1.85E+05	1.27E+05	7.50E+04	1.47E+05

Nitrogen oxides (NO_x)	6.14E+04	1.03E+05	2.22+05	1.33E+05	7.63E+04	1.69E+05
Nitrous oxide (N_2O as N)	4.38E+02	6.95E+02	1.47E+03	8.94E+02	5.12E+02	1.13E+03
Particulates	4.53+04	1.07E+05	2.57E+05	1.42E+05	7.45E+04	1.87E+05
Sulfur oxides (SO_x)	8.08E+04	1.71E+05	3.88E+05	2.22E+05	1.25E+05	2.87E+05

Oliver et Jackson [81] analyzed energy and economic aspects in order to assess the application of PVs (1 m^2 of poly-crystalline silicon frameless modules) in buildings and compared the electricity supply to centralized PV plants and to conventional electricity sources. The comparison was made considering a supply of a kWh of electricity to the point of use. The data used for the energy analysis results based on an LCI database (ETH Zurich and the Paul Scherrer Institute) and then converted by the authors to primary energy equivalents using energy conversion coefficients. The system was assumed to produce an average of 850 kWh/kWp/year; this value was referred to an average of PV system outputs in Europe. In addition, the electricity produced by the BIPV system was consumed within the building on which the system was installed. Results showed that, despite the higher output performance of a central PV plant, BIPV system required less embodied energy per kWh of electricity generated (2.9 against 5.3 of PV plant). Regarding the energy saved, BIPV and PV plant had the same results (13.2 MJ). In conclusion, the EPBT of the BIPV system was 5.5 years while the EPBT of PV plant was 7.9 years.

The evolution of BIPV, in particular considering semi-transparent photovoltaic (STPV), has allowed to intervene in spaces previously occupied by traditional glass (skylights, windows, glass facades). For this reason, in addition to the production of electricity, aspects such as solar heat gain reduction and daylighting play an equally important role in assessing the effective efficiency of the devices in the interior spaces. For STPV devices, it is often essential to find a compromise between the production and the internal lighting, considering that a part of the radiation that is intercepted for the production of energy cannot arrive inside the environment. In fact, due to their structure, STPV creates areas of shade or penumbra, which depend on the degree of visible transmittance of these devices, on

the WWR, and which have consequences on the daytime illuminance factor and on the thermal balance of the environment. Although energy production can compensate for the use of artificial lights, as demonstrated in some of the following studies, the effect of the lack of natural light and the discomfort that derive from it are aspects that are often overlooked and that would certainly require greater attention.

An evaluation of one of these technologies was discussed by Sun et al. [82], which analyzed the energy and daylight performances of a CdTe PV glazing integrated into windows. The simulation was conducted through Energy Plus software; simulation regarded a private office occupied by two people from 8.00 to 17.00 on weekdays. The annual energy performance of the PV window was calculated for an office under five different climatic conditions in China; the results were then compared to a conventional double glazing (DG) system. The application of CdTe glazing, from 50% to 100% PV area of the whole window, was tested for different window-to-wall ratio (WWR):

- For 30% WWR there were no advantages in terms of saving on energy consumption reduction.

-From 45% to 75%, the energy saving potential became appreciable. In particular, covering 67%, 75% and 80% of the window area by PV glazing gave rise to the lowest overall energy consumption for 45%, 60% and 75% WWRs, respectively.

- From 75% WWR there was the most significant energy saving potential (73% under the tested climates) when coving 80% of the window area by PV glazing for 75% WWR.

Regarding the daylighting, using WWR 75% in the half office near the window, the percentage of hours where the useful daylight illuminance (UDI) was in the useful range (100-3000 lux) increased from 30-55% for the conventional DG to 40-90% for the window with CdTe PV glazing. The study wanted to underline the important of the right proportion between STPV and window, also providing a basis for possible future applications. Since STPV absorb a fraction of solar radiation (to produce electric energy) that hit window surface, a fraction of solar energy and

daylight cannot penetrate into the space; this is one of the main controversial aspect of the technology.

In their study, Martellona et al. [83] analyzed two promising technologies in the field of STPV: one involving the use amorphous silicon cells (NSTC = 3-6% and Tvis 7-40%) and the other the use of perovskite-based cells (NSTC = 6.6% and TVIS = 42.4%). The first type has a red-brown color, due to the absorption of most of the blue-green radiation, while the other has a neutral color, like gray glass. The authors investigated the use of these technologies in two types of buildings in order to evaluate the effect on their energy balance. The first reference building was a medium-sized office building that has three floors and five thermal zones, with a wall window ratio (WWR) of 30% and a total window area of 652 m^2. The second reference building was an apartment building with four floors and a wall window ratio of 15%. Energy yield results showed that, despite the lower STC value, a-Si cells performed better than perovskite cells under low-radiation conditions; also considering an average over a full year, a-Si cells outperform perovskite cells (from 30% on the South façade to 180% on the North façade). When the maximum energy yield is achieved, a-Si cells may provide up to 45 kWh/m^2year, while perovskite cells may provide up to 34.4 kWh/m^2year. These results were independent from the type of building, since they referred to the facade exposition. Considering the HVAC consumptions in the office, when the PV yield is taken into account, the results showed that BIPV solutions determined an energy saving of 33.3% (a-Si) and of 24.5% (perovskite cells), compared to the clear glass. The percent variation connected to HVAC consumptions in the apartment ranged from 12.8% (a-Si cells) and 9.5% (perovskite cells). Finally, authors showed that the visual comfort of perovskite cells offered a more balanced performance, since they limit both under-illumination and over-illumination, allowing to reduce the amount of electricity for office lighting.

Kapsis & Athienitis [84] evaluated the potential benefits of STPV in a cooling dominated commercial building located in Toronto. Authors used an integrated approach considering three different models for the evaluation of the performances of the STPV window: a daylighting, an electrical and a thermal model. In addition, they investigated the impact of various design parameters (WWR, façade

orientation, etc.) and different PV cell technologies. All results were expressed as a function of the visible effective transmittance of the STPV module (10%, 20%, 30%, 40%, 50%): the use of a STPV module with 10% visible effective transmittance (STPV_10%) resulted in the lowest annual electricity consumption (as low as 5 kW h/m^2/yr), when the STPV annual electricity production was considered. On contrary, when excluding STPV electricity production, authors found that the selection of STPV_20% resulted in the most energy-conserving design. Particularly relevant in the study is the attention for different simulation scenarios: the use of a roller shade device inside the room and its operation, the schedules with "active" and “passive” occupants, and finally the use of an absence sensor coupled with dimming control sensor, which both allowed maintaining the right levels of illumination, according to the external natural light. A limitation of the study is that no consideration has been made regarding the type of integration into the building, in particular on some aspect such as window frames or window structure.

A similar work was made by Lok et al [85]. First, authors evaluated the electricity generated by three BIPV windows located in exterior walls of a sample building (residential/office); the windows differed for the degree of transparency (BIPV 1 = 40%, BIPV 2 = 20%, BIPV 3 = 10%). According to their efficiency values, BIPV 3 showed the largest amount of generated power (efficiency of 9.91%) and BIPV 1 the lowest (efficiency of 6.65%). Regarding the electric lighting energy saving, authors made a comparison of two scenarios: with and without a daylight-dimming system. Results showed that there was a significant energy saving (from 2.7% to 14.2%), depending on different windows and the more transparent window glazing had better energy saving potential, compared to a base-case conventional double-panel window. In addition the BIPV windows significantly reduced the total annual building loads (from 6.0% to 15.4%) depending upon the BIPV type and daylight-dimming systems, compared to results of the traditional double glazing window. Finally, a parametric analysis was conducted considering an increase in the BIPV window area (WWR from 10% to 90%): this led to an increase of energy used for cooling and heating, but it also allowed to produce more electric power. Since this electric surplus was sufficient to compensate the greater cooling and heating energy

use, the annual total energy use was overall reduced. The percent savings from the various BIPV windows resulted to range from 7.8% to 38.9%. One of the limitation of the study was that the properties of the window (glass conductance, shading factor and visible transmittance) were only estimated; therefore, the validation of the window model was not conducted using measured data. In addition, further studies are necessary to measure unwanted sunlight glare, and to evaluate the energy benefits for building that require larger windows area.

Tae et al. [86] studied the performances of three different semi-transparent solar cell types (BIPV window), through a simulation of the annual energy consumption of a whole building in six different climate conditions (from tropical to cool summer). The three types of semi-transparent solar cells (a-Si:H) had different optical and electrical properties and were fabricated by the authors in order to evaluate the energy performance of buildings incorporated with BIPV windows . This was an importance aspect, since the thermal-optical properties of the BIPV windows come directly from measurement and tests conducted on the fabricated semi-transparent cell types. All results were compared to a base-case (a double-glazing with air-filled window):

- In lower latitude sites, the first two alternative (called PV1 and PV2) allowed saving both cooling and heating energy usage thanks to lower values of solar transmittance and U-factor compared to the baseline model.

In semiarid middle latitude or arid subtropical PV3 could save 34% and 66% of annual cooling and heating energy, respectively.

-In humid continental (warm summer) climate, all BIPVs increased heating energy requirement compared with the baseline model.

- In humid continental and cool summer all BIPV systems increased heating energy requirement.

Although BIPVs could save cooling energy consumption similar to other cases, the additional annual heating energy requirement is 45.4% (PV1), 53.5% (PV2), and 63.9% (PV3), respectively, compared to the baseline model configuration. In conclusion, this study provides information for not only to design a new BIPV

window system for the similar type of building, but also to plan energy retrofitting strategies involved in the fenestration of existing buildings to save energy cost and reduce environmental effects from the building.

Wang et al. [87] compared the energy saving potential of an optimized PV Insulating glass unit (IGU) to more common window systems: a single clear glass and a Low-E glass window. The simulation model of PV IGU was created through the optical characteristics of the semi-transparent a-Si PV laminate measured by a spectrometer while the electrical characteristics were tested under the standard testing conditions with a solar simulator. The outdoor experimental tests (based on data measured by sun tracker, a pyranometer and a weather station) were conducted in order to evaluate the accuracy of the model proposed, though the comparison between these experimental data and the simulation results. In particular, it were chosen two statistical indices, mean bias error (MBE) and mean square error (MSE), to assess the accuracy of the simulation model. Authors found that the energy saving potentials of the optimized IGU compared with these windows were 25.3% and 10.7%, respectively. However, the electricity generated by the PV IGU is partially balanced by the increasing in artificial lighting use, due to the relatively low visible transmittance.

Olivieri et al. [88] analyzed the overall energy performance of five STPV elements; each element had a specific degree of transparency (visible transmittance between 0% and 32%) and the results, in terms of energy saving potential, were compared to a conventional solar control glass compliant with the local technical standard. Once again, authors focused on daylighting, electrical and thermal aspects of the STPV systems. In order to perform the optical characterization of the different elements considered, an experimental campaign was conducted, using a spectrophotometer equipped with an integrating sphere. The results of the work were expressed considering different aspect:

- for small façade openings (WWR = 22%), the best STPV solution performed worse than the regular glass, considering the potential energy save;

- for intermediate and large façade openings (WWR 33%), the STPV solutions provided an energy saving potential ranging between 18% (WWR = 33%) and 59% (WWR = 88%).

Focusing on the degree of transparency effect:

- for relative small façade openings (WWR = 33%), the energy performance of all STPV elements was similar.

-For intermediate façade openings (33% < WWR < 66%) the second less transparent STPV element (visible transmittance of 16%) outperformed the other solutions, being about 25% more efficient than the least efficient STPV element (visible transmittance of 32%);

- for large façade openings (WWR 66%), the less transparent STPV element (visible transmittance of 10%) provided the most efficient energy balance.

Xu et al. [89] investigated the optimal PV cell coverage ratio (PVCCR) for semi-transparent photovoltaic facades in terms of the overall energy consumption of office building in China, through various combinations of architectural variables as room depth, WWR, and orientation. The experimental room had length, width, and height of 4.65 m, 3.4 m, and3.6 m, respectively, and the semi-transparent PV were installed to the roof. Regarding electricity PV generation, results showed that conversion efficiency decreased with increasing temperature; in particular, a temperature difference of 7° C corresponded to a 5.5% conversion efficiency as PV cell coverage ratio was increased from 10% to 80%. A greater WWR allowed more daylight to penetrate into the room and allowed greater window area upon for the installation of semi-transparent PV panels. However, the benefit of WWR on daylight illuminance was less accentuated if compared with the room depth increase. Finally, considering the optimal PV cell coverage ratio, the electricity savings ranged from 5% to 30%; the savings depending on the combination of room depth and WWR adopted: in rooms with large WWR, optimal PV cell coverage ratios resulted to be relatively larger if compared to rooms with small WWR. Building orientation affected the optimal ratio, with changes of 5–10%, based on specific orientation and optimal PV cell coverage ratio.

Karthick et al. [90] evaluated the electrical, thermal and daylight performance of STPV skylights on the rooftop window of an experimental room (surface area 18 m^2 and height 3 m) in India. The PVCCR values were 0.62, 0.72 and 0.85. The experimentations were conducted from January 2016 to December 2016 and the measurement taken from 9:00 a.m. until 5:00 p.m. for every 60 min interval. Regarding the electrical performance, results showed that the electrical efficiency is higher in 0.62 than in 0.85 PVCCR. 0.85 PVCCR should be higher energy due to the larger area of the STPV skylight covered by solar cells as compared to 0.62 PVCCR. The maximum annual electrical energy was 98 kWh 0.62 PVCCR), 105 kWh (0.72 PVCCR) and 130 kWh (0.85 PVCCR). The maximum reduction in cooling capacity (thermal performance) during summer was 208 kWh, 234 kWh, 248 kWh, respectively for 0.62, 0.72 and 0.85 PVCCR. The annual energy savings (lighting load) per square meter of STPV was 131.4 kWh, 102.2 kWh, and 87.6 kWh respectively 0.62, 0.72 and 0.85 PVCCR. The minimum EPBT was 4.08 years for 0.85 PVCCR.

Cheng et al. [91] analyzed the daylighting and energy performance of STPV facades in cold climatic regions of China, in order to study the conflict between daylighting and energy efficient that affect this type of technology. Results showed that, when the transmittance increased from 30% to 80%, the heating energy use of the office room reduced of 12.5 kWh/m^2 (from 27.6 kWh/m^2 to 15.1 kWh/m^2 per year), while the cooling energy use only increased of 5.6 kWh/m^2 (from 22.3 kWh/m^2 to 27.9 kWh/m^2 per year). Contrary, the power generation of STPV facades also decreased dramatically with increased transmittance. The annual energy yield of STPV facades decreased by 71.3% (from 23 kWh/m^2 to 6.6 kWh/ m^2 per year), when the transmittance increased from 30% to 80%. Regarding the orientation, the best daylighting quality and overall energy performance was achieved for STPV facades with south facing. In conclusion, the best performances were obtain when the transmittance and WWR recommended for the STPV façade ranged from 50% to 60% and from 40% to 50%, respectively, especially for buildings located in cold climatic regions.

Ng et al. [92] evaluated the lifetime performance of STPV integrated to different glazing systems (Table 17) located in tropic climate through an LCA study. The

boundary system included the manufacturing of BIPV components from raw materials, transport to the site (Singapore), installation, operation and maintenance, disposal/recycling of waste. The lifetime of the module was assumed 25 years while for the inverter was 15 years, with one replacement of the same type. The results showed that the EPBT ranged from 1.8 – 3.5 with an average value of 2.73. Among six different type of modules, the first one had lower GHG emissions (-951 kg CO_{2eq}) than the double-glazed window.

***Table 17** - Technical data and specification of the six semi-transparent BIPV modules*

	Module 1	**Module 2**	**Module 3**	**Module 4**	**Module 5**	**Module 6**
Module area [mm x mm]	980 x 950	1300 x 1100	1300 x 1100	1300 x 1100	989 x 930	980 x 950
Efficiency [%]	8.02	5.90	3.32	4.43	5.01	4.75
SHGC	0.289	0.413	0.298	0.387	0.154	0.123
U-value [W/m^2 K]	5.08	4.80	5.08	5.10	1.67	2.14
Visible light transmittance [%]	8.17	5.19	1.84	4.17	6-91	7.34
PV technology	a-Si	c-Si	c-Si	c-Si	a-Si	a-Si
Construction assembly	Single-glazed laminate	Single-glazed laminate	Single-glazed laminate	Single-glazed laminate	Double glazed unit	Double glazed unit
Appearance	Standard	Red	Golden	Dark blue	Standard	Standard

The remaining modules had GHG emissions of between 573 and 1647 kg CO_{2eq}. The cumulative energy demand for the six systems ranged from 29 to 106 GJ. Always the first module had also lowest energy and emissions intensities (240–310MJ/kWh and -5 g $CO_{2\ eq}$/kWh respectively) while the double-glazed modules GHG emissions ranged from 45–62 g CO_{2eq}/kWh and energy intensities ranged from 823 to 1265 MJ/kWh. The worst performing modules were the coloured-tinted ones, due to a lower visible transmittance, energy intensity and higher thermal conductivity.

Another work by Ng et al. [93] regarded the energy analysis of semi-transparent BIPV in Singapore. Authors analyzed six semi-transparent BIPV modules included two double glazed units equipped thin-film amorphous silicon solar cell technology but with different layers (single glazing, double glazing, double low-e glazing and double low-e tinted glazing), solar transmittance and visible transmittance. First, authors calculated the Net Electricity Benefit (NET) for the six BIPVs: NEBs strongly dependent on the WWR adopted. Double low-e glazed BIPVs showed a good performance due to their better thermal performance, even though they have slightly lower photovoltaic efficiencies. Together with single glazed, these modules generated positive NEBs for all WWRs on north/south orientations. Regarding the energy saving, if compared with conventional glasses, all BIPV modules showed an increase in savings rate between 16.7% and 41.3% (WWR ranged of 70–100%) while glasses as double-glazed, low-e tinted and low-e glazing, had energy savings of approximately 5.4%, 7.3% and 12.0%, respectively.

Khai et al. [94] investigated the energy savings and performance of a semi-transparent photovoltaic window in Singapore's tropical climate. The building (30m (L) x 30m (B) x 3m (H) and 4 thermal zones) with PV windows was modelled and simulated with EnergyPlus. The space was assumed to be occupied between 800 – 1800 hrs during the weekdays and the lighting level was fixed to 500 lux. In order to do a comparison of results, the simulation was repeated with single and double-glazed windows, instead of the PV windows, under the same conditions. The WWR ranged from 10 – 100% for the four-façade orientations. Results showed that for east and west orientation the maximum net total savings was at 30% WWR and decreased sharply with over 70% WWR. For north and south orientations, the net total savings increases consistently with the WWR. At 100% WWR, the net total savings were 7.38 and 8.85 kWh/(m^2.yr), respectively. In conclusion, semi-transparent BIPV showed overall better net total energy saving: in particular, for east and west orientation the net energy saving ranged from 8.2 to 10.0 kWh/(m^2.yr) respect to single glazing and from 1.1 to 2.3 kWh/(m^2.yr), respect to double glazing. For north/south orientation the net energy saving was around 70 and 58 kWh/(m^2.yr), if compared to single and double glazing, respectively.

2.4 Smart-Windows

Regarding the term "Smart Windows", it refers to a category of glass (smart glass) or other transparent materials whose light transmission properties change following the application of electrical voltage (electrochromism), light (photochromism) or heat (thermochromism). These technologies can be classified as active (thermochromic and photochromic) or passive (electrochromic). In comparison to traditional windows, smart windows have the ability to adjust their optical properties in response to the change of some boundary variables and hence have the potential to improve the energy performance of buildings and the comfort of the residents, thanks to their dynamic and adaptive functioning. Therefore, the aim of dynamic glazing systems is to control incoming solar radiation, in order to guarantee visual comfort for residents and to manage solar contributions in hot and cold seasons. To obtain the maximum potential from all these technologies, it is however necessary that these devices are managed through appropriate control strategies, in order to compensate the currently limits of these technologies (for example, the time between the switching from one state to another). These strategies should include at least one shading device, which could be the most suitable compared to the analyzed technology. In addition, for future application, a better compromise between energy balance and luminous comfort for the occupants must be achieved. The state of the art was developed about three categories, which will be briefly described at the beginning of each paragraph: photochromic window, thermochromic window and electrochromic window.

2.4.1 Photochromic Window

The literature research showed a lack of studies connected to the evaluation of photochromic (PC) windows performances. Photochromic materials (Fig.8) change their transparency in response to light intensity but remain unchanged with temperature changes, so windows made from these materials are not regulate by the temperature level outside. For this reason, the current research focuses on the development of hybrid PC materials and combinations of electrochromic (generally WO_3-based) and photoactive films. Photochromic materials found success in eyeglasses but are not probably ready for large-scale application in building, since

there are some problems such as photo-response time, stability, durability, visible light coloration, reversibility, etc. [95].

Figure 8 *– The visual effect of a photochromic window during different phases*

An example of possible application of photochromic property could be find in photochromic films, which can be used for smart window applications to partially block the sunlight and provide comfort vision [96]. The problem lies in the high cost and some difficulties related to production processes for large-scale applications: for this reason, Wu et al. [97], in their work, reported the development of a simpler photochromic coating (based on sol-gel matrix embedded with organic PC dyes) on glass substrate. The application of the PC films allowed to reduce G-value and U-value (from 0.87 and 5.2 to 0.26 and 1.58) resulting in high potential energy saving for end users especially in tropical climate.

Hočevar & Krašovec [98] developed photochromic window, based on a simplified version of a PEC capable of coloring under solar illumination, without the option to vary its transmittance. The important advantages were there that no electrodes were required and the realization consisted in a single smart glass pane. An improvement in the characteristics of the glass was reached (Tvis down from 76% to 35%) together with a good stability, for more than 12 months.

2.4.2 Thermochromic Window

Thermochromic windows (Fig. 9) base their functioning on a temperature structural phase change, which depends from the material used. This structural change allows changes in infrared optical and electrical properties of the material. The technology may be suitable for future applications since it allows reducing glare and solar heat gain, but currently it is still not totally ready for large-scale production, since some aspects related to high transition temperatures and low visible transmittances are not yet fully exceeded [99]. The challenge is to find materials whose structural change occurs at a temperature connected to that of the room (20-25 °), and that this change is rapid enough to adapt to the conditions required.

Figure 9 *- An example of thermochromic window*

According to this scope, Warwick et al. [100] examined the effect of thermochromic transition hysteresis width on energy demand, finding that a low transition temperature in a warm climate could reduce energy demand up to 54% in comparison with standard double glazing. The internal conditions of the building were chosen to represent the conditions of an office bloc (internal temperature between 19° C and 26°C; the lighting was fully dimmable between 0% and 100% and was automated and zoned; the occupancy was set to be from 8:00 to18:00, for five days a week. Finally, external conditions were controlled by use of weather files. The main limitation of the model proposed was its simplicity and its directional confinements, assuming only a South facing façade, but could be expanded by the introduction of further units with different orientations or window sizes. This work showed that thermochromic (passive) systems could achieve or

exceed the performance of standard systems, but also the difficulty of adapting the hysteresis temperature to the different conditions of use, especially in cold climates.

In their review, Aburas et al. [101] focused on thermochromic smart window technologies for building application. Authors analyzed many studies to determinate the energy efficiency of these components in building, underlining that a directly comparison of results was not possible since each study used specific room conditions, HVAC set point temperatures and glazing sizes.

Xu et al. [102] found that the highest energy saving overall for double glazing could be obtained when VO_2 films were deposited on the inside surface of the outer pane (84.7% energy saving in comparison with white glass), but heating energy consumption was found to be higher. The analysis regarded five cities that were representative for five climate zones: hot summer and warm winter, mild, hot summer and cold winter, cold and severe cold. The size of the chosen room was 6 m × 5 m × 3 m and the building occupancy was set as occupied from 08:00 until 18:00, five days a week. The south wall was exposed to the external environment while the remaining three walls were not affected by external conditions. The main limitations of the study were that no assessment of the illuminance level was conducted and no options of possible shading devices were considered.

Ye et al. [103] found that during the cooling period of a year, VO_2 glazing's application in a residential room could save 21.7 kWh annual electricity consumption (electrical energy saves near 9.4%) in comparison to ordinary glazing (when excluding the effect of associated lighting electricity consumption). In addition, authors found that cooling load could be reduced in the range of 10.2-19.9% respect to a standard clear glazing. Also, in this study, the focus is on energy consumption and therefore the internal lighting aspect has not been analyzed.

Yang et al. [104] simulated the heating and cooling energy consumptions of three different VO_2 films in five typical Chinese cities; then they compared the results with white glass and Low-E glass. The dimensions of the room were 4 m x 3.3 m x 2.8 m (length x width x height) and only a single window (1.5 m x1.5 m) was contained in the middle of the exterior wall. Results showed that cooling energy consumptions for the examined technologies could decrease by 81.7% and 70.5%

compared with white glass and Low-E glass, respectively. Also, in the heating period, the energy consumption of the thermochromic glass resulted to be better than Low-E glass. Anyway, all these positive results were influenced negatively by the transition temperature (that in some case was too high) and by the visual transmittance (that in some case was too low); in addiction, the effect of these parameters on internal lighting has not been calculated.

Kokogiannakis et al. [105] investigated the energy benefits for heating and cooling consumption in a highly glazed office building (66% of external surface area covered by window) using thermocromic glazing system. The results were compared to the performance of two heat mirrors units and a clear triple glazed window. Authors showed that TC glazing could reduce cooling load in hot climates (about 30%), however the same system had a negative performance in cold climates, where the highest energy saving was offered by the use of mirror glazing.

Costanzo et al. [106] analyzed the application of TC windows in an existing office building in Italy, showing that the energy saving could range from 5% to 25%. In addition, the study considered a series of theoretical thermochromic glazing and the expected performance was compared to static clear and reflective insulating glass units. The simulations were repeated in different climatic conditions and a detailed description of the simulation room and building was made. Few studies were shown to have explored thermochromic windows from a visual and thermal comfort performance perspective. Lastly, authors collected values (g-values,U-factor, Tsol and Tvis) of the different technologies from the analyzed studies.

- For thermochromic windows: The g-value range between 0.62 and 0.2 for the clearest state and between 0.449 and 0.1 for the darkest state; Tsol varies between 0.499 and 0.09 for the clearest state and between 0.357 and 0.02 for the darkest state; Tvis varies between 0.6 and 0.26 for the clearest state and between 0.13 and 0.043 for the darkest state. The U-values vary between 2.76 and 1.31 (W/ (m^2K)) depending on the product and the number of window panes.

- For photochromic windows: g-values ranged between 0.48 and 0.31 for the clearest state and 0.41–0.22 for the darkest state, Tvis ranged between 0.78 and 0.13 for the clearest state and 0.73–0.09 for the darkest state, while information about

Tsol is very limited. Few U-values were found, and the ones listed are significantly high and vary between 5.7 and 5.9 W/(m^2 K).

For electrochromic window: g-values vary between 0.63 and 0.27 for the clearest state and between 0.31 and 0.04 for the darkest state, Tsol varies between 0.52 and 0.19 for the clearest state and between 0.06 and 0.01 for the darkest state, Tvis varies between 0.75 and 0.35 for the clearest state and between 0.17 and 0.01 for the darkest state. The maximum U-value is 5.5 (W/(m^2 K)) and the minimum is 0.5 (W/(m^2K)), most values lie, however, in the span of 1–1.6 (W/(m^2 K)) depending on the amount of window panes.

2.4.3 Electrochromic window

Electrochromic glasses (Fig. 10) can regulate light penetration and transmission by responding to an electrical voltage. The main advantage is that generally they require a low voltage power source (DC 0–10 V) and that, compared to other types of smart glasses, they can be actively controlled with fast response speed and in real time, also preventing local glare phenomena within the rooms and solar modulation. Unfortunately, the systems are still quite expensive and the modulation levels are still rather limited [107].

Figure 10 *– An example of electrochromic glasses in two different states*

In their work, Lee et al. [108], evaluated different electrochromic glazing control parameters (outdoor air temperature, room air temperature, solar radiation incident on the window (SRW), and global horizontal solar irradiance (GHI) to improve the

energy performance and sustainability of medium-sized commercial building in different climates (six climates zones in US). The tested building had a total area of 41% of the total and the window-to-wall ratio (WWR) is 0.33. When the electrochromic window was installed on the south face of the buildings, the annual heating and cooling energy consumption of the unit floor area could be reduced at the most locations compared to a static glazing window; anyway, saving potentials depended on the climate and control parameters. Regarding this aspect, outdoor air temperature was the simplest and the most effective in reducing both heating and cooling energy in all locations, but other parameter, such SRW and GHI, were the most critical control parameters, causing a clear distinction of electrochromic window performance between the various locations. The authors have not clearly defined the structure of window and window frame, as well as the possibility of using internal of external shading systems.

Tällberg et al., in a recent review [109], made a comparison of the energy saving potential of these window technologies. The authors found that there only few studies were related to thermochromic and photochromic windows, while mostly focused on electrochromic window.

With reference to the latter, most studies referred to office buildings located in different European cities. Mäkitalo et al. [110] simulated the performance of electrochromic window applying different control strategies (always on, always off, different operative temperature, light and schedule, etc.), showing that this technology allowed an improvement in energy performance compared to a traditional window with blinds, in particular electrochromic windows should have greater potential for energy savings in a sunnier climate. Anyway, the energy saving regards the consumption related to zone cooling, while the regular window with blind was a better option considering the energy consumption for zone heating. Each strategy has its advantages on the one hand and disadvantages on the other, and the challenge is to find a compromise between the various situations, based on the type of building, the needs and habits and the environmental conditions of the geographical location.

In a similar way, Reynisonn et al. [111] compared three different models of windows: a traditional window without a shading, a traditional window with an external blind and a dynamic electrochromic window. They calculated that the energy saving for different locations (Kiruna, Reykjavik, Stockholm, Copenhagen, Paris and Madrid). was between 10-30% compared to traditional window with operable blinds and 50–75% compared to a window without blinds; authors also shown that the energy benefit is greatest for warm climates.

Ajaji & André [112] found that, for an office building in Bruxelles, the primary energy consumption could be reduced by 61%, mainly thanks to a lower cooling demand. Authors used two scale models of an office in the south of Belgium to assess visual comfort: one was equipped with an electrochromic window while the second one with a reference window. Moreover, they assessed through experimental tests the risk of overheating, the internal gains and the outdoor climate in the buffer zone in a climatic chamber. The greater assumptions were that the south face of the office was 90% glazed and that an external shading closed the opening at 50% when the solar irradiation on the window exceeded 180W/m^2 and opened when the solar irradiation dropped below 140 W/m^2.

Gugliermetti & Bisegna [113] analyzed thermal and visual performances of EC devices, with their transparency state regulated with on/off (OCS) and linear control strategies (LCS). EC devices operated with the dimming of the electric light output, in order to maintain the right level of illuminance in spaces. The analysis was performed for office spaces for three cities (Rome, RM, latitude 42◦, Bolzano, BZ, latitude 46◦, Catania, CT, latitude 37◦) that represent the typical different outdoor condition in Mediterranean climate. The comparison performances were conducted between the two different control strategies: results showed that primary energy total requirements were similar for both control strategies, while comfort aspects were in favor of LCS; in addiction reducing the minimum illuminance level makes LCS more favorable also for the energetic aspects. Once again, optimal set points depended mainly on EC device solar transparencies and on orientations of offices, while latitude had only a small influence in this study.

In his work, Aldawoud [114] compared different conventional fixed shading devices coupled with a double glazing window and an EC window. The study was conducted in a typical office building, covered by glazing for 50% of his envelope, in hot dry climate. Even if exterior shading devices (overhangs and side vertical fins) lower the direct solar heat gains (from 36% to 47% in winter and 34% to 44% in summer for overhangs, by 34-43% in winter and 32-41% for vertical fins) compared to unshaded windows, their performance depended on the design and size of these devices. Authors demonstrated that EC window performed better in reduction of solar heat gains (from 53 to 59%) in all season, offering an high potential for the reduction in annual peak cooling load in all windows orientations. For this reason, despite the maintenance cost and higher initial cost compared to other shading devices, EC windows allowed to recover the initial expenditure through the reduction of solar loads.

Fernandes et al. [115] calculated the interior illuminance and luminance level for a south-facing private office where was installed a window split into two independently-controlled EC panes. The transmittance of these was optimized and adapted hourly based on the illuminance target in a work plane. Authors wanted to determinate if EC window could allow reducing energy consumption maintaining occupant visual comfort. The space chosen for the study and modelled with Radiance was a one-person office (4.57x3.05x2.74m) situated in California. Results showed that, with the control target set to 600 lux, annual energy use was higher for EC than for the reference window equipped with venetian blind. Authors underlined that these results could be linked more with the shading system used than with the glass type; in fact, venetian blinds allow to redirect light, where EC absorb it, and this has a benefit in terms of internal illumination, as well as in energy savings for artificial lights. Finally, the results indicated that windows with ordinary glass, coupled with continuously controlled Venetian blinds, could result in equal or lower energy consumption than split electrochromic windows.

Frattolillo et al. [116] compared the performance of two different glazing system: a traditional high thermal performance glass and an electrochromic glass controlled by remote. The experimental characterization were conducted in two identical test rooms (with respect to the surface and size) and they assessed the energy saving

achievable in a Mediterranean climate, through the simulation of the models developed. The experimental characterization of the test rooms was made through the measurement or the calculation of some data such as the external air temperature, the total solar radiation on vertical surfaces (SE and SW) and the operative indoor temperatures. Results showed that the use of electrochromic glass in summer allowed a reduction of cooling energy requirement greater than 80%, if compared to traditional low emission glass. On the other hand, electrochromic glass caused an average increase of the heating energy demand, greater than 35%, in winter.

2.4.4 Venetian blind shading system

Window shading systems (Fig.11) help to reduce energy consumption, since they allow the control of solar inputs, and provide the right visual comfort of the occupants thanks to the control of daylight, preventing the phenomenon of excessive direct light or glare, especially when they are correctly managed at depending on the variations in the external and internal environment conditions. In the case of venetian blinds, their success as a shading system is due to the fact that they allow different levels of light regulation, thanks to different opening levels and the adjustment of the slat angle. In addition, these devices can be completely withdrawn in a small space if not active. Venetian blinds can be manual or motorized (as in the case of SW-LSC), even in some cases automatic and managed by a control logic. With regard to the latter type, the advantage that can derive from the automatic regulation, according to the outdoor weather condition, can be greater compared to the manual or motorized venetian blinds.

Figure 11 *– Venetian blind system*

According to this scope, Kim et al. [117] evaluated thermal and visual performance of automated venetian blinds compared with those of manual and motorized. The automated system was managed by a sun sensor, measuring vertical outdoor illuminance, and by two different control logics (Energy Saving Mode and Comfort Mode). The experimental tests were carried out in two rooms, with identical dimensions (5.8 m (W) x 4.8 m (D) x 2.7 m (H)) and internal/external conditions. The thermal performance was evaluated by analysing the average temperature difference and the rate in which the temperature decreased over time while the visual performance was evaluated by the average room illuminance. Results showed that, in terms of cooling energy consumption, automated blinds performances were equal or better compared to manual blind; in terms of visual comfort, automated blinds allowed to reduce the discomfort from excessive solar radiation and direct sunlight and an automatic control of daylight. A limitation of the study is that it was not developed a control method that simultaneously considered the energy saving of lighting and cooling through the right control of both the occlusion index and the slat angle.

In their work, Carletti et al. [118] analyzed thermal and lighting performance of an external motorized venetian blind system with different operation configurations, based on different slat angle (closed in horizontal, 45°, closed in vertical, completely packed). In addition, they compared the performance of this motorized

shading system with those of an automatic one, controlled by two parameters, air temperature and illuminance. The test room, located in a residential building in Italy, was monitored in two different periods (spring and summer) and the window was integrated in a wood frame and equipped with an high performance double glazing system air filled camera (SHGC 42% and U 1.3 W/m^2K). The study confirmed that automated venetian blinds could be an optimal solution not only in office buildings with large glazed surfaces, but also in residential buildings, where the glazing area is limited. Results showed that automatic controlled systems could improve indoor thermal conditions and saving energy for cooling, allowing a good control of the mean radiant temperature and guaranteeing an adequate indoor illuminance. On other hand, motorized blinds had limitations in their effectiveness, since occupants tend to move the blinds only when direct solar radiation makes conditions uncomfortable and consequently blinds were often completely closed or open.

A limitation that the previous studies had in common was that the aspect related to the electrical consumption of the automated or motorized system has not been analyzed, as well as the management of the internal lights according to the configuration of the shading devices.

Lee et al. [119] compared the energy savings and peak demand reductions related to the use of an automated Venetian blind compared to a static venetian blind, both equipped with the same dimmable electric lighting system. The analysis was conducted in two side-by side rooms with identical building materials, furniture and dimensions (3.71 m wide, 4.57 m deep and 2.68 m high). The windows in each room were simultaneously exposed to approximately the same interior and exterior environment (south-est exposition). Results showed that dynamic system allowed daily cooling load reductions of 7-15% and 17-32% and an average daily lighting energy reduction of 19-52% and - 14 to f 11%, respectively for 45° and 0° blind angle, compared to static venetian blind with the same dimmable lighting control system. With no daylighting controls, the daily lighting energy savings was 22-86% for overcast to clear sky conditions, while an average daily cooling load reduction of 25% (0° blind angle) were obtained on clear days in July. In addition, the use of dynamic system allowed a peak cooling load reductions of 18-32% with daylighting

controls and of 28% reductions without daylight controls, compared to static blind on clear days in July. Since the article is rather dated, the system used was not equipped to control the interior lighting levels or for operate in synchronization with the daylight control system.

3 - Case study

In this chapter, the case study of the Smart Window-LSC (SW-LSC) will be shown, together with the traditional window used as element of comparison and the location description (including the weather data and the test room). SW-LSC is a prototype window designed in collaboration with Politecnico di Milano, that is based on the Eni Ray Plus® technology developed by Eni, within the partnership with PMMA manufacturer Arkema/Altuglas. The term ”smart window” refers to a technology that allows to actively or passively participate in the energy performance and energy saving of the building, thanks to dynamic solar control and to the intrinsic characteristics of the device (transmittance of glass and frame). In the case of SW-LSC, which also includes the use of Luminescent Solar Concentrators, the contribution is also in terms of energy production and daylight improvement. The functioning of the SW-LSC, which will be explained in detail below, is based on a passive and motorized shading system exploiting the electrical energy of LSC modules integrated into the frame. In particular, the SW-LSC is designed to offer advanced energy performance, while guaranteeing its own energy self-sufficiency for the purpose of the operation of automatic solar control systems (automated venetian blind).

3.1 Smart window-LSC

The SW-LSC prototype consists in a two-part window: an extra window in the upper part (upper window, UW) and double-wings window that opens inwards in the lower part (lower window, LW). The upper window is coloured semi-transparent, since it integrates four LSC modules installed inside a double glazing; the lower window can be considered as a normal double-wings window with a double-glazing filled with air. In detail, the SW-LSC frame is made with thermal break aluminum profiles (Uf = 1.9 W/m^2 K). For the upper window the frame had dimensions of 0.724 x 2.342 m while for the lower part was 1.407x2.342 m. The coloured-semitransparent (yellow) modules are four LSC slabs, 50 x 50 cm each. LSC module efficiency range from 1.1 to 1.4 %. Every LSC modules is equipped

with 88 sc-Si solar cells (22x7mm) and the total PV area is 0.048 m^2. The electrical features of PV cells are showed in Tab. 18.

Table 18 *– Electrical characteristics of PV cells*

Maximum power P_{mpp}	mW	22.3
Maximum power voltage V_{mpp}	V	0.5
Maximum power current I_{mpp}	mA	44.6
Short circuit current I_{sc}	mA	50
Short circuit voltage V_{oc}	V	0.63
Temperature coefficient αV_{oc}	%/°C	-0.33
Cell efficiency	%	22

The dimensions of the whole SW-LSC are 2.252 m x 2.332 m (L X W) and the layout of the device is shown in Fig. 12

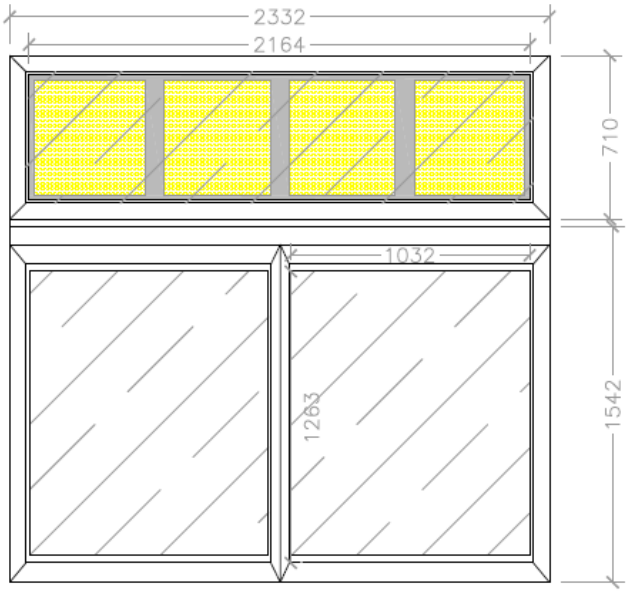

Figure 12 *– Sketch of the SW-LSC system*

In details, the layering of the upper double-glazing (transom window) with U-value of 1.2 W/m^2 K, is shown in Fig. 13 and described below.

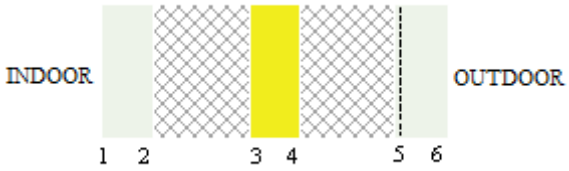

Figure 13 *- Stratigraphy of the upper double-glazing (transom window) with LSC technology integrated*

1 – 2 An extra-clear laminated glass of 6.76 mm on the outside;

2 - 3 A gap of dehydrated air, 12 mm;

3 - 4 The central element is a (yellow) PMMA slab that incorporates the Eni Ray Plus® technology, 6 mm thick;

4 – 5 A gap of dehydrated air, 12 mm;

5 - 6 An extra clear low emissive laminated glass, 6.76 mm thick, with the low emissive layer applied in face 5, as internal glass.

The total thickness of the double-glazing is 49.52 mm.

Each window sash of the lower part of the window is made of double extra clear glass filled with air with a 4 + 4.2 / 22/ 4 + 4.2 stratification. (Ug = 1.1 W/m^2 K). The internal glass is covered with a low emissive layer applied in face 3, as shown in Fig. 14.

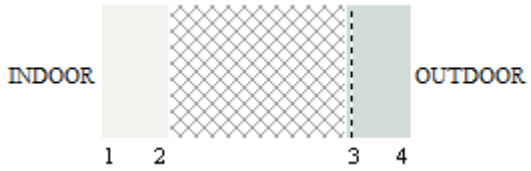

Figure 14 *– Stratigraphy of the lower double-glazing*

The upper and lower part of the window are divided by a horizontal highly reflective aluminum shelf (coefficient of reflection 0.92). The light-shelf (1 m x 2.342) extends from the inside to the outside of the window (0.4 m inside and 0.6 m outside) for the entire length of the window (2.342 m). The function of the light shelf is to avoid direct sunlight into the environment and minimize glare: it intercepts part of the incident solar radiation and spreads it in the internal

environment with greater depth and uniformity, while ensuring shading near the window and reducing glare. In addition, the light-shelf helps to mix the coloured light that passes through the LSC panels with the clear light that passes through the neutral glass below, in order to obtain a natural light characterized by a lower colour temperature [120]. Unlike the external shelf, the internal shelf is made with a perforated sheet (with Ø1.5 holes, 3 mm pitch), and this is considered within the analysis. Solar control is achieved through metal venetian blinds, placed inside the double-glazing of the lower window, adjustable according to the conditions of the sky and the irradiation level. The movement of the blinds is driven by electric motors (DC motors, 3 W each), one for each wing, integrated into the window frame and powered by LSC panels. In order to guarantee electrical conservation and continuity of operation even in low solar radiation days, the SW is equipped with two 12 V batteries (6 Ah capacity each), incorporated in the frame, charged by the electricity generated by the LSC modules. The batteries energy is sufficient to move the shading system even on cloudy days and for relative long periods (5 days) [121]. The shatters movement is guided by an external sensor (a light/radiation meter) connected to a computer with an adaptive control logic, which allows for the best setting in terms of interior comfort and energy saving. The solar irradiation sensor is placed at about 1/4 of the height of the upright of the window frame starting from the sill [126] and it is showed in Fig.15.

Figure 15 *- (a) The solar irradiation sensor placed on the external side of the window. – (b) Position of the solar radiation sensor*

The control logic, connected to the external solar radiation sensor, adjusts the opening level of the slats. The irradiation sensor is a monocrystalline silicon photovoltaic cell, type IXYS KXOB22, with voltage and current values in STC equal to 0.5 V and 44.6 mA, respectively [127]. The system detects the level of solar irradiance on the external surface of the window and, when the measured value exceeds a certain threshold, the solar shading system is activated by lowering the blinds in order to completely shield the direct incident solar radiation (Fig. 16a). When the irradiance value is reduced below the set threshold the blinds are completely opened (Fig 16b). The system provides the possibility for the user to redefine the irradiance threshold that controls the closing/opening of the slats [128]. The irradiance value set during the analysis was 180 W/m^2 and all the data used in the analysis (in particular, the motors energy consumption) refer to this value. This value was chosen by trial and error during the monitoring phase since it ensured, for the reference location, that the mechanism would operate on a regular frequency. In fact, during the monitoring period, it was noted that lower values caused a high consumption on cloudy days, as the device operated with a higher frequency.

Figure 16 *- (a) Shading system in the configuration of the window completely closed – (b) Shading system in the configuration of the window completely opened*

In addition to the aluminum frame, the upper window is equipped with an aluminum mask that protects the modules, and cables and connections among the various photovoltaic cells. The aluminum mask has dimension of 0.592 x 2.193 m. An additional aluminum box (0.110 x 0.080 x 2.342 m), placed between the upper and lower window, is used to protect and hide electrical components and equipment. This box is made with a "C" profile to which a second lid "C" profile is inserted.

In order to compare the performances of SW-LSC, a traditional window located on the corresponding room on the first floor was used. The traditional window is a single glass panel (5 mm glass, Ug = 5.6 W/m^2 K) with an aluminum frame and roller shutters as shading device. The window has the same dimension of the SW-LSC but due to the different configuration, it resulted to have a higher glassed area. The traditional window is shown in Fig. 17.

Figure 17 *- The traditional window located on first floor*

The window models have the characteristics shown in Table 19.

Table 19 *- Thermo-optical characteristics of the SW-LSC and of the traditional window*

Name	SHGC	Solar Transmittance at Normal Incidence	Visible Transmittance at Normal Incidence
SW-LSC (upper window)	0.49	0.409	0.678
SW-LSC (lower window)	0.507	0.383	0.631
Traditional window	0.819	0.775	0.881

The above characteristics of SW-LSC where provided by an external body, which tested the optical and thermal characteristics of LSC slabs and glazing. Subsequently, these information were implemented through Window7 software, which allowed the creation of SW-LSC and traditional window stratigraphy and finally, the extrapolation of the data shown in Tab.19.

In conclusion, the functioning of the SW-LSC is to use the energy produced by the integrated LSC modules in order to power the motors that regulate the shading

system. Furthermore, thanks to the use of the sensor placed outside, the mechanism performs its function passively and autonomously, without the intervention of the inhabitants. Finally, since the modules produce energy even with diffused radiation and thanks to the use of storage batteries, the system guarantees operation even for several cloudy days.

In the case of the SW-LSC, the transparent matrix is made by polymethylmethacrylate (PMMA) while the photovoltaic cells used to convert the concentrated light beam into electrical energy are the common silicon cells of the monocrystalline (mc-Si) type. These photovoltaic cells are glued on the edges of the slab and they are protected by a perimeter frame; they can be connected both in series and in parallel, according to the specific needs of use [122].

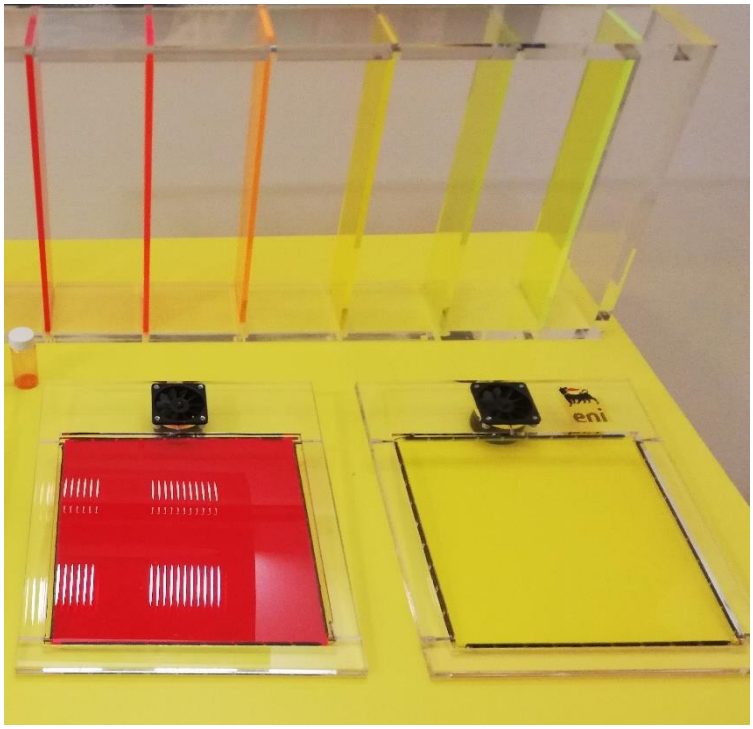

Figure 18 *- Different LSC modules and dyes*

The fluorophore inside the matrix determines the final colour of the slabs and the final performance of the modules (Fig.18). The “color” of LSC modules is static and is mainly due to the electrical operation of the same; it also has a beneficial effect on the internal light of the environment [123]. Thought different synthesis processes it is possible to obtain a variety of fluorophores and colours (those synthesized by Eni are red, yellow and orange). The colour variation obviously also

affects the final product, the LSC slab, and consequently the spectrum of the radiation filtered into the environment by the SW. In the case study, the use of the "yellow dye" was analyzed, since gave the best response from the point of view of efficiency and optical performance when used for the production of the modules [124]; it is also the one used at the time of the analysis.

The luminescent dye used into SW-LSC modules is a derivative product of 4,7-di (2-thien-2'-yl) -2,1,3 benzothiadiazole (DTB). The specific concentration of the dye within the support material is in the order of 100-200 ppm; with these values it is possible to absorb 25% of the radiation coming from the front surface, while the remainder passes through the device. This "yellow" dye has a large Stokes shift and this allow to greatly reduce the re-absorption of emitted photons by other luminophores (η_{self}).

To conclude, the main elements of the SW-LSC prototype are:

- The LSC modules, consisting mainly of three elements: the transparent matrix of polymeric material (polymethylmethacrylate, PMMA), the luminescent dye, called fluorophore, i.e. the element that allows to absorb and re-emit part of the solar radiation; the solar cells, suitably arranged at the edges of the slab.

- The aluminum structure: the LSC panels are integrated in the upper part of the SW. The lower part consists of a double-glazing window (with air-filled cavity). Both the upper window and the lower part are enclosed by a thermal break aluminum structure, which constitutes the frame of the SW-LSC.

- The accessory elements: the venetian blinds, the two electric motors, the venetian blinds management and control system, the radiation sensor, the accumulation batteries and the horizontal aluminum light shelf.

3.2 Location and climate data

The SW-LSC was assembled and tested at the Eni Research Centre in Novara (Italy). Novara is located 169 m above the sea level and it is characterized by a warm and temperate climate. There is significant rainfall throughout the year, even

in the driest month. According to Köppen and Geiger [132], this climate is classified as Cfa (Humid subtropical climate).

A weather station placed on the roof of the building, monitored the following data with a timestep of one second:

- External Temperature;

- Global solar radiation;

- Diffuse solar radiation;

- Direct solar radiation;

- Wind speed:

- Wind direction;

- Atmospheric pressure.

The weather station is represented by (Fig. 19):

- one pyroheliometer model CHP1;

- one solar tracker;

- two model CMP11 pyranometers equipped with ventilation unit model CVF3.

Figure 19 *- Components of the weather station: (a) pyroheliometer, (b) solar tracker, (c) pyranometer*

The weather data was used for the simulations of this study. Below are reported some information regarding the local climate of Novara:

- minimum annual temperature is -7.9 °C;

- maximum annual temperature is 35.6 °C;

- mean annual humidity is 69%;

- mean annual horizontal solar radiation is 281.6 W/m^2.

The monthly mean Global Horizontal Radiation ranged from 118 W/m^2 (December) and 429 W/m^2 (July). Fig. 20 shows the mean daily values for global horizontal, direct normal and diffuse solar radiation [133].

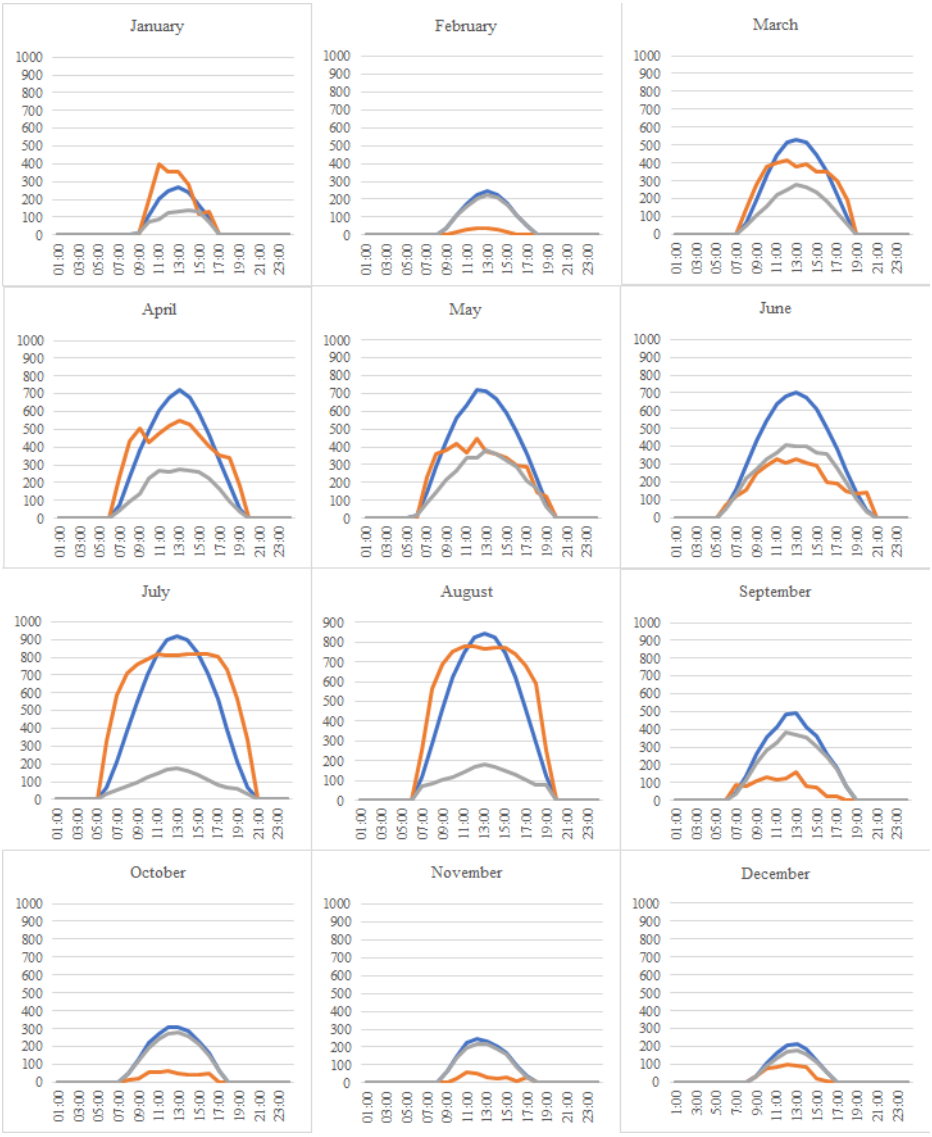

Figure 20 *- Mean daily values for global horizontal, direct normal and diffuse solar radiation [W/m^2] [133]*

The outdoor dry-bulb temperature reached 34 °C during summer, the minimum value was -8 °C during winter, while the annual mean temperature was about 12 °C.

February resulted to be the coolest month with a mean temperature of 1.7 °C: the minimum temperature was -7.8 °C while the maximum was 16.1 °C, respectively. July was the hottest month with a mean temperature of 23.5 °C: the minimum temperature was 13°C while the maximum was 34.6°C

As shown in Tab. 20, the relative humidity varies from 61.6 % in July to 78.7 % in November, while the annual mean value was about 69 %. The year average wind speed wind was about 1.34 m/s: it ranged from 0.87 m/s (January) to 1.66 m/s (May).

Table 20 – Monthly mean relative Humidity and wind speed for Novara.

Month	Relative Humidity [%]	Wind Speed [m/s]
January	74.57	0.87
February	68.01	1.26
March	62.22	1.46
April	67.00	1.65
May	65.88	1.66
June	63.84	1.65
July	61.58	1.65
August	66.49	1.44
September	69.19	1.34
October	75.51	1.04
November	78.73	1.14
December	74.91	0.95
Year	68.99	1.34

Finally, the SW-LSC prototype is installed in a test room where the input and output data from the device are monitored and the control logic of the same is managed via computer. For our case study, the room is treated like an office. The room have dimensions of 3 m x 4 m x 3.5 m (L x W x H) and is located on the second floor of a building in Novara (latitude 45.45°, longitude 8.64°, altitude 156 m). The traditional window is installed in the room corresponding to the first floor. Since this second room is opened on one side (for the presence of a stairwell), it has been

closed and made of the same size as the test room through a thick curtain that simulates a clear white wall (Fig. 21). This step is necessary in order to validate correctly the model based on the lighting measurements made into the rooms.

Figure 21 *– The curtain used to reproduce the white wall*

Both windows face south south-east, with an azimuth of 27° and there are no obstacles due to others building or others obstruction where the windows are exposed. The stratigraphy of the walls involves the use (from outside to inside) of natural stone (travertine), mortar, brick and a layer of plaster. The walls and ceiling are characterized by a clear white color (reflection coefficient 0.75) while the floor by a smoke gray color (reflection coefficient 0.35), due to the rubberized carpet pad.

4 - Model and method

In this chapter, the research method used in order to reach the main goals of this work are defined. In addition, all models created and the experimental setup are described. In detail, the daylight, thermal and optimal performances of SW-LSC are investigated; then, the analysis of the life cycle of the SW-LSC is described, in order to evaluate the environmental impacts of window case study. The thermo-physical models of SW-LSC and traditional window were implemented with EnergyPlus [134] and Window7 [135] software. Then, the models were calibrated through the data collected during the on-site experimental test. The LCA methodology was used to evaluate the impacts of the SW-LSC prototype.

Section 4.1 regarded the daylighting performances of SW-LSC and traditional window; the analysis was conducted starting from experimental tests in order to evaluate the illuminance level inside the test rooms. The data collected during the experimental test were used to calibrate the models created. Section 4.2 focused on electrical performances; in particular, through the analysis of monitored data, a regression model was used to estimate the electric generation of the SW-LSC. Section 4.3 concludes the performances analysis; in this section, the performances of multiple SW-LSCs where simulated in a large building, in order to evaluate the energy saving that could be obtained in comparison with the traditional window. Section 4.4 based on the LCA methodology (goal and scope, system boundaries, functional unit); the data collection, the processes connected with the main elements of SW-LSC and the Life cycle Inventory were described in this section.

4.1 Daylighting performances

4.1.1 Experimental tests

In order to validate the SW-LSC model in terms of lighting, a campaign of data collection was carried through the measurement of illuminance level (lux) in different points of the room where the SW-LSC prototype is installed (Fig. 22_a). At the same time, the measurements were also carried out in the room located on

the first floor of the same building, in correspondence with the test room, which have the same dimensions but is equipped with a traditional window (Fig. 22_b).

Figure 22 *– (a) Inside view of second floor room (SW-LSC) – (b) Inside view of first floor room (traditional window)*

The monitoring studies were conducted using a lux meter that is the instrument generally used for measuring illuminance and light intensity in environments and workplaces. The measurements were conducted in 5 points in both rooms at a height of 0.8 meters, the height recommended by the regulations UNI EN 12464-1 [136] for the workplace; the map of the test room and the position of the five points are shown in the Fig. 23.

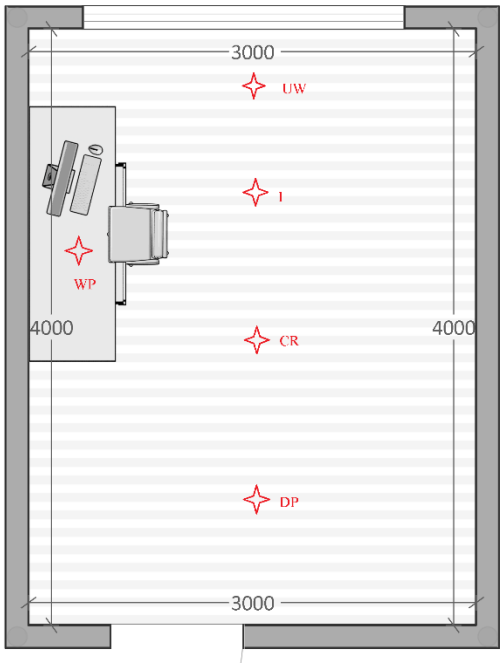

Figure 23 *- Location of measuring points inside the room*

The points were named as follow:

- Under window (UW) with coordinates: x=1,5 ; y = 0,5;

- Work plan (WP) with coordinates: x=0,8 ; y = 1,5;

- Intermediate (I) with coordinates: x=1,5 ; y = 1;

- Center of the room (CR) with coordinates: x=1,5 ; y = 2;

- Door proximity (DP) with coordinates: x=1,5 ; y = 3.

The measurements were carried out on February 18 2020 from 11 a.m. to 4 p.m. with half an hour interval for both rooms and with the shading devices deactivated; in the case of SW-LSC the venetian blinds were positioned in the "fully open" mode and the same was done with the shutters of the traditional window. The day was chosen as completely sunny, to prevent the passage of clouds from affecting the measurements. The artificial lights were switched off during the whole duration of the measurements. The only internal load inside the rooms was the computer (250 W) that monitored the performance of the SW-LSC and regulated the shading system.

The monitoring data relating to the electrical performance of SW-LSC referred to two years of monitoring. The data concern the generation of electricity, the accumulation of energy in the batteries and the consumption of the motors, recorded with a timestep of one second. The data re-processing made it possible to take into account the daylight savings time period (aligning the times with the monitoring ones), the accidentally consumption due to a movement of the blinds activated manually (and not through the threshold set by the control system) for system maintenance and lockouts and, finally, to aggregate the same as daily production and consumption. The re-elaboration was carried out by exploiting the recorded climatic data concerning the external temperature and radiation on the vertical surface of the window.

4.1.2 Modeling

The modeling of the two windows (frames and structure) was performed in Energy plus environment. The stratigraphy of the glasses, both of the traditional windows

and of the SW-LSC, has been built using Window_7 software that allows creating and managing more complex stratigraphy and layers such as that of the upper window. This model was subsequently uploaded to EnergyPlus and Open studio environment.

The assumptions on the modeling were that heat exchanges occur only through the south facade, while the other surfaces are adiabatic. The materials used for the walls are those listed in the previous section (Section 3.2) as well as their reflective coefficients. The office room was set to be occupied by one person from 7:00 a.m. until 6:00 p.m. during working days, with a break for lunch from 00:00 p.m. to 1:00 p.m. The other parameters have been set to match what was prepared during the experimental setup.

Two models were created one per each room. The windows have the same dimensions but due to the different layout, the glazed surface of the traditional window is slightly greater. The model has a single room and a single thermal zone, and is shown in Fig. 24.

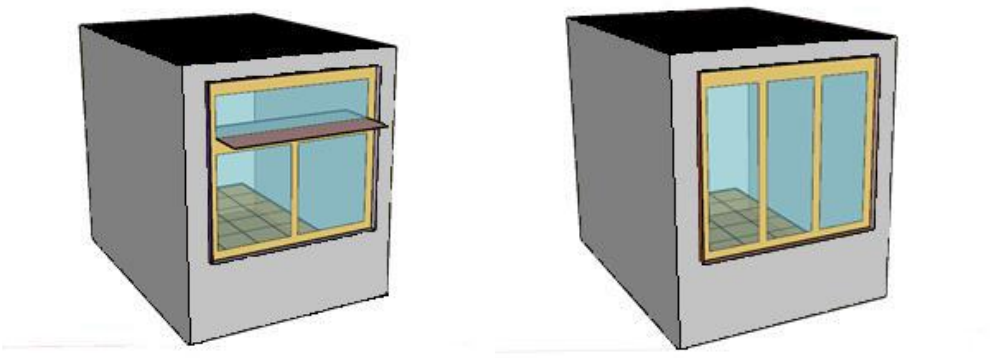

Figure 24 – (a) Room model with the SW-LSC – (b) Room model with the traditional window

The data output from the weather station described in the previous paragraph was implemented into a weather data file imported into the building simulation tool used.

Subsequently, these data were re-elaborated in order to obtain these variables with a one-minute timestep, in order to be consistent with the monitored data.

Simulation have been run with one-minute timestep.

The calibration process was performed for the optical properties of the internal walls (reflection coefficients: wall 0.75, ceiling 0.75, floor 0.35), of the outside obstructions and of the light shelf. In particular, since the light shelf was covered with a high reflectance layer, it was necessary to proceed by attempts in order to simulate correctly the characteristics and functioning of this element. The light shelf reflection coefficient was calibrated in the range from 0.81 to 0.95; the final value chosen was 0.92. Due to the limited measurement range of the luxmeter used (resolution 0.1 lux, precision ±4% ≤ 20000 lux and 5% ≥ 20000 lux), especially for high illuminance values, and due to some localized shading due to the structure of the windows, an error of 10% with respect to the monitored data was considered acceptable.

4.2 Electrical performances

4.2.1 Energy generation statistical modeling

Due to the limited availability in the physical generation models for the technology investigated a simple regression model was used to investigate the relationship between power output from LSC modules and incident solar radiation. A regression model is a statistical linear model that, in case of more input variables, can be expressed as (2):

$$y = \beta_0 + \beta_1 x_1 + \beta_2 x_2 + \ldots + \beta_r x_r + \varepsilon \quad (2)$$

In which:

y is the real output

$\beta_0, \beta_1, \beta_2, \ldots, \beta_r$ are the regression coefficients

$x_1, x_2, \ldots, x_r$ are the independent variables

ε is the random error

In case of r=1, the model become a simple linear regression one (3):

$$y = \beta_0 + \beta_1 x_1 + \varepsilon \quad (3)$$

In which β_0 is also called intercept. Estimation of regression coefficients β_0 and $\beta_1$is usually done through the Least Squares method, that aim to minimize

the error between predicted and real targets. Function to minimize, denoted as SS function, can be expressed in the following way (4):

$$SS(\beta_0, \beta_1) = \sum_{i=1}^{n} (y_i - \hat{y}_i)^2 = \sum_{i=1}^{n} (y_i - \beta_0 + \beta_1 x_i)^2 \quad (4)$$

In order to minimize SS function, it is compulsory to find two estimators, the so-called least-square estimators and denoted as $\widehat{\beta_0}, \widehat{\beta_1}$. This is done deriving function SS with respect to the estimators and putting the results equal to zero (5):

$$\begin{cases} \dfrac{dSS}{d\widehat{\beta_0}} = -2 \sum_{i=1}^{n} (y_i - \widehat{\beta_0} + \widehat{\beta_1} x_i) = 0 \\ \dfrac{dSS}{d\widehat{\beta_1}} = -2 \sum_{i=1}^{n} (y_i - \widehat{\beta_0} + \widehat{\beta_1} x_i) x_i = 0 \end{cases} \quad (5)$$

Results for $\widehat{\beta_0}$ and $\widehat{\beta_1}$ are obtained introducing new variables $\bar{y}\ and\ \bar{x}$, and solving latter equations (6-7):

$$\widehat{\beta_0} = \bar{y} - \widehat{\beta_1} \bar{x} (6)$$

$$\widehat{\beta_1} = \frac{\sum_{i=1}^{n} (x_i y_i) - \bar{x} \sum_{i=1}^{n} y_i}{\sum_{i=1}^{n} (x_i)^2 - n\bar{x}^2} \quad (7)$$

In which $\bar{y}\ and\ \bar{x}$ are expressed in the following way (8-9):

$$\bar{y} = \frac{1}{n} \sum_{i=1}^{n} y_i \quad (8)$$

$$\bar{x} = \frac{1}{n} \sum_{i=1}^{n} x_i \quad (9)$$

The simple linear regression can be expressed as (10):

$$\hat{y} = \widehat{\beta_0} + \widehat{\beta_1} x_1 \quad (10)$$

Variable $\hat{y}$ represents model output in equation (10).

Assessment of the model can be done using model performance metrics, such as

the coefficient of determination R2, the root mean square error RMSE and the mean bias error MBE. The former one represents the goodness of fit of the model and can be expressed in the following way (11):

$$R^2 = 1 - \frac{SS}{SS_{total}} = 1 - \frac{\sum_{i=1}^{n}(y_i - \hat{y}_i)^2}{\sum_{i=1}^{n}(y_i - \bar{y})^2} \quad (11)$$

In which SS is the residual sum of squares and SStotal is the total sum of squares. In other words, R-square relates variance explained by the model with respect to the total variance. It ranges within the interval [0,1], assuming value equal to 1 in case of perfect fit of data. RMSE, instead, represents standard deviations of the residuals and it is used to evaluate accuracy of the model itself. Lower is the RMSE value, better the accuracy. In mathematical terms (12):

$$RMSE = \sqrt{\frac{1}{n}\sum_{i=1}^{n}(y_i - \hat{y}_i)^2} \quad (12)$$

Finally, MBE represents the average distance between predicted and real targets (13):

$$MBE = \frac{1}{n}\sum_{i=1}^{n}(y_i - \hat{y}_i) \quad (13)$$

4.2.2 Energy generation regression analysis

As mentioned in previous paragraph, a statistical analysis between electrical power produced by LSC modules and incident solar radiation was performed. A stochastic model is usually used when there are is a lack of information regarding physics involved within natural phenomena under study. Raw data for three variables were provided by sensors installed near LSC modules. Particularly, data on electricity produced, incident solar radiation on the modules and cell temperature were collected (through the external sensor connected via computer) from 30 April 2017 to 18 November 2019 by historical performance monitoring, with a sub-minutely time-step (each measurement was performed every 30 seconds). Daily time range of observations goes from 7 am to 7 pm. Firstly, anomalies were detected and

removed. Then, raw data were merged into hourly values, averaging values through the arithmetic mean. In Fig.25, Fig. 26, Fig. 27 were reported hourly variations for the variables accounted within the analysis. Solar radiation, expressed in W/m^2, and the generation (W) show an analogous daily trend, reaching high values during midday. Instead, the temperature of the cell, expressed in Celsius degree, shows minor daily oscillations, increasing during the month, up to 32 °C as maximum value. The cell temperature increase (Fig. 27) can be justified by the change in external conditions (solar irradiation and external temperature) and the presence of the double glazing that encloses the modules and acts as a heat accumulator. The temperature jump is contained (12°C) compared to other technologies (20-30°C) and this is mainly due to the fact that only a small fraction of the radiation directly affects the cells, that located at the edges of the module.

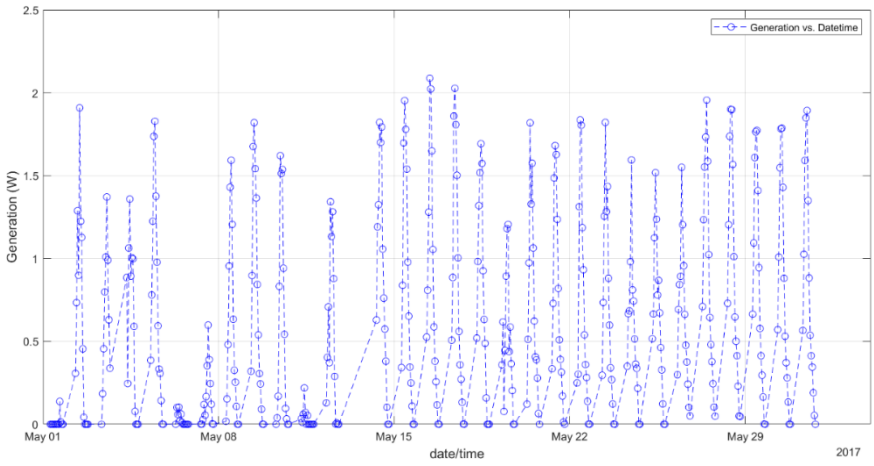

Figure 25 *– Generation monthly trend (1.1% LSC efficiency)*

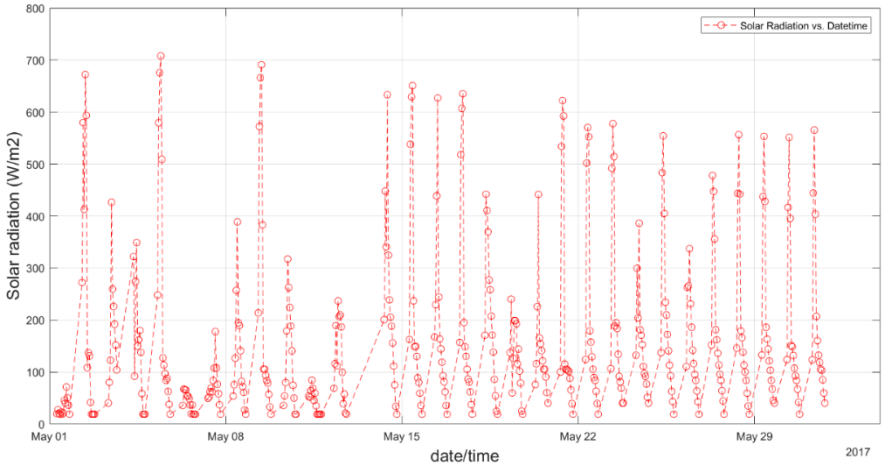

Figure 26 *– Solar radiation monthly trend*

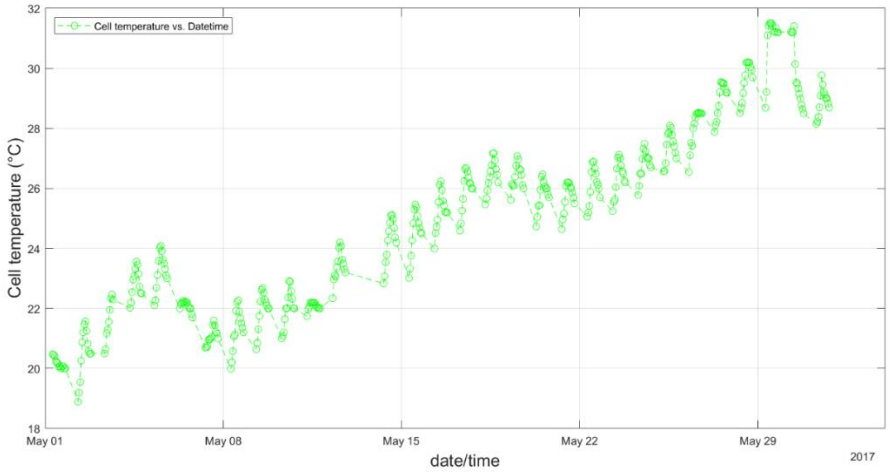

Figure 27 *– Cell temperature monthly trend*

Hourly mean values were normalized in the interval [0,1], applying min-max scaling method (13):

$$z(x) = \frac{(x - \min(x))}{(\max(x) - \min(x))} (13)$$

In which z represent the normalized hourly variables. Further step was to split data into two groups, one for training the regression model, the other for the testing. Within former cluster 2017 and 2018 data were included, instead testing sample includes 2019 data. Fig. 28 below reports two graphs, the former one shows trend of normalized solar generation w.r.t. normalized solar radiation, the latter w.r.t. cell

temperature. It can be seen, in a clear way, the correlation between LSC power output and solar radiation. Instead, cell temperature appears has a null or weekly correlation with the component generation. Since that, regression analysis was conducted exploiting only solar radiation as independent variable and, therefore, a simple regression linear model was analyzed to explore a possible correlation between the above-mentioned variables. Mathematical details of the model were formulated in the previous paragraph. Analysis was conducted on MATLAB environment and a bisquare robust option exploited, that is less sensitive to anomalous values, allowing analyst to do not remove manually outliers. In Fig.29 real and fitted data are report for two datasets used within the analysis.

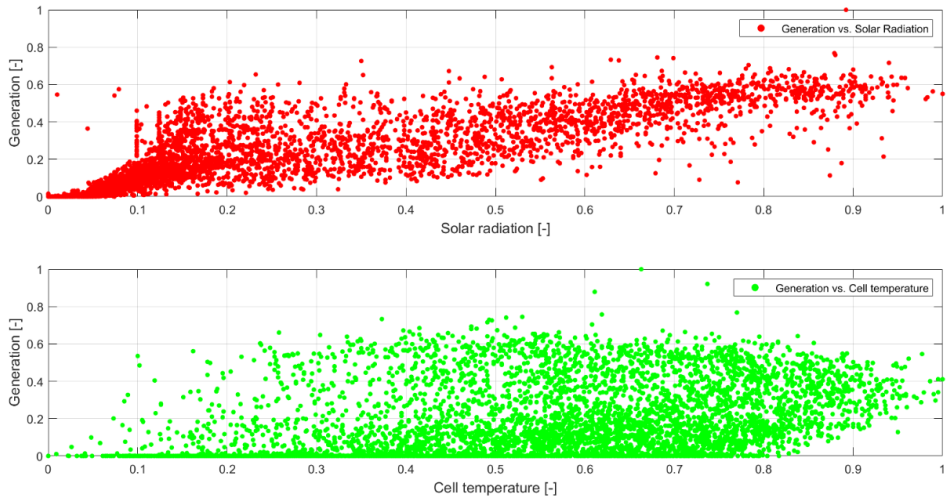

Figure 28 *- LSC energy generation vs. other variables*

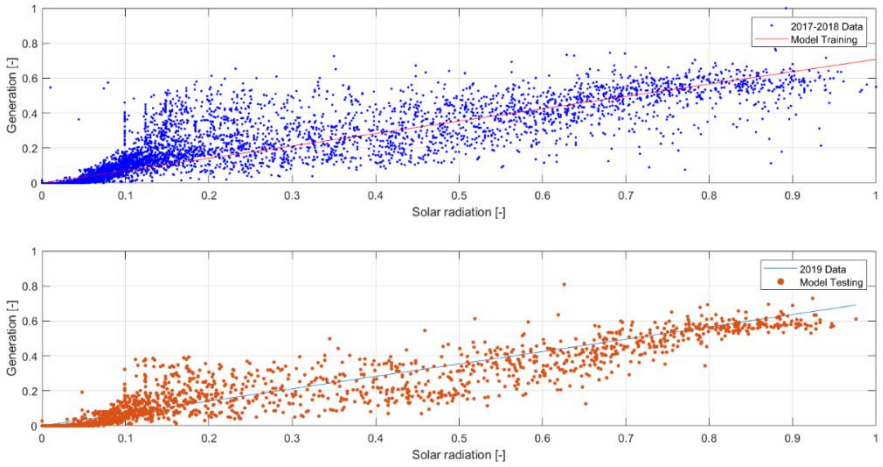

Figure 29 *– Linear robust fitting for training and testing data*

Finally, Fig. 30 reports real and predicted values for a selected period of 2019, that ranges from 14 March up to 8 May. Near values for each time-step shows goodness of fit of the model exploited, as can be seen also in Tab. 21 (where x in formula is the solar radiation).

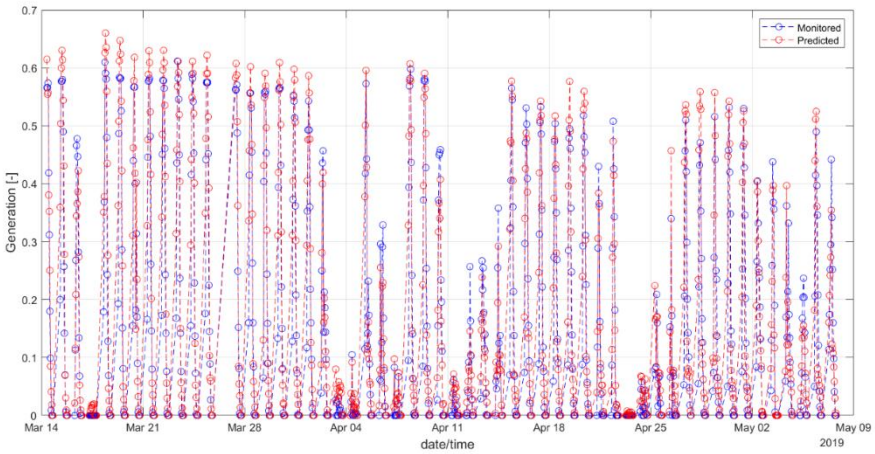

Figure 30 *- Real vs. predicted LSC energy production values for a selected period*

Table 21 *– Main features of the regression model*

	Regression model	R^2	RMSE	MBE
Training set (2017-2018)	$Y=0.7077*x+6.024*10^{-6}+\varepsilon$	≈0.95	≈0.04	≈0.02
Testing set (2019)		≈0.87	≈0.07	≈−0.01

4.3 Building performance simulation

After the experimental system was characterized and calibrated, the models created were tested on a larger building, in order to evaluate the thermal performances of the system in a real building environment.

The small office model proposed by ASHRAE Standard 2019 is a building with a floor area of 511 m^2; the building plan and the perspective view of the building are shown in Fig.31. The building is composed by one attic and fives thermal zone; among these five thermal zones there is a central area that has no external walls and four perimeter areas which are each exposed towards a respective direction (north, south, west, east). The perimeter areas are the only ones equipped with window surfaces (four windows for west and east surface, six windows for south and north surfaces).

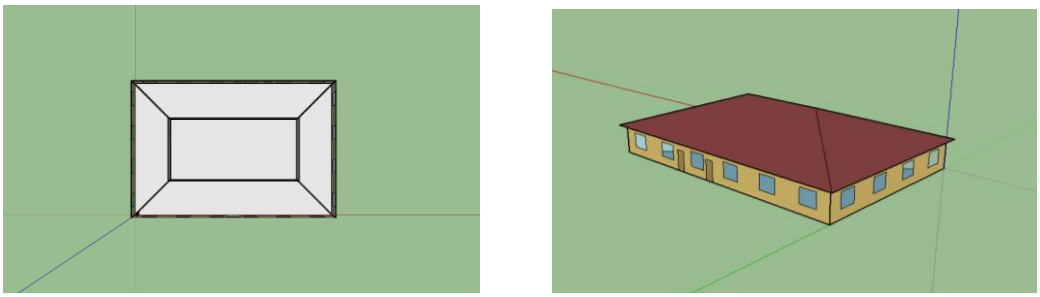

Figure 31 *- Plan and perspective view of the small office*

For the analysis carried out, the windows of the reference model were entirely replaced, in the first model, by the traditional window (traditional window scenario) and, in the second model, by the SWs-LSC (SW-LSC scenario), keeping the original dimensions for both.

Author chose four days that had particular characteristics of irradiation and temperature and that were therefore representative of the most critical periods and seasons from a thermal point of view, as described in other literature works [137] [138]. These days were:

• Cold cloudy (24 December);

• Cold sunny (15 January);

• Warm cloudy (28 August);

• Warm sunny (22 July).

The choice of the days had been made using the hourly climate data for the city of Novara.

Table 22 shows the outdoor dry-bulb temperature (Dbt) and the global horizontal radiation (GlobHorRad) for the four selected days. Moreover, the chosen days are significant for the differences or similarities to the average monthly values.

***Table 22** - Reference days characteristics*

Reference days	Mean Dbt	Mean GlobHorRad	Month	Mean Dbt	Mean GlobHorRad
	°C	Wh/m^2		°C	Wh/m^2
24 December (cold cloudy)	- 1.8	68.2	December	2.8	118.3
15 January (cold sunny)	-4.5	136.2	January	1.7	136.2
22 July (warm sunny)	27.2	550.5	July	23.6	429.3
28 August (warm cloudy)	24.8	219.8	August	22.9	349.4

In particular, the cold cloudy day (24 December) shows an average temperature lower of about 4.6 degrees than the average monthly value while the solar radiation on horizontal value is about 41% of the monthly one. The cold sunny day (15 January) shows the lowest temperature of the year (-4.5 °C), while the solar radiation on horizontal value (136.2 W/m^2) is the same order of the monthly value. The warm sunny day (22 July) shows a temperature 3.6 degree higher than the monthly mean (the temperature is one of the highest of the year for the reference location) and a solar radiation on horizontal value (550.5 W/m^2) higher than the monthly value (429.3 W/m^2). The warm cloudy day (28 August) shows an average temperature of 24.8 (1.9 degrees higher than the monthly mean) while the solar irradiation is about 37% of the monthly one.

4.4 Life cycle assessment

LCA is a systematic tool for analysing the environmental impacts of a product system throughout its life cycle, from the extraction of resources, through the production of materials, parts, and the product itself, to its use and the management required by reuse, recycling, or final disposal. LCA, based on the standards of the ISO 14040 [139] and ISO 14044 [140], compiles and evaluates the inputs and

outputs and the potential environmental impacts associated with the life cycle of the product system [141].

4.4.1 Goal and scope definition

The final goal of the analysis is to assess the environmental impacts of SW-LSC prototype that is currently installed at Eni research center in Novara. Considering the dual nature of the whole device (photovoltaic modules + smart window), it is necessary to clarify that the initial focus was to calculate the impacts relating to LSC modules and, subsequently, to consider the impacts relating to the integration of the modules in the SW frame and all the accessory elements that allow the device to work correctly. This approach allowed to obtain a clearer picture of the impacts of the entire SW-LSC and, at the same time, to evaluate the impact of the LSC modules separately, considering also the possibility of using them for other types of applications different from that of the SW (direct integration into the building, skylights, etc.).

After the impacts evaluation of each phase, the study involved a dominance analysis to assess the relative impact of individual components of the SW-LSC. In addition, two different scenarios for the SW-LSC frame were explored. The first scenario considered the use of a primary aluminum for the thermal break aluminum frame, and the other one involved the use of thermal break aluminum frame with 75% recycled material.

Another goal of the analysis was to compare the SW-LSC prototype, , with other traditional windows on the market, on the basis of some assumptions and simplifications,. Similarly, LSC modules were also compared with other photovoltaic technologies that can be integrated into the building. The comparison of LSC modules with other PV technologies was carried out on the basis of two different functional units; 1 m^2 of module surface and 1 kWh of generated energy. The use of two functional units (both widespread in LCA of PV technologies) allowed to evaluate different aspects: on the one hand, the burden linked to the production of the module surface (which is useful in comparing technologies that

can be integrated in the building facades or glazed building[1]) and, on the other hand, the production of electricity (which takes into account PV performance and yield).

The function of the system is to guarantee lighting and thermal comfort in internal environment through the motorized venetian blind system powered by LSC modules and the thermal and optic characteristics of the whole SW-LSC. In addition, it must be considered the generation of renewable energy through the surplus power output. The functional unit (FU) chosen was a 5,27 m^2 automated shading system window (Uw = 1,6-1,8 W/m^2K), equipped with coloured LSC fanlight (tvis = 77% and g = 85%) [128, 129, 130] and which can produce about 1.5 kWh/year. Electricity generation was calculated through the analysis of monitored data; these data referred to the city of Novara (Italy) and depended to the local climatic conditions.

The approach used was “from cradle to gate with options” [142], considering the maintenance of SW-LSC during its life cycle. The assembly phase involved all the operations that made it possible to obtain the SW-LSC prototype starting from its disassembled elements. Loads and credits deriving from energy and materials recovery at the end of life were analysed separately, since it was not possible to collect data on this phase (because the SW-LSC is a prototype); in addition, there was a lack of data and information about the possible recovery of LSC modules, since the technology is relatively new. The study of this phase was mainly based on assumptions/predictions that will be shown during the work.

Author did not consider the transport of the materials and the packaging. The choice was motivated by the fact that the SW-LSC analyzed was a prototype not commercially widespread, so the transport of the materials as well as the packaging of the chemical elements that make up the dye could vary significantly in the future, especially considering a large-scale production of the device, both geographically and quantitatively. Also, for this reason, the results of the analysis must be considered as the "worst case", or laboratory case, as they refer to the specific object of the study. In addition, large-scale production generally leads to improved process

[1] For example the opaque technologies of third generation PV or the semi-transparent PV of first generation)

efficiency and material use. The datasets used to model materials and processes derived from Ecoinvent database [147]. No allocation or cut-off procedures were performed in the analysis.

Life cycle impact assessment (LCIA) was conducted using SimaPro 8.1 software and CML-IA baseline method, which is the new update of the CML2001. CML-IA is one of the mostly used models in PV-LCA analysis but also for window related LCA [143,144,145,146]. It considers a broad set of 11 impact categories which are shown in table 23:

Table 23 *– CML-IA impact indicators*

Categories	Unit
Global warming potential(GWP100a)	kg CO_2 eq
Abiotic depletion potential (ADP)	kg Sb eq
Abiotic depletion potential fossil fuel (ADPff)	MJ
Photochemical oxidation potential (PO)	kg C_2H_4 eq
Human toxicity (HT)	kg 1,4-DB eq
Acidification potential (AP)	kg SO_2 eq
Eutrophication potential (EP)	kg PO_4--- eq
Ozone layer depletion potential (ODP)	kg CFC-11 eq
Fresh water ecotoxicity (FWE)	kg 1,4-DB eq
Marine aquatic ecotoxicity (MAE)	kg 1,4-DB eq
Terrestrial ecotoxicity (TE)	kg 1,4-DB eq

In conclusion, the main objectives of this work can be summarized as follow:

- assessment of the environmental impacts of the SW-LSC prototype; furthermore, to identify the most impacting components of the device through a dominance analysis.

- assessment of the impacts relating only to LSC modules, which could be used for types of installation other than the window (for example for direct replacement in glazed buildings), also to maximize energy generation.

- comparison of the environmental impacts of SW-LSC with those of other commercial windows (functional unit: 1m^2);

- comparison the impacts of LSC modules with other photovoltaic (PV) technologies that can be used for building integration (functional units: 1 m^2 and 1 1 kWh).

4.4.2 Life Cycle Inventory (LCI)

This section describes the activities carried out for the collection of information and the processing of data relating to the SW-LSC system and its components. Thanks to the collaboration and involvement of the company where the prototype was assembled and installed, it was possible to find information relating to the SW-LSC, through data collection campaigns and questionnaires. The company assembled in loco the SW-LSC components after that all the components have been manufactured in different places; for this reason, it was necessary to define the different production paths of the main components required for the final product.

In order to simplify the description of the SW-LSC elements and the related data collection, this paragraph has been divided into 3 sections, connected to the SW-LSC macro-components:

- LSC module, which included the luminescent dye (fluorophore), the PMMA matrix and the photovoltaic cells;

- Aluminum structure (frame);

- Auxiliary components, which included light shelf, DC motors, cables and connections, batteries, Venetian blind.

• LSC module elements

The following elements (dye, PMMA slabs, PV cells) were assembled to obtain the LSC module. In particular, as described below, the dye was dispersed inside the PMMA matrix before the polymerization step of its monomer, the methyl methacrylate (MMA); then PV cells were glued to the edges of the coloured slabs and connected in series or parallel, obtaining the LSC module.

- Fluorophore

Eni company has synthesized and patented the luminescent dye.

All data related to the dye synthesis process were collected through the dye patent and interviews with some team members who contributed to the synthesis of the dye. In addition to the quantities of substances used in the synthesis process and the production methods, the technical data sheets relating to the machinery used (i.e.

chemistry vacuum system, rotary vane pump, motors) and the operating times of the same were collected. These data allowed to calculate the electrical energy consumed for the production of the dye; all data, as well as efficiencies and the yields of chemical reactions, referred to laboratory scale production.

For this study, the concentration of dispersed dye was set at 200 ppm, in order to analyze the "worst" case possible from the point of view of the quantities of chemicals used in the synthesis process.

The final yellow dye (which had the best results for efficiency and optical characteristics) was obtained in laboratory in three steps through two intermediate precursors. Each precursor was synthesized with its own procedure that foresaw different process times and quantities of chemical substances, and then used for the next step. During the analysis, all the quantities involved during the synthesis process were related to the concentration of final dye required for 1 m^2 of module, which was the modules dimension referred to the FU (5.27 m^2 window).

The synthesis process is shown in Fig. 32

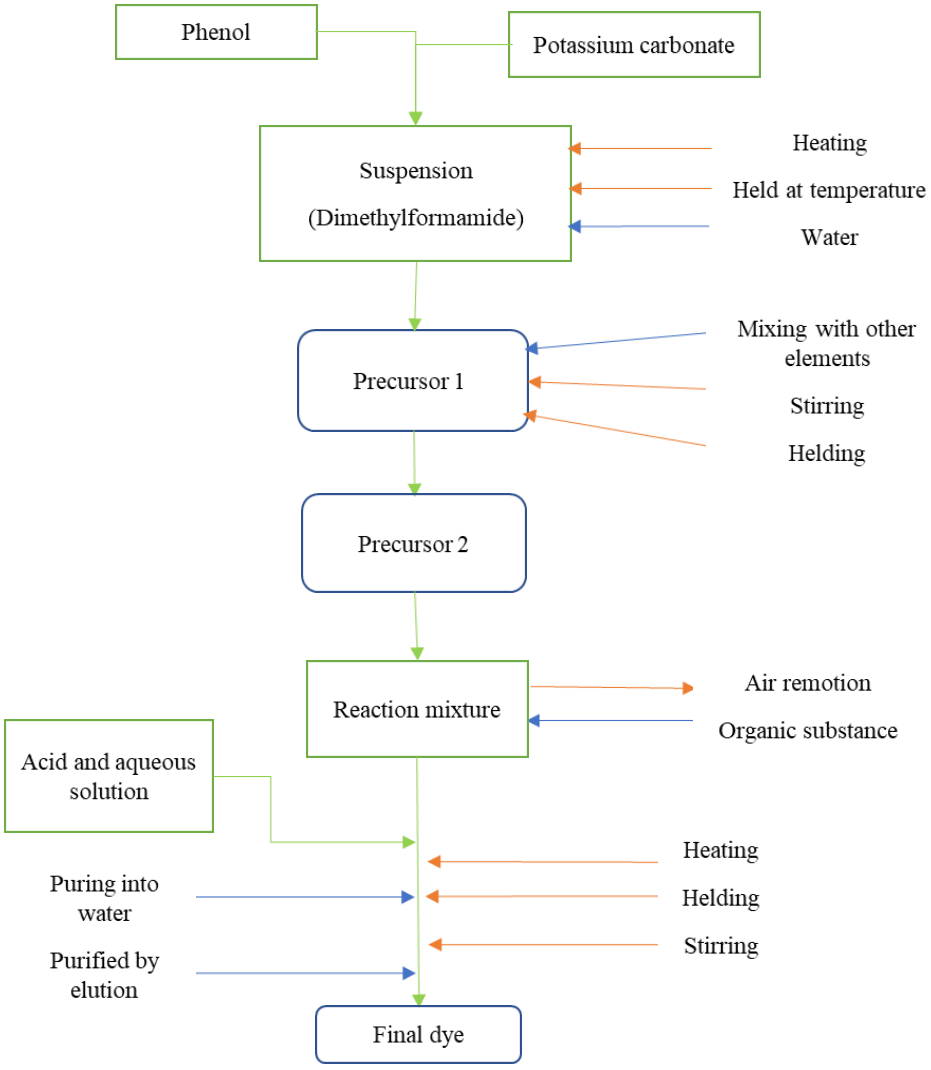

Figure 32 - Synthesis process of the "yellow" dye**.**

Table 24 shows the three-steps synthesis of the final dye and its composition. In the event that the chemicals used in the intermediate precursors and in the final dye were not present in Ecoinvent database, similar substances from a chemical point of view or that had similar synthesis processes were used.

Table 24 *- Composition of the final dye referred to 1 m^2 of LSC modules*

Chemicals (Eni patent)	*Secondary data*	*Quantity*
STEP 1		
Phenol	Phenol/RER	1.14 g
Potassium carbonate	Potassium carbonate/RER	1.08 g

5,6- difluoro - 4,7 bis (2 metyl) 2,1,3 Benzothiadiazole)	Benzothiadiazole/RER	0.97 g
N.N-dimethylfermammide	N.N-dimethylfermammide/RER	0.01 l
Water	Water /RER	0.08 l
Precursor 1 (Step 1 product)		1.32 g
STEP 2		
N-bromosuccide	Phenol/RER	1.03 g
Precursor 1		1.32 g
Tetrahydrofuron	Tetrahydrofuron/RER	0.02 l
N.N-dimethylfermammide	N.N-dimethylfermammide/RER	
Water	Water/RER	0.08 l
Precursor 2 (Step 2 product)		1.54 g
STEP 3		
2,5-dimethylphenylboronoic acid	Boric acid/RER	0.9 g
Potassium carbonate	Potassium carbonate/RER	2.74 g
Precursor 2		1.54 g
1,4 Dioxane	Dioxane/RER	0.03 l
Water	Water/RER	0.71 l
Palladium-tetrakisiphenyl	Triphenyl phosphate/RER	0.13 g
Final dye (yellow)		1.43 g

- PMMA

PMMA is the most used material as a waveguide for LSC sheets. PMMA cast sheets are produced starting from its monomer, methyl-methacrylate (MMA), via a bulk polymerisation process. The process consists of casting liquid monomer in a flat mould (between two sealed glass sheets) and to heat it (in hot water baths or in ovens) in order for the MMA to polymerise. Typically, as happens in our case, the luminescent dye is dissolved in the monomer before this step; this process has no further impact compared to the neutral PMMA sheet, since the dye is simply added and mixed together with the other elements. The PMMA slab is then withdrawn from the mould. Coloured PMMA slabs used into the SW-LSC device were produced by a European company that is part of the CEFIC (European Council of Chemical Industries); this company was also responsible to dope PMMA slabs with the "yellow" luminescent dye. PMMA data used in this study are based on the results of 4 individual LCA studies performed independently by European producers (including the one involved in the SW-LSC project) of PMMA cast sheet and they refer to the production of 1kg PMMA cast sheet as a cradle-to-gate system. The primary PMMA data used in the above LCA studies comes different plants located in European countries. [161]

- Photovoltaic cells

The industrial processes with which these cells are produced are now widespread in the literature and will not be explored in this work. The only additional process for applying photovoltaic cells to the LSC slab is that of laser cutting, which allows to adapt the PV size to the thickness of the slabs. Once the LSC sheet has been obtained, the photovoltaic cells are glued to the edges using silicones or resins with a high degree of transparency. The data referring to PV wafer, resin and laser cutting process were taken from the Ecoinvent database [147] and are shown in Tab. 25. The system boundary used for these elements was "cradle to gate".

Table 25 *– Photovoltaic cells profile*

Material/process	***Secondary data***	***Quantity***
Photovoltaic cells	Photovoltaic cell, single-Si wafer, production/RER	0.048 m^2
Resin	Epoxy resin, production/RER	96 ml
Laser cutting	Laser machining, metal, with YAG-laser, 500 W power/RER	0.53

- Aluminum frame

Due to reasons of confidentiality, the manufactory company has not provided detailed data on the production process. The author therefore calculated the quantities of materials and energy resources thanks to the technical data sheet, the detailed measurements of the frame and its section, and from third data of Ecoinvent database. The data referring to 1 m^2 of aluminum frame are shown in Tab. 26.

Table 26 *– Aluminum frame profile*

Material/Process	*Secondary data*	*Quantity*
Thermoplastic	Acrylonitrile-butadiene-styrene copolymer/RER	0.31 kg
Adhesive	Adhesive, for metal/RER	0.22 kg
Aluminum frame	Aluminum, wrought alloy/RER	30.90 kg
	Electricity, Medium V/IT	0.99 kWh
Plastic extrusion	Extrusion, plastic film/RER	0.19 kg
	Glass fiber reinforced, polyamide, injection moulded/RER	4.10 kg
	Isopropanol/RER	0.02 kg
	Metal working factory	1.80E-08 p
	Nylon 6/RER	0.01 kg
Thermoplastic	Polyethylene, high density/RER	0.19 kg
Coat	Powder coat, aluminum sheet/RER	7.63 m^2
	Reinforced steel/RER	0.44 kg
Aluminum process	Section bar extrusion, aluminum/RER	29.58 kg
Aluminum process	Section bar rolling, steel/RER	0.68 kg
	Steel, chromium steel 18/8, hot rolled/RER	0.36 kg
	Synthetic rubber/RER	3.79 kg

The base scenario for SW-LSC aluminum frame considered the use of only primary aluminum.

The manufactory company has provided the certification that the aluminum used in the SW-LSC has a recycled content of 75%. For this purpose, as already mentioned, a "recycling scenario" for the frame was explored in this study. The comparison between the two scenarios is necessary to quantify the advantages of using recycled aluminum compared to primary aluminum for the SW-LSC prototype. The results of the comparison could be useful for evaluating alternative solutions, since the use of aluminum frame is not binding in the final product, and for other companies wishing to market other similar devices / products following different logistical choices for the window frame.

- Auxiliary elements

Since there was no detailed information on the manufacturing process of these elements, they were modelled in a simplified way from the Ecoinvent database [147]. Aluminum box and mask where modelled considering the primary aluminum used and the process to produce the sheets, as shown in Tab. 27.

***Table 27** - Aluminum mask and box profile (1 m^2)*

Material/process	Description	Quantity
Aluminum (box and mask)	Aluminum, wrought alloy aluminum ingot, primary, to market |GLO	49. 8 kg (box) 5.4 kg (mask)
Aluminum sheet	Sheet rolling, aluminum, processing/RER	49.8 kg (box) 5.4 kg (mask)

Also, the light shelf was modelled in a simplified way, as shown in Tab. 28.

***Table 28** - Light-shelf profile (1 m^2)*

Material/process	Description	Quantity
Aluminum (light shelf)	Aluminum, wrought alloy aluminum ingot, primary, to market/ GLO	21.8 kg
Aluminum sheet	Sheet rolling, aluminum, processing/RER	21.8 kg
Aluminum perforated sheet	Aluminum removed by drilling, aluminum drilling/RER	4.52 kg

The double-glazing (both for the upper and lower windows), an acid lead battery, the venetian blind system and two DC motors were then considered in the analysis and all these elements completed the profile of the whole SW-LSC.

The profiles of these elements are shown in the following tables 29-32. Double-glazing profile was modelled on the basis of glazing with similar transmittance in Ecoinvent database (U = 1.1 W/m^2 K). Lead acid battery profile was modelled based on a literature work and it is included in the analysis [148,149]. Venetian blind was modelled in a simplified way like other elements such as the aluminum mask. Finally, DC motors were modelled from an EPD of motors for rolling blinds, similar to the one used into SW-LSC [150]

Table 29 *- Double glazing profile (1 m^2)*

Material/process	Description	Quantity
Aluminum	Aluminum, wrought alloy/GLO	0.51 kg
Process	Sheet rolling, aluminum/ GLO	0.51 kg
Electricity	Electricity, low voltage/RER	5.46 kWh
Glass	Flat glass, coated/ GLO	16.5 kg
Glass	Flat glass, uncoated/ GLO	16.5 kg
Synthetic rubber	Polybutadiene/ GLO	0.02 kg
Sealant	Polysulfide, sealing compound/ GLO	0.75 kg
	Argon, liquid/ GLO	0.04 kg
Water	Water, completely softened, from decarbonised water, at user/GLO	1.7 kg
	Zeolite, powder/GLO	2.24 kg

Table 30 *- Acid lead battery profile (1 kg)*

Material/process	Quantity
Lead, primary lead production from concentrate/ GLO	0.32 kg
Lead, treatment of scrap acid battery, remelting/ RER	0.28 kg
Water, deionised, from tap water/ CH	0.13 kg
Sulfuric acid, production/RER	0.1 kg
Polypropylene, granulate, production/RER	0.1 kg
Antimony, production/ RoW	0.01 kg
Glass fibre, production/RER	0.02 kg
Copper, production, primary/RER	0.002 kg
Copper, treatment of scrap by electrolytic refining/RoW	0.0004 kg
Barium sulphide, barium sulfide production/GLO	0.002 kg

Electricity, medium voltage/IT	0.31 kWh
Heat, central or small-scale, natural gas/ Europe without Switzerland	2.73 MJ
Heat, district or industrial, other than natural gas/ Europe without Switzerland	0.25 MJ
Wire drawing, copper, processing/RER	0.003 kg
Injection moulding, processing/RER	0.1 kg

Table 31 *- Venetian blind profile (1m^2)*

Material/process	Quantity
Aluminum, wrought alloy/GLO	0.54 kg
Sheet rolling, aluminum/ RER	0.54 kg

Table 32 *- DC motors profile (1 kg)*

Material/process	Quantity
Cable, connector for computer, without plugs/GLO	0.123 m
Cable, network cable, category 5, without plugs/GLO	1.11 m
Cable, ribbon cable, 20-pin, with plugs/GLO	0.032 kg
Injection moulding/GLO	0.2 kg
Polyethylene, high density, granulate/GLO	0.2 kg
Printed wiring board mounting facility/GLO	2.08E-07 p
Printed wiring board, surface mounted, unspecified, Pb containing/GLO	0.02 kg
Printed wiring board, surface mounted, unspecified, Pb free/GLO	0.05 kg
Printed wiring board, through-hole mounted, unspecified, Pb containing/GLO	0.02 kg
Printed wiring board, through-hole mounted, unspecified, Pb free/GLO	0.05 kg
Sheet rolling, steel/GLO	0.5 kg
Steel, low-alloyed, hot rolled/GLO	0.5 kg

Eni research center provided all information relating to type and number of auxiliary components, as well as the assembly procedures of SW-LSC prototype. This information was elaborated and completed through literature studies or data from Ecoinvent database.

4.4.3 SW-LSC assembly phase, manufacturing and end of life

- Assembly

Using the information collected in the company, it was estimated a total time of about 3 hours to assemble the SW by hand. During this phase, the environmental impacts were only related to the electricity consumption due to the use of some machinery and tools, such as a drill and a welding machine for aluminum parts. Energy consumption was assessed by estimating the times of use of these tools,

which is also linked to the thickness and length of aluminum sheets to be processed (4.8 m). The assembly phase profile is shown in table 33.

***Table 33** - Assembly phase modelling*

Material/process	Description	Quantity
Aluminum for welding	Aluminum, wrought alloy/ GLO U	0.0183 kg
	Argon, crude, liquid {GLO}| market for | Cut-off, U	0.00357 kg
Energy consumption (welding)	Electricity, medium voltage/IT U	0.075 kWh
	Electronics, for control units/GLO U	1.0E-5 kg
Energy consumption (drilling)	Electricity, medium voltage/IT U	0.036 kWh

As previously described, the first phase was to obtain the LSC modules by gluing the photovoltaic cells to the edges of the coloured PMMA plate. Furthermore, the interconnections between the cells have been prepared in order to ensure the correct functioning of the modules. LSC modules edges were incorporated into an aluminum mask in order to protect the photovoltaic cells and the interconnections. In the second phase, the lower window and the upper window (where LSC modules were arranged) were combined through an aluminum box where batteries, wires, connections and control system will be placed.

The connections and cables for the management of SW-LSC control system allowed the connection with LSC panels, batteries, irradiation sensor and Venetian blinds. Data referred to these elements were taken from Ecoinvent database.

After the completion of the prototype structure, the LSC modules are placed inside the upper window, covered with the aluminum mask and encapsulated between two glass sheets.

The light shelf, placed between the upper and lower window, is composed of an internal and an external shelf, both hinged to the fixed part with metal hinges along the entire length. The internal shelf is placed above the aluminum box also in order to facilitate its anchoring. The internal shelf is fixed with stainless steel cables and forks fixed with a detachable pin.

- Maintenance

Although there is not much information in the literature regarding the use phase of LSC modules it is possible to estimate a life span of 15 years for LSC modules in SW-LSC, since good protection is offered by both aluminum mask and glass encapsulation. The life span of the SW-LSC in its entirety can be estimated around 30 years. The replacement of LSC modules is always possible, also in the event of a malfunction, since the upper window is equipped with an easy opening system and LSC modules are not welded but only housed in the cavity. It is hypothesized that SW-LSC maintenance should not require any special precautions, other than cleaning the glass covering LSC modules, in order to ensure optimal functioning. For all these reasons, in this work, a single replacement of modules after 15 years was considered in all scenarios.

- End-of-life

Although the end of life phase has not been evaluated for all the elements of SW-LSC due to the lack of information, it is possible to hypothesize the material recycling or the energy recovery after the disassembly of the prototype; the elements considered for this analysis were the glass, the aluminum and the PMMA. Kikuchi et al [151,152], in their study, showed that it is possible to recover PMMA, like other types of thermoplastic, through a particular depolymerisation process; however, reference is made to transparent PMMA plates, and there are no bibliographical references on the recovery of PMMA doped with a fluorescent dye. For this reason, the end of life assumptions related to PMMA considered the energy recovery and loads connected to the PMMA incineration, rather than its recycling.

In order to evaluate the impact avoided considering the end of life phase of these elements, secondary data from the Ecoinvent database were used for the following materials.

• Recycling of 62% of glass from SW-LSC; the remaining percentage goes to landfills.

• Recycling of 80% of aluminum from frame, mask and box; the remaining percentage goes to landfills.

• Energy recovery from PMMA incineration.

Many considerations need to be made regarding window glass recycling. Generally, the glass container is easily recycled while post-consumer float glass (including flat window glass) is rarely recycled due to the contaminants it may contain. The Waste Framework Directive sets a 70% target for the reuse and recycling of construction waste materials, including glass. The main problem is that individual targets are not set on specific types of waste. Furthermore, in the case of window glass, the type of glass used must be considered, which may require several additional treatments. In our case, since SW-LSC is equipped with an insulated glass, the removal of the spacer bars and edge seals would be required but no particular limitations would be implemented. In addition, the techniques to separate the glass from other window components (window frames, hinges, sealants, insulation materials, etc.) are currently available, but need to be improved and become more widespread. The recycling percentage of 62% was therefore chosen according to a window EPD [153] (same Ug and glass type of SW-LSC). The recycling benefit and costs were allocated to the production of the recycled glass: virgin glass (100 kg) was used as avoided product and packaging glass (100 kg) was used as input from technosphere.

The percentage of aluminum of 80% was choose considering that the material is easily recyclable without loss of quality, even from windows; the percentage of end-of-life aluminum from building parts recycled in Europe is around 90-95% [154]. Once again, the recycling benefit and costs were allocated to the production of the recycled aluminum: aluminum, primary, ingot (210 kg) was used as avoided product.

Finally, the incineration route was chosen for PMMA, since recycling should be evaluated on the basis of the presence of the dye. The scenario was modelled thought Ecoinvent as waste incineration of plastics (PMMA) (7.14 kg)

This EOL analysis aims to quantify what could be the credits benefit deriving from the recycling of glass and aluminum, directly avoiding the use of raw materials. This means that the modelling of the end of life does not consider the costs due to recycling operations itself. The remaining percentage of materials not counted in recycling is destined for landfill (in the case of glass) and sanitary treatment and

landfill (in the case of aluminum). As regards PMMA, the incineration operation considers both the energy recovery and its costs.

The contribution of burdens and credits deriving from EOL was calculated in the base scenario of the analysis.

5 – Results

In this chapter, results of all the analyses are showed. In particular, Section 5.1 focused on the calibration of the models created. through the comparison between daylight data monitored and simulated. In Section 5.2 are showed all the results related to the test room analysis; in particular, the daylight simulation results and the comparison between the SW-LSC and traditional window. Then, the analysis of the electrical data relating to the SW-LSC was made. In section 5.3, the models created are used in a whole building. The first part of this section focuses on the daylight analysis of the entire building thought the annual calculation of the Daylight Autonomy (DA) and the light distribution inside the various zones. The second part regards a comparison of thermal performances of SW-LSC and traditional windows and an evaluation of energy savings. Finally, the LCA results are shown, followed by the comparison between SW-LSC and other windows on the market and the comparison between LSC modules and other PV technologies, on the basis of two different FUs.

5.1 Daylighting model calibration

The models of the traditional window and the SW-LSC were used inside the test building; the simulations using the illuminance map made it possible to obtain the illuminance value at the points of the experimental test. The result of the illuminance map is shown as an example in Tab. 34; the reference points value are marked in red.

Table 34 – Example of the illuminance map (SW-LSC case, 11.00 AM)

x/y	0.4	0.8	1.2	1.5	1.8	2.2	2.6	3
0.5	2743	2908	3163	3784	3923	3844	3860	3905
1	14190	15670	5480	4593	3590	3680	3520	3290
1.5	10234	18452	6543	3740	3476	3405	3289	2190
2	4796	3790	3590	4089	3244	2543	2690	2354

3	2945	2971	2994	3690	3038	3048	3043	2996
3.5	2286	2312	2340	2146	2369	2383	2409	2420

The comparison between the simulated and monitored values after the calibration process in the test room is shown in Fig. 33 and Fig. 34:

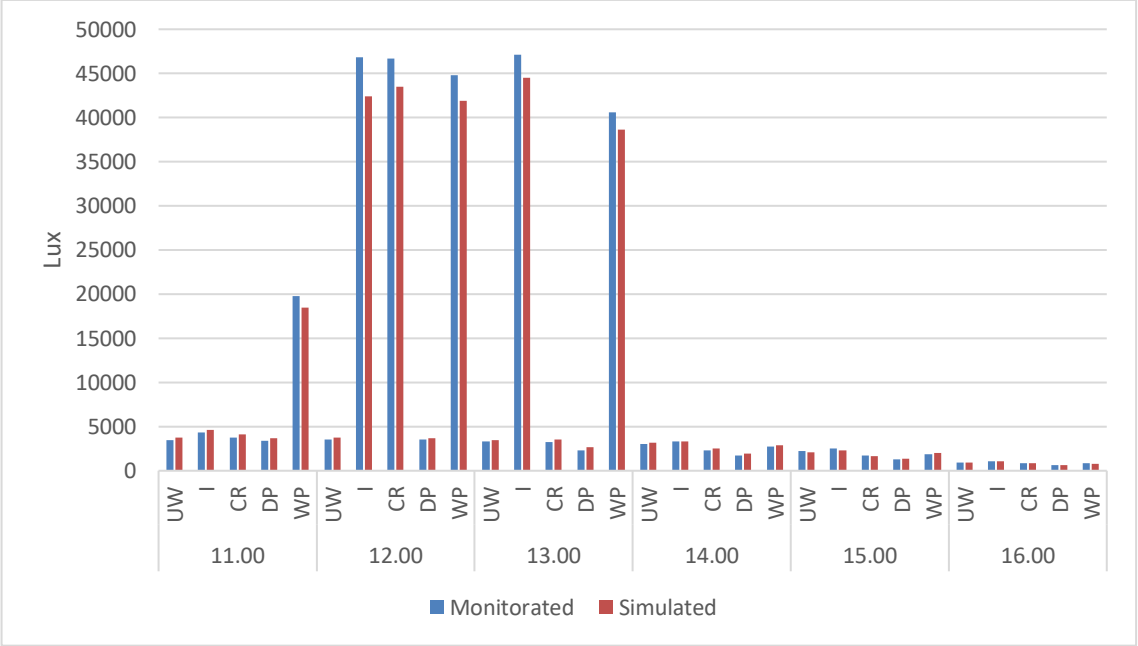

***Figure 33** - Gap between monitored and simulated value [lux] for SW-LSC model*

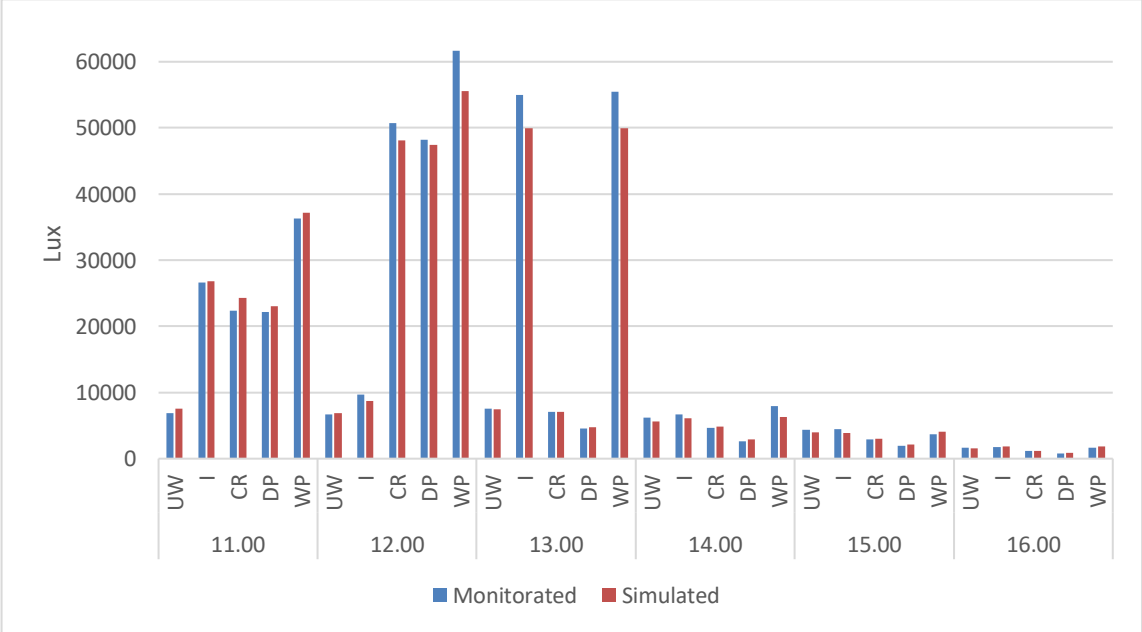

***Figure 34** - Gap between monitored and simulated value [lux] for traditional window model*

In order to evaluate the accuracy of the models created, the percentage error between the measured and the simulated value was calculated; the percentage error is expressed as the absolute value of the difference between the measured and estimated value, divided by the absolute value of the value measured, multiplied by 100. Table 35 and 36 show the percentage error for the five points described in section 2.2 (UW, WP, I, CR, DP) during the measurement period (from 11.00 to 16.00), for SW-LSC and traditional window models respectively:

***Table 35** - Percentage error between monitored and simulated values [%]*

SW-LSC					
Time	Points				
	UW	I	CR	DP	WP
11:00	8.11 %	6.81 %	9.33 %	8.53 %	6.81 %
12:00	7.19 %	9.46 %	6.80 %	3.88 %	6.47 %
13:00	3.64 %	5.43 %	10.19 %	14.44 %	4.9 %
14:00	3.73 %	0.27 %	9.66 %	9.26 %	4.65 %
15:00	5.23 %	8.52 %	6.47 %	8.35 %	8.22 %
16:00	1.43 %	0.09 %	0.36 %	0.79 %	7.18 %

***Table 36 -** Percentage error between monitored and simulated values [%]*

Traditional window					
Time	Points				
	UW	I	CR	DP	WP
11:00	9.32 %	0.89 %	8.67 %	3.92 %	2.34 %
12:00	2.92 %	9.87 %	5.17 %	1.68 %	9.98 %
13:00	0.92 %	9.22 %	0.77 %	5.58 %	10.03 %
14:00	9.58 %	8.34 %	4.89 %	8.86 %	19.63 %
15:00	9.61 %	11.95 %	1.98 %	9.74 %	9.11 %
16:00	3.64 %	5.38 %	1.72 %	12.75 %	9 %

In both cases (SW-LSC and traditional window) the percentage errors calculated are around or below 10%, except for WP at 14.00 (traditional window case) that showed a higher error (19.63%), probably due to localized shading at the measuring point during the simulation phase.

In conclusion, however, the models are a good approximation of reality and resulted to be validated for the cases of the traditional window and SW-LSC. The calibrated models will be used in the whole building analysis.

5.2 Test building results

The daylighting monitoring study performed with a lux-meter made it possible to obtain the level of illumination in different points of the two rooms where the SW-LSC and the traditional window were installed.

The results of the monitoring are shown in Tab. 37 - 38.

***Table 37** - Illuminance values recorded during the monitoring study for and traditional window*

Traditional window - Monitoring results [lux]					
Time	Points				
	UW	I	CR	DP	WP
11:00	6900	26600	22400	22200	36300
12:00	6720	9700	50700	48200	61700
13:00	7530	55000	7050	4530	55500
14:00	6220	6690	4620	2640	7900
15:00	4390	4420	2930	1930	3720
16:00	1650	1710	1160	800	1700

***Table 38** - Illuminance values recorded during the monitoring study for SW-LSC*

SW-LSC - Monitoring results [lux]					
Time	Points				
	UW	I	CR	DP	WP
11:00	3500	4300	3740	3400	19800
12:00	3520	46800	46660	3560	44800
13:00	3350	47100	3240	2340	40600
14:00	3060	3300	2320	1760	2750
15:00	2220	2500	1730	1270	1850
16:00	910	1107	825	630	864

Results show that for the UW point, the presence of the light shelf allows to reduce excessive illuminance on the work plane. In general, in the case of the SW-LSC, the mix between the yellow light that filters from the LSC modules and that of the lower part window as well as the presence of light shelf, allows to obtain lower values of the illuminance in most points in the room.

The analysis of the electrical data relating to the SW-LSC made it possible to obtain the generation and consumption of the device. The analysis covered about two years of monitoring, from 30 April 2017 to 18 November 2019. Fig.35 and Fig.36 show the average monthly energy generated by LSC modules in SW-LSC and absorbed by electric motors during this period.

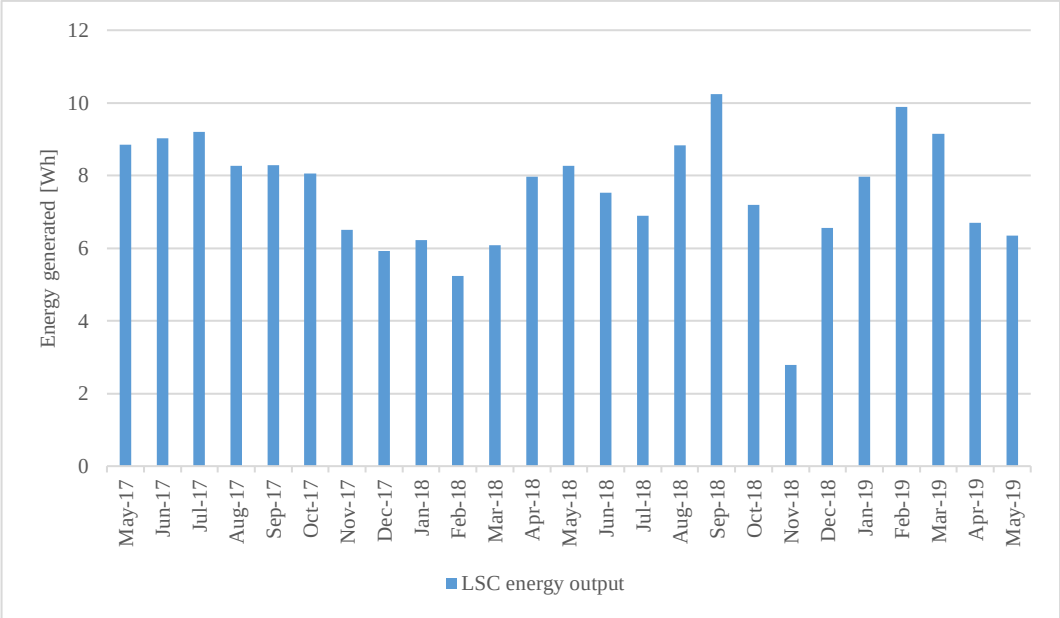

Figure 35 *- Average monthly electric energy generated [127]*

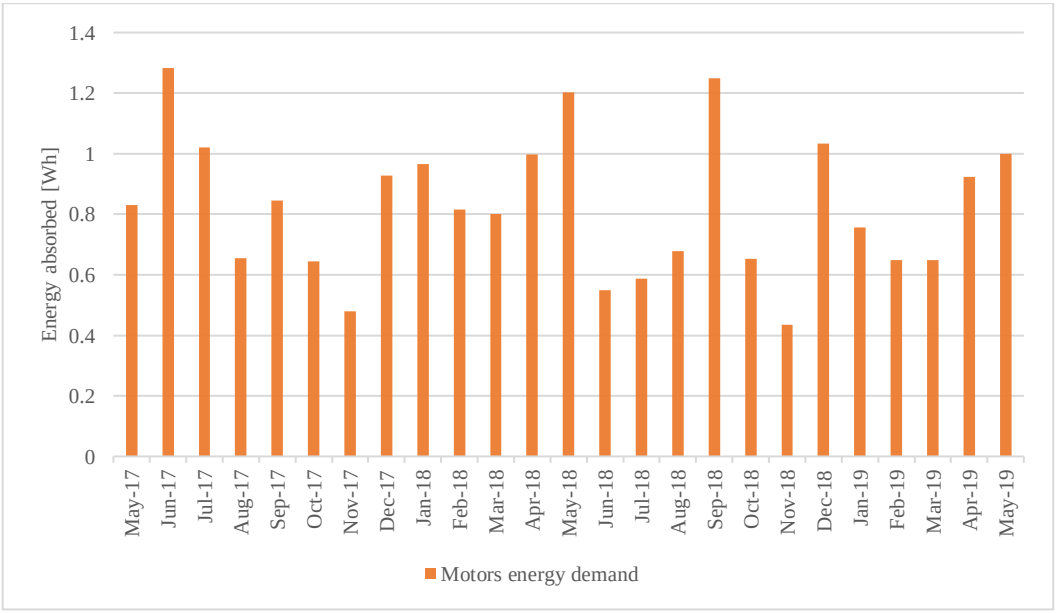

Figure 36 *- Average monthly electric energy absorbed [127]*

Then it was chosen to express the results of the data relating to 2018, which is the only one including an entire year. The net electricity generation for 2018 was approximately 1.5 kWh, with an average daily production of 5 Wh/day. Fig. 37 shows the net daily output for year 2018.

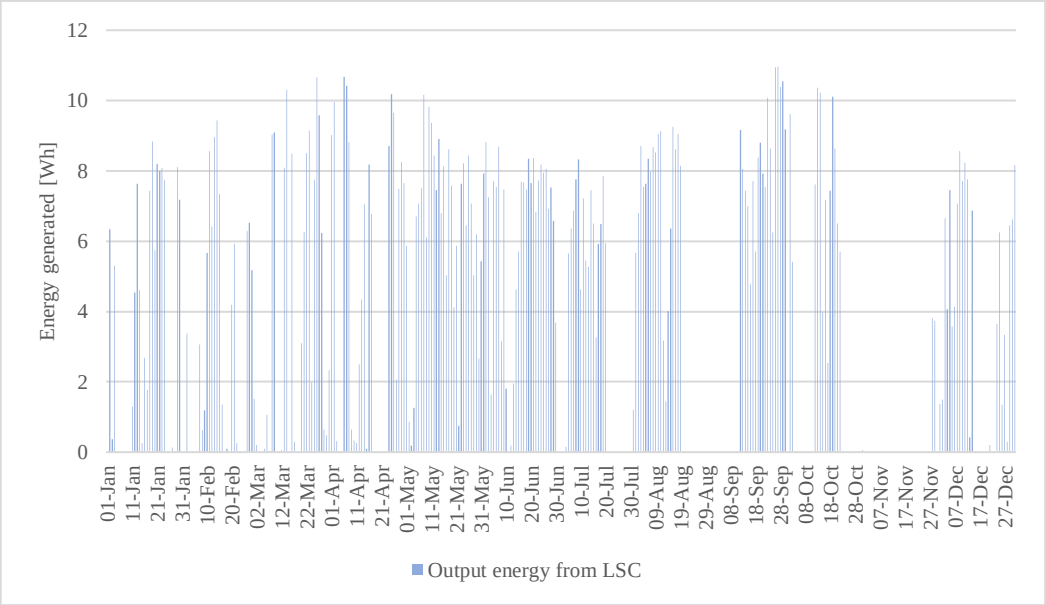

***Figure 37** - Output energy from LSC modules for year 2018 [127]*

The annual consumption was about 0.27 kWh, due to the movement of venetian blinds system and in rare cases, to the recharging of small devices connected via USB at the output of the production system. In some periods of high production, the non-consumed energy that exceeded the capacity of the batteries was released on a resistor. Fig- 38 shows daily energy consumption during the year 2018.

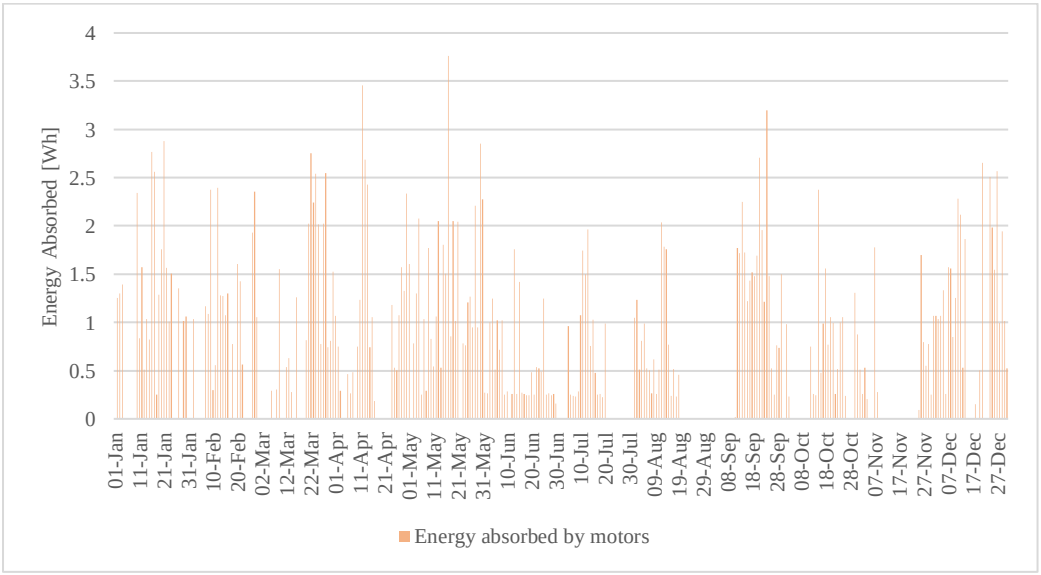

***Figure 38** - Energy absorbed by electric motors for year 2018 [127]*

The highest average monthly production was recorded in September (8.9 Wh) while the lowest (2.4 Wh) in November as shown in Fig. 39.

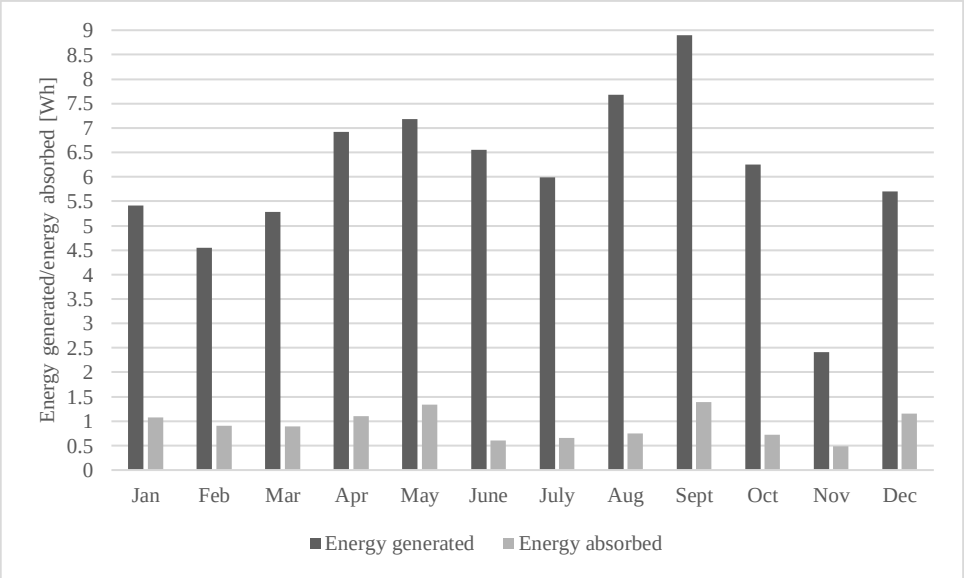

Figure 39 *– Monthly energy generated and absorbed for year 2018[128]*

The maximum net daily production was 11 Wh / day (September 26), while the maximum daily consumption was 3.7 Wh / day (May 17) as shown in Fig. 40 and Fig. 41.

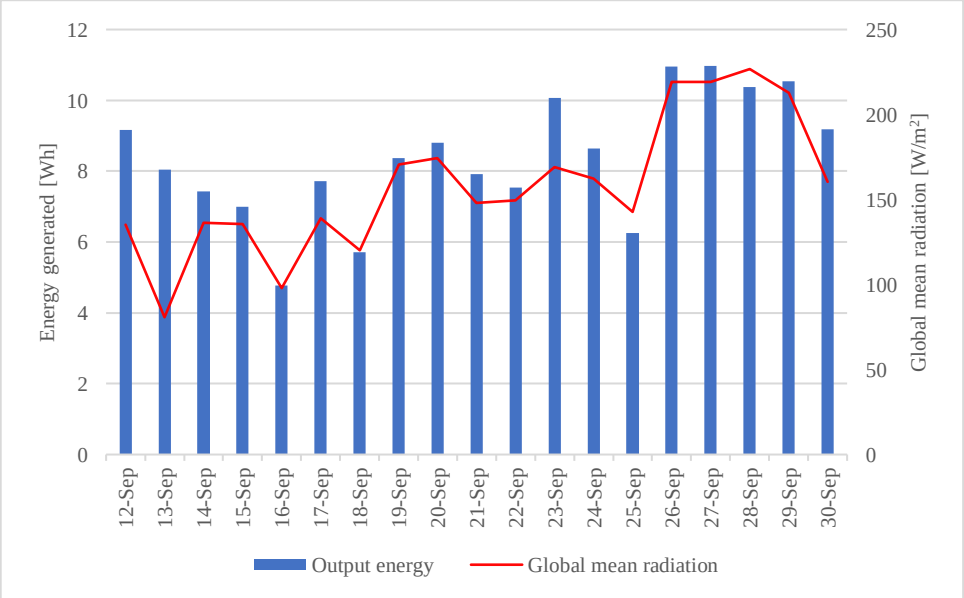

Figure 40 *– Daily energy generated during the period 12 - 30 September*

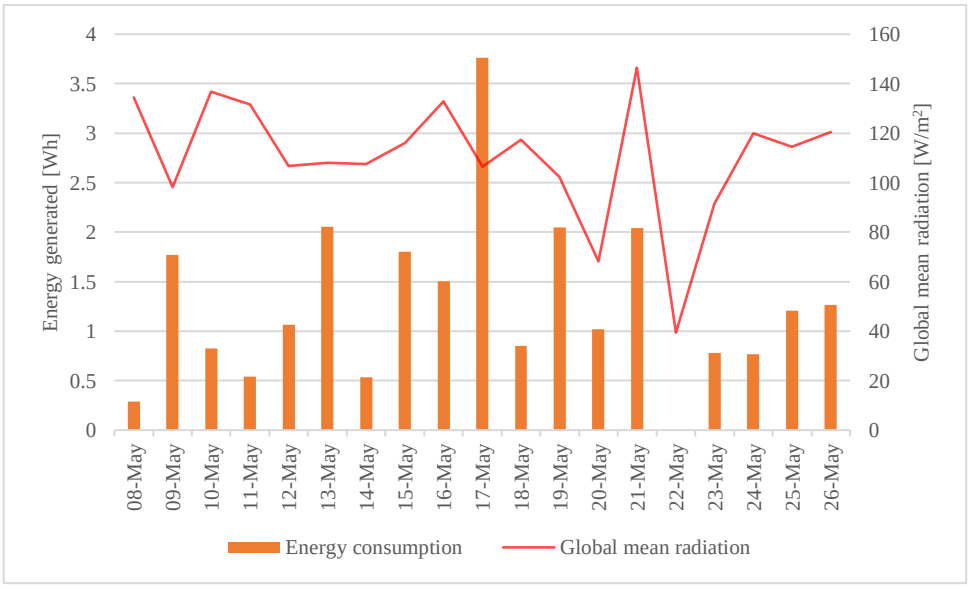

Figure 41 *– Daily energy absorbed during the period 08 - 26 May reported with global mean radiation*

It should be noted that consumption is strictly linked to the threshold set for the activation of the shadowing system and the climatic conditions. In fact, in some particular days of partial cloud, it may happen that the activation of the shading system occurs frequently due to oscillations above and below the threshold value, causing a higher consumption than normal, how showed in Fig. 42.

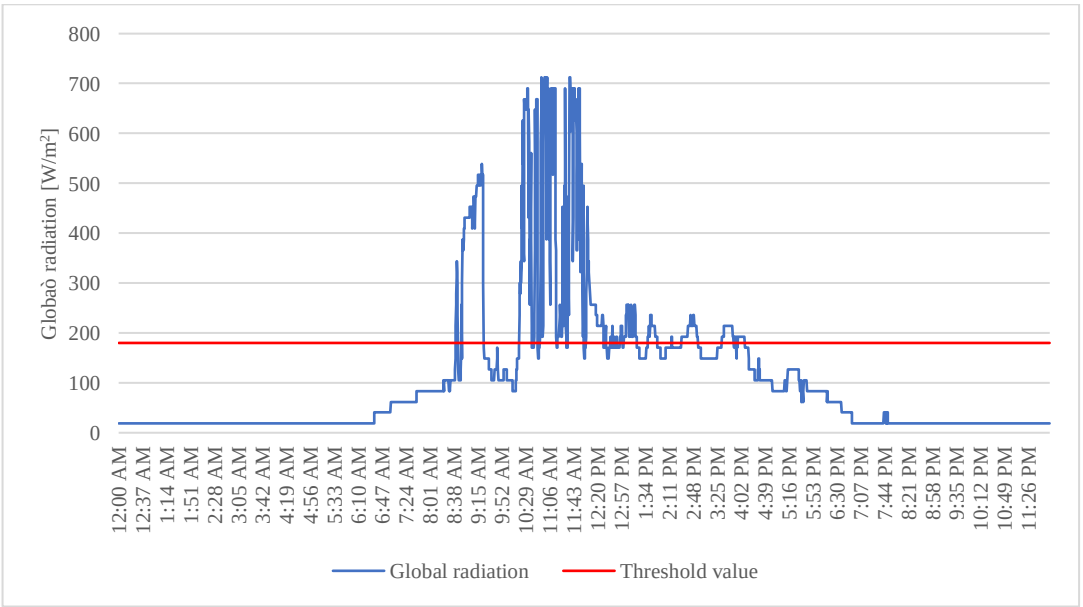

Figure 42 *- Daily irradiation trend (May 17 2018) compared with the threshold for the activation of venetian blinds (180 W/m²) [127]*

Generally, on totally sunny or totally cloudy days, the shading system makes a minimum of two movements, while on sunny but very variable days they can reach up to 10. For this reason, before the shading system is operated, the control system carries out repeated measurements over 15 minutes. If the radiation value remains in the activation range after 15 minutes, the shading system is activated.

In any case, thanks to the batteries and the characteristic of LSC modules, which generate electricity even with diffused radiation, there has never been a higher consumption than the energy stored and produced, even in continuous periods of low irradiation.

5.3 Whole building results

5.3.1 Daylight results

For the daylight analysis of the entire building, the annual calculation of the Daylight Autonomy (DA) is proposed to quantify the annual daylight and to determinate the level of direct sunlight both in the case of the SW-LSC and the traditional window. DA is defined as the percentage of time in a year that daylight can provide a given illuminance for a chosen point.

The method used (incremental method) expects that the illuminance of daylight must exceed the illuminance required for the given time. In this study we chose to analyze the DA for two values: a minimum threshold value of 300 lux and a maximum value of 500 lux, which is the recommended one for normal office work and PC work. The analysis period was a full year and we assumed the occupied hours to be standard office work hours from 8am to 6pm and 9am to 5pm, depending on the season. In both cases (SW-LSC and traditional) no blind system were taken into account, since it would have been onerous for the calculation to predict both the automatic movement of the Venetian blind and manually operation of the traditional window shading system. In addition, no blind system was considered in the test building analysis. An acceptable value of DA has been set at 50%, i.e. if the set threshold of illuminance has been reached for at least 50% of the hours during the year.

The illuminance map grills were created for all four perimeter areas of the building (facing north, south west and east) excluding the central area and the attic, which are not equipped with windows and are not exposed to direct solar radiation. The illuminance map grills cover most of the area useful for office work, excluding the perimeter areas of the rooms, as shown in Fig 43.

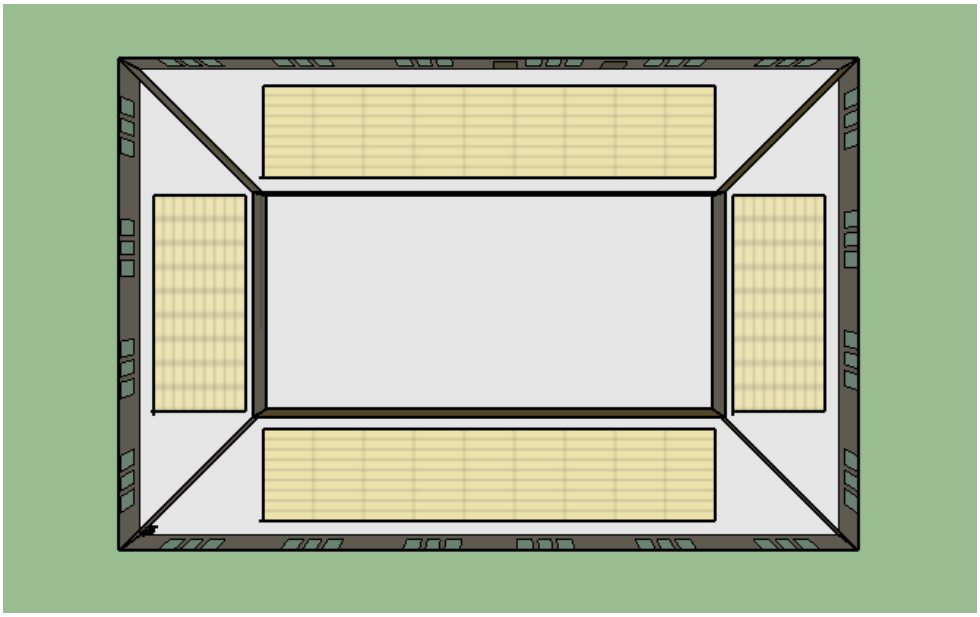

Figure 43 *– Illuminance maps grill for the whole building*

Within the illuminance map grill, three useful and strategic points were chosen for each room, where the limit values in which to analyze the DA were set. These points are: left point (LP), central point (CP) and right point (RP). The results of analysis are show in the following Tab.39:

Table 39 *– Daylight autonomy (DA) for the reference points*

	SW-LSC_South zone			**Traditional_South zone**		
	LP	CP	RP	LP	CP	RP
DA_{300}	56 %	58 %	56 %	65.8 %	68.5 %	65.9 %
DA_{500}	43.2 %	46.1 %	43.6 %	57.1 %	61.2 %	57.0 %
	SW-LSC_East zone			**Traditional_East zone**		
	LP	CP	RP	LP	CP	RP
DA_{300}	40.3 %	55.0 %	63.1 %	57.7 %	67.4 %	71.5 %
DA_{500}	22.7%	37.1 %	51.5 %	41.5 %	55.8 %	63.2 %
	SW-LSC_North zone			**Traditional_North zone**		
	LP	CP	RP	LP	CP	RP
DA_{300}	42.9 %	43.6 %	38.9 %	63.0 %	62.8 %	62.8 %
DA_{500}	16.3 %	16.9 %	11.2 %	44.0 %	44.4 %	44.1 %

	SW-LSC_West zone			Traditional_West zone		
	LP	CP	RP	LP	CP	RP
DA_{300}	63.1 %	59.5 %	42.2 %	71.6 %	66.0 %	58.9 %
DA_{500}	51.9 %	44.3 %	23.6 %	63.4 %	54.1 %	43.3 %
	SW-LSC_TOT			**Traditional_TOT**		
	LP	CP	RP	LP	CP	RP
DA_{300}	50.9 %	54.2 %	50.1 %	64.0 %	65.8 %	64.3 %
DA_{500}	33.2 %	35.5 %	31.8 %	51.4 %	53.7 %	51.9 %

The results show that the traditional window generally allows to obtain higher DA values in both cases (300 lux and 500 lux). Considering the single zones, the traditional window made it possible to reach the desired value of DA300 (50%) in all points; LP of East zone, all point of North zone and RP of West zone showed a threshold percentage of less than 50% for DA500. Considering the entire building, the threshold of 50% was reached for both DA300 and DA500.

Regarding SW-LSC, considering the single one, DA300 (50%) was reached in all points except LP of East zone, all points of North zone and RP of West zone. It was not possible to reach the 50% threshold in the case of DA500 in most points, except for the RP points of East zone (51,5%) and LP of West zone (51,9 %). Considering the whole building, the 50% threshold was reached in the case of DA300 but not in the case of the DA500. This is due both to the characteristic of SW-LSC and to the presence of the light shelf, which in any case has the beneficial effect of reducing glare phenomena near the window and guaranteeing greater uniformity of the radiation inside the rooms thanks to the reflection of the same towards the ceiling. This can be observed by analysing and comparing all points (10x10) of the illuminance maps created. For this purpose, five categories have been defined:

- low daylight (< 300 lux);
- acceptable daylight (between 300 and 500 lux);
- medium daylight (between 500 and 1000 lux);
- high daylight (between 1000 and 2000 lux);
- very high daylight (> 2000 lux).

The categories and ranges have been chosen considering the final destination of the analyzed building which is that of an office. The results of the analysis are expressed as a percentage of points for which the illuminance value was that established in the range considered (Tab 40).

Table 40 *- Percentage of points in the illuminance map with an illuminance value that falls within the defined range*

Illuminance range	**SW-LSC**				**Traditional window**			
	North	South	West	East	North	South	West	East
>300	48.8%	34.9%	38.6%	39.5%	29.7%	25.2%	26.7%	27.1%
300 < x < 500	28.8%	12.6%	17.5%	17.7%	18.8%	8.5%	12.3%	13%
500 < x < 1000	17.8%	24.8%	21.6%	20.8%	38.2%	17.3%	24%	24.1%
1000 < x 2000	3.9%	18.3%	14.7%	14.3%	10.9%	26.2%	20.3%	19.1%
< 2000	0.7%	9.4%	7.6%	7.7%	2.4%	22.8%	16.7%	16.7%

Tab. 38 shows that in the case of SW-LSC there are more points whose illuminance value falls in the area between 300 and 500 lux (acceptable daylight). In the case of the traditional window, the percentage of points which falls in the area of “high daylight” and “very high daylight” is average more than 6% and 8% if compared to the case of SW-LSC in the same range.

5.3.2 Thermo-physical results

The results related to the thermo-physical analysis are shown in the following figure (Fig. 44 to 49). First the monthly heat balance in the small office was calculated for traditional window and SW-LSC model (Fig. 44 – 45); then the daily heat balance (heating and cooling) (Fig.46-47) and the heat gain/loss from windows (Tab. 39) for the selected four days, and for the day before and after the reference day, were calculated. Results refer to the total heat balance relating to the four peripheral areas and the central area; the attic was always excluded.

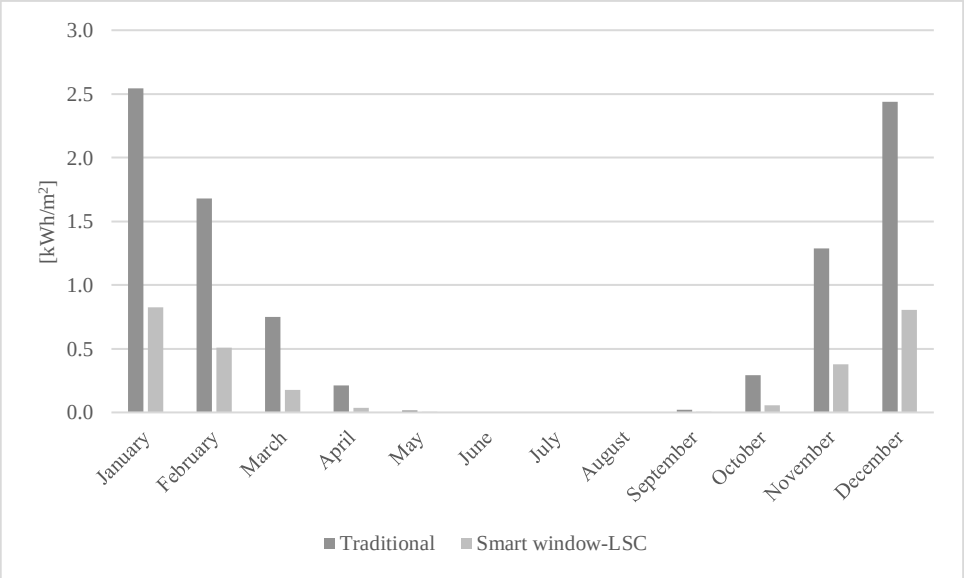

***Figure 44** - Monthly heating requirements for the two alternatives*

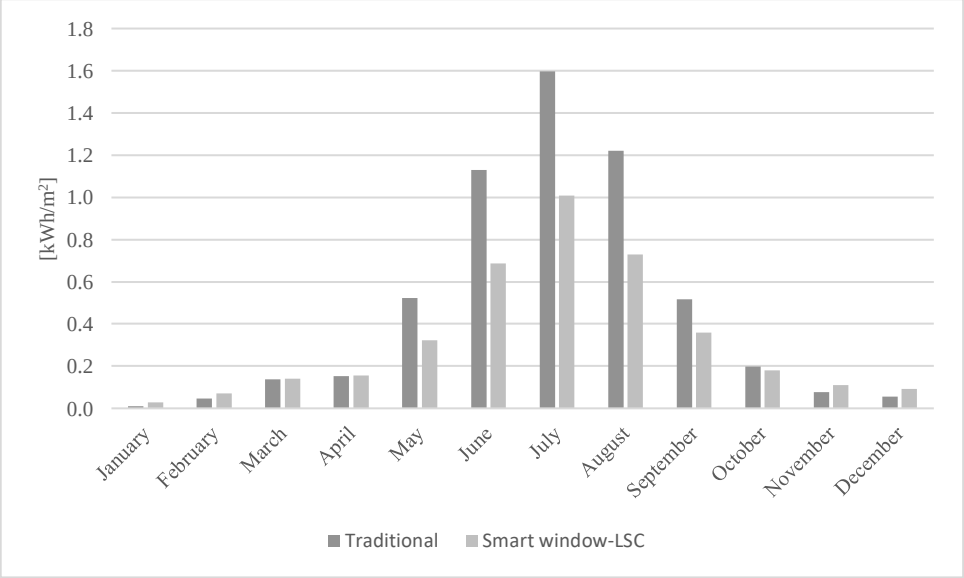

***Figure 45** - Monthly cooling load for traditional window and SW-LSC office models*

Fig 46-47 show that for the traditional window scenario, the monthly heating load is always higher than in the SW-LSC scenario (from 200 to 300%); the highest difference is recorded in January and it is equal to 1,723 kWh / m^2.

In the case of the cooling load, the scenario of the traditional window shows higher values (from 10 to 67%) from May to October; the highest difference is recorded in July and is equal to 0.589 kWh/m^2.

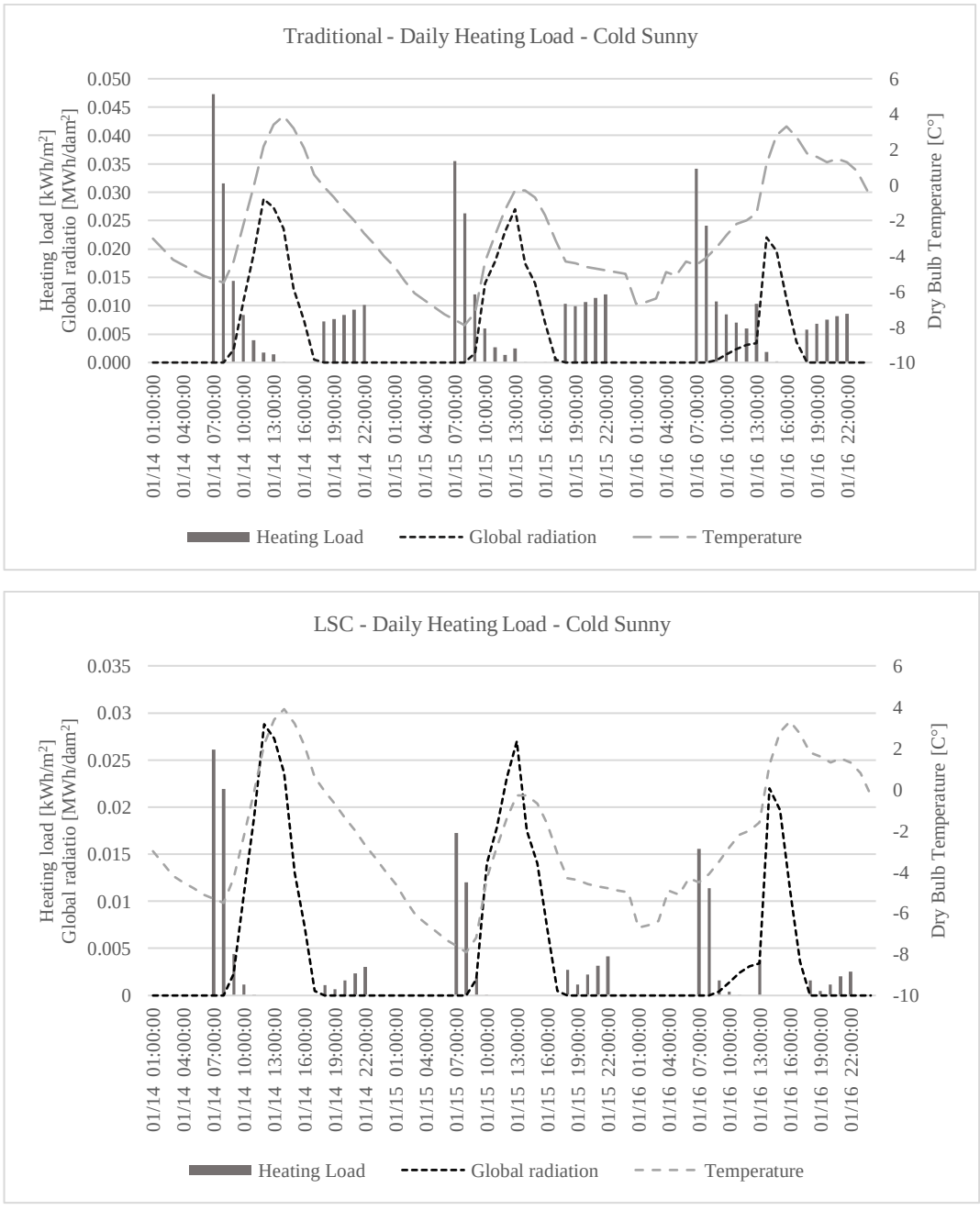

Figure 46 *- Daily Heat balance for traditional window and SW-LSC (cold sunny period)*

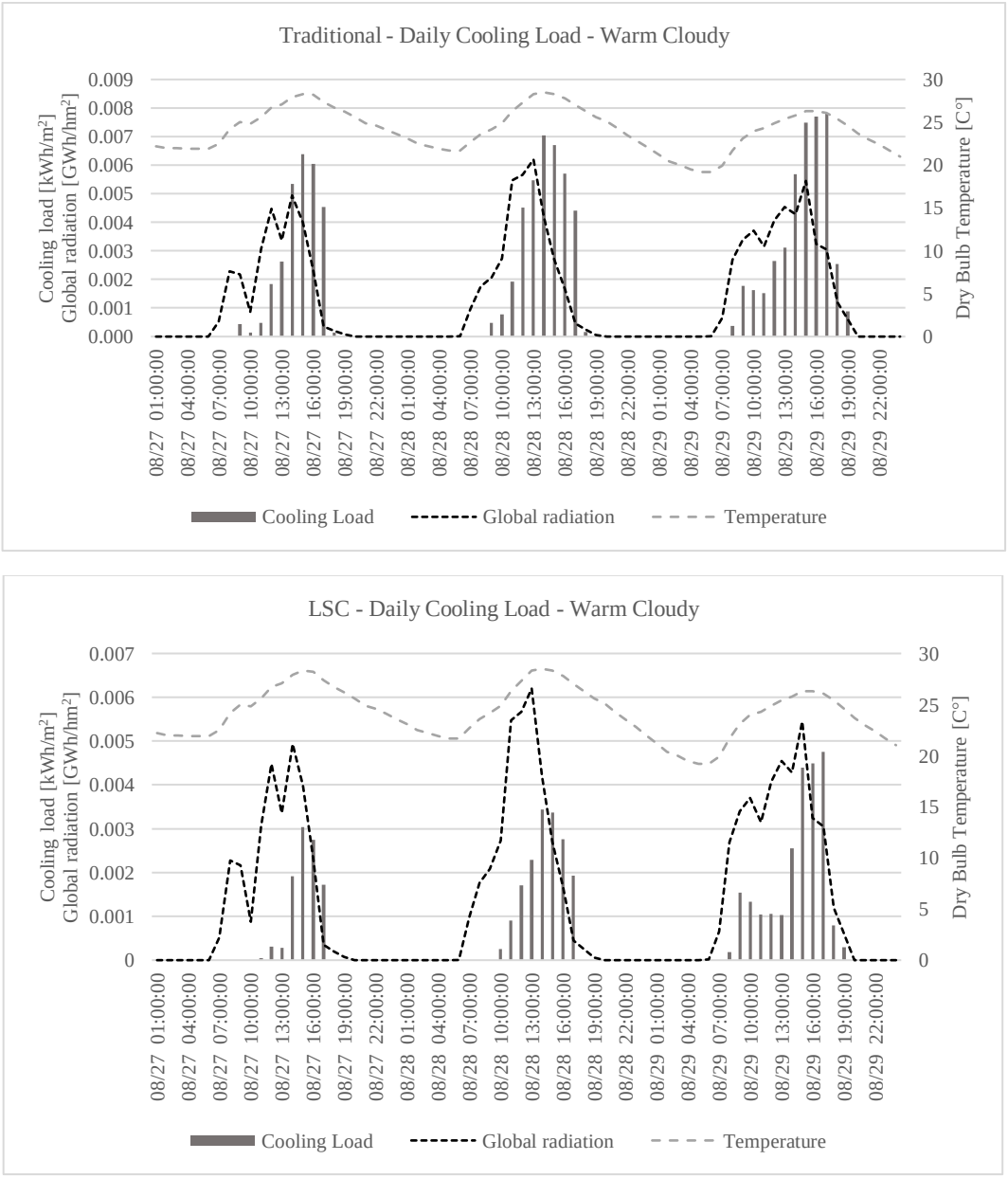

***Figure 47** - Daily Heat balance for traditional window and SW-LSC (warm cloudy period)*

The results showed that:

- During the cold sunny period (14 – 16 January), the maximum heating energy demand for the traditional window scenario occurs was 0.048 kWh/m^2. For the reference day (1/15) this value was 0.035 kWh/m^2. The maximum heating energy demand for the SW-LSC scenario was 0.026 kWh/m^2 (1/14) while for the reference day was 0.017 kWh/m^2.

- During the cold cloudy period (23 – 25 December), the maximum heating energy demand for the traditional window scenario was 0.033 kWh/m^2. For the reference day of this period (12/24) this value was 0.031 kWh/m^2 at 07.00. The maximum heating energy demand for the SW-LSC scenario was 0.015 kWh/m^2 (12/25) while for the reference day was 0.014 kWh/m^2. Thanks to a higher mean temperature (-1.6°C), the heating energy demand is lower if compared with those of the cold sunny period (Tm = -2.6°C; MeanGlobHorRad = 119.5 W/m^{2}K) for both scenarios, despite the lower solar input caused by the presence of clouds (83.1 W/m^{2}K).

- During the warm sunny period (21 – 23 July), the maximum cooling energy demand for the traditional window scenario was to 0.015 kWh/m^2 (7/22). The maximum cooling energy demand for the SW-LSC scenario was 0.0095 kWh/m^2 (7/22).

- During the warm cloudy period (27 – 29 August), the maximum cooling energy demand for the traditional window scenario was 0.008 kWh/m^2 (8/29); for the reference day (08/28) this value was 0.007 kWh/m^2. The maximum cooling energy demand for the SW-LSC scenario was 0.0048 kWh/m^2 (8/29). For the reference day (08/28) this value was 0.0035 kWh/m^2. Due to the lower solar radiation and mean temperature (Tm = 24.3 °C; MeanGlobHorRad = 255.7 W/m^{2}K), the cooling energy demand is lower if compared with those of the warm sunny period (Tm = 27.1°C; MeanGlobHorRad = 533.9 W/m^{2}K) for both scenarios.

These results are strictly related to the different optical and thermal characteristics of the two windows; in particular the u-value, which is significantly lower in the case of the SW-LSC.

Table 41 summarizes the results for heat gains and loss in both scenarios.

Table 41 *– Heat gain and loss for traditional window and SW-LSC scenarios*

	Cold sunny day (01/15)	
	Traditional window	SW-LSC
Max heat gain	0.0055 kWh/m^2	0.007 kWh/m^2
Max heat loss	0.013 kWh/m^2	0.0045 kWh/m^2
	Cold cloudy day (12/24)	
	Traditional window	SW-LSC
Max heat gain	0.011 kWh/m^2	0.003 kWh/m^2
Max heat loss	0.012 kWh/m^2	0.003 kWh/m^2
	Warm sunny (7/22)	

	Traditional window	SW-LSC
Max heat gain	0.024 kWh/m^2	0.016 kWh/m^2
	Warm cloudy (8/28)	
	Traditional window	SW-LSC
Max heat gain	0.021 kWh/m^2	0.011 kWh/m^2

5.3.3 Electricity balance

The whole building was finally analyzed from the point of view of electricity consumption, both in the cases of SW-LSC and of traditional window. Furthermore, the electricity generation of SWs-LSC installed in the south perimeter of the office building was quantified. It was decided to use only the south-facing façade since the experimental data collected on the prototype refer to this direction of exposure.

The electricity consumption in the office building was divided in interior lighting, external lighting and internal equipment. Since the difference of the two models (SW-LSC and Traditional) refer only on the characteristics of the windows, the electricity consumption gap between the two cases regarded only internal lighting, how can be seen in Tab. 42.

***Table 42** - Electrical consumption for whole building case*

	Traditional	SW-LSC
Interior Lighting	11619.44 [kWh]	11702.78 [kWh]
Exterior Lighting	1597.22 [kWh]	
Interior Equipment	13716.67 [kWh]	

The use of the traditional window involves an electrical energy saving of about 83 kWh per year for internal lighting. As confirmed by daylighting tests, the perimeter areas of the building have a higher DA and this also affects electricity consumption.

As regards the generation of electricity by the SW-LSCs, the relationship obtained statistically in the paragraph was exploited.

Since LSC modules also generate energy with diffuse radiation, the calculation of the generated energy refers to all the radiation that hits the upper part of the SW-LSC, also considering the diffuse component from the sky and the ground.

The results of the analysis showed that, for the office building, the SW-LSC (6 m^2 modules) facing south allowed to produce 22 kWh of electric energy. In the case of

the building analyzed, the shape of the roof penalized the possibility of generating energy in the months with high global radiation as shown in Fig.48.

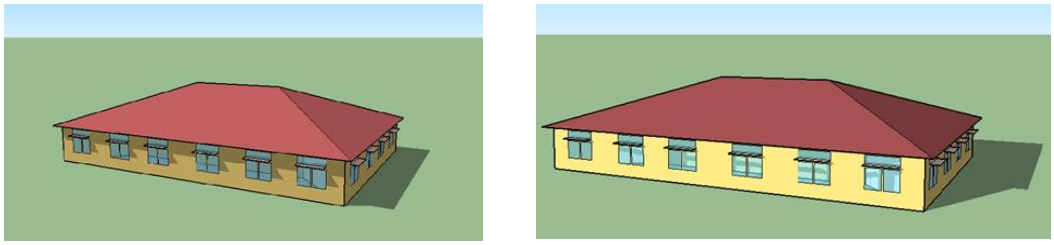

Figure 48 *– Smart windows exposed to south in the whole building model*

In fact, due to the solar position during the period from April to October, the modules are often shaded and therefore the generation of energy is reduced compared to other months (from October to March).

A further simulation was carried out in order to exclude the shading caused by the roof and to evaluate the full production potential for the SWs-LSC facing south. The results showed that, in this case, the electric generation is 59 kWh/year, with an increase of 62% compared to the previous case.

Further studies and investigations will be necessary in order to determine the potential for generating electricity for exposures other than the south, finding a relationship between irradiation and generation and evaluating the production for the other SWs-LSC installed in the building.

5.4 LCA results

The main results of the life cycle assessment study (excluding EOL phase) are showed in Tab.43

Table 43 *- Environmental impacts of SW-LSC*

Impact categories	Unit	Total	Production	Assembly	Maintenance
Abiotic depletion potential	kg Sb eq	3.08E-02	3.04E-02	3.00E-07	3.82E-04
Abiotic depletion potential (fossil fuels)	MJ	5.63E+04	5.42E+04	3.59E+00	2.11E+03
Global warming potential	kg CO2 eq	5.91E+03	5.76E+03	4.02E-01	1.45E+02
Ozone layer depletion potential	kg CFC-11 eq	2.20E-04	2.10E-04	1.55E-08	1.01E-05
Human toxicity	kg 1,4-DB eq	5.28E+03	5.26E+03	3.51E-01	2.03E+01
Fresh water aquatic ecotox.	kg 1,4-DB eq	3.57E+03	3.56E+03	2.21E-01	1.56E+01
Marine aquatic ecotoxicity	kg 1,4-DB eq	4.67E+07	4.67E+07	3.31E+03	4.85E+04
Terrestrial ecotoxicity	kg 1,4-DB eq	1.21E+01	1.19E+01	1.36E-03	1.60E-01

Photochemical oxidation potential	kg C2H4 eq	2.01E+00	1.98E+00	1.39E-04	3.00E-02
Acidification potential	kg SO2 eq	3.26E+01	3.20E+01	2.31E-03	5.57E-01
Eutrophication potential	kg PO4--- eq	8.39E+00	8.30E+00	5.60E-04	8.89E-02

Results include the SW-LSC elements production, the assembly phase and the maintenance, which consist of the substitution (1 time) of LSC modules during the life cycle of the SW-LSC. The assembly phase is manly carried out by hand, as well as the replacement of the modules. For this reason, the assembly phase impacts could to be considered negligible (about 0,01% of total impacts); the maintenance phase impacts (around 2% of total impact) coincide with the impacts referred to the production of new LSC modules. The production phase contributes more than 96% in all categories, as might be expected from a hand-assembled prototype, not large-scale produced.

Considering only the production phase, SW-LSC components contribution to the impact categories is shown in Fig. 49.

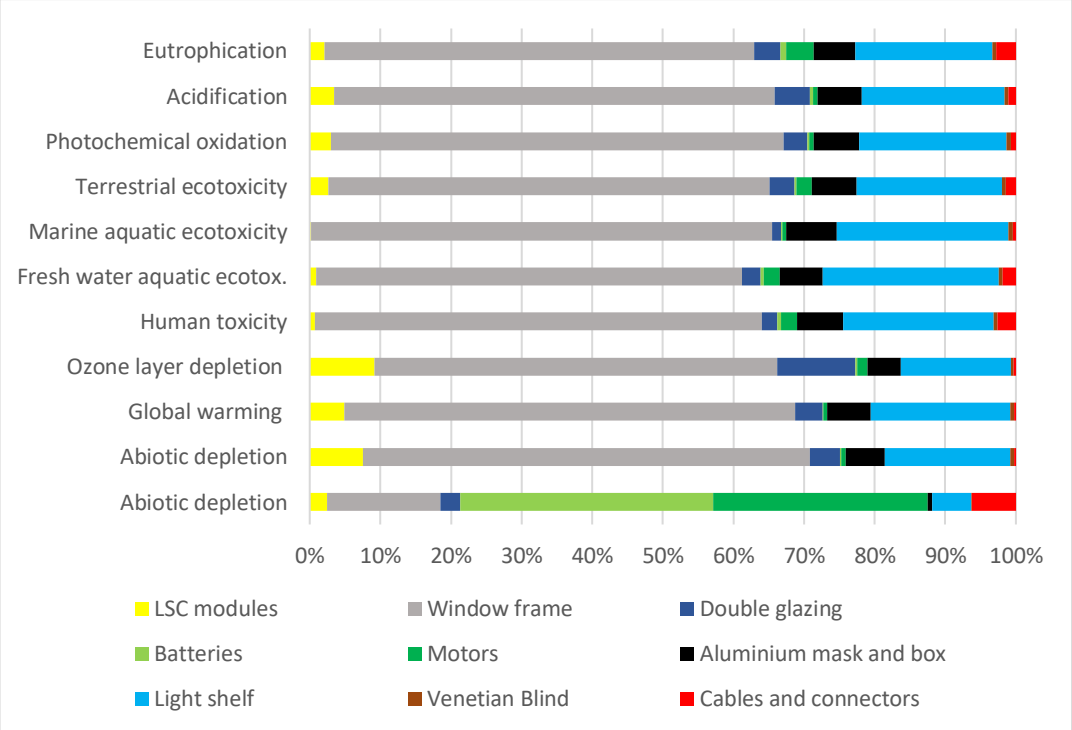

***Figure 49** – Contribution of SW-LSC elements*

The most impactful components of SW-LSC system in the base scenario are:

- Window frame: the contribution of this component to the environmental impact was above 60% in all categories, from 59. 78% (ODP) to 65.80% (ADP fossil fuel), except for ADP where the contribution was 16.22%.
- Light shelf: the contribution of this component ranged from 16.29% (ODP) to 25.02% (FE) in all categories, except ADP where the contribution was only 5%.
- DC motors and batteries: these components had a great contribution (30.74% and 36.26%, respectively) in ADP but a low contribution (less than 4% for DC motors and 1% for batteries) in all other categories.

Aluminum box and mask had a mean contribution of 6% in all categories, from 4.96% (OPD) to 7.24% (ME), except for ADP where it was less than 1%. The other components of the system had an impact lower than 5% in all categories; the only exception is the window glazing which was the third contributor to ODP (11.52%). These results show that the aluminum frame is one of the most impacting elements in the life cycle of a window. This is due both to the higher percentage of the material in the total structure and to the fact that its processing requires extremely energy-intensive processes. The impact of batteries and motors is limited to the ADP category, since these elements involve a greater use of raw materials raw materials or specific materials characterized by limited availability and high-quality value, compared to other SW-LSC elements. A limitation to these results is that it was not possible to calculate the energy saving potential related to the use the light shelf and the venetian blind system and, consequently, it is not possible to make an overall balance between the benefits and the environmental burdens that these elements can add to the system as a whole.

It should be noted that the LSC modules, which represent one of the main elements of the system, provide a low contribution in all categories, from 0.39% (HT) to 4.82% (ODP). However, it is useful to report the relative impact of the various components of LSC modules, which is shown in Fig. 50

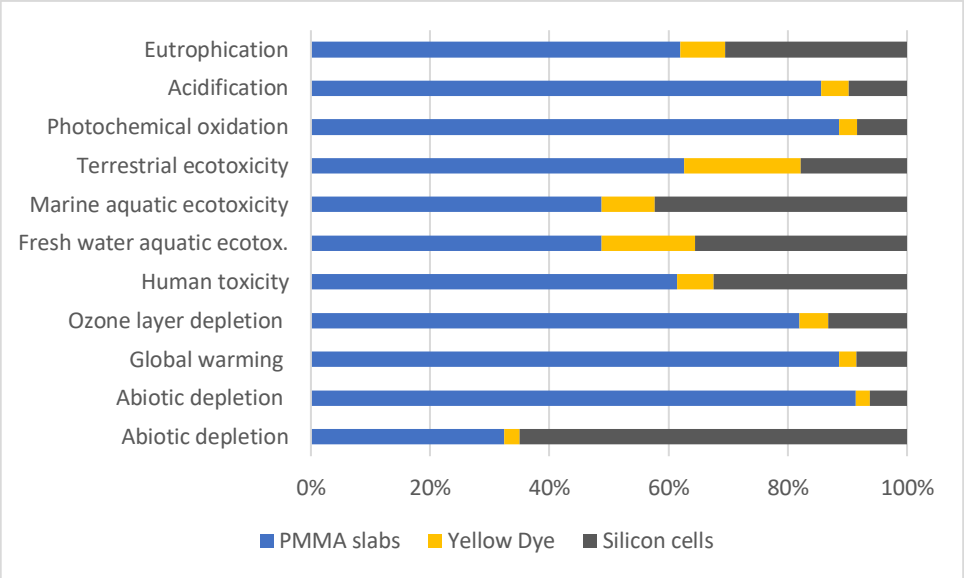

Figure 50 *– Environmental impacts of LSC module (1 m^2)*

Considering the LSC module, the major contributors in all categories (except ADP) are PMMA slabs (from 32% (ADP) to 91% (ADP fossil fuel), followed by the photovoltaic cells (from 6% (ADP fossil fuel) to 65% (ADP)) which are the major contributors in ADP category. The contribution of the dye is lower than 8% in all categories, except fresh water ecotoxicity (16%) and terrestrial ecotoxicity (20%).

Considering the EOL phase, the impacts connected with the disposal / landfill phase were analyzed together with the credits deriving from the recycling (aluminum and glass) and the energy obtained from the PMMA incineration. The total impacts could be reduced by the following percentages (Tab.42).

Table 42 *– Total impacts and credits*

Impact categories	Total	Disposal	Credits from recycling	Reduction (%)
Abiotic depletion potential	2.73E-02	1.81E-05	-2.17E-02	80%
Abiotic depletion potential(fossil fuels)	5.33E+04	4.40E+01	-1.79E+04	36%
Global warming potential	5.67E+03	2.85E+00	-4.36E+03	79%
Ozone layer depletion potential	2.06E-04	3.72E-07	-1.13E-04	60%
Human toxicity	5.04E+03	1.48E+00	-1.20E+03	25%
Fresh water aquatic ecotox.	3.26E+03	1.98E+00	-1.68E+03	52%
Marine aquatic ecotoxicity	4.53E+07	2.77E+03	-6.01E+06	14%
Terrestrial ecotoxicity	1.15E+01	5.68E-03	-3.56E+00	32%
Photochemical oxidation potential	1.94E+00	1.05E-03	-7.40E-01	40%
Acidification potential	3.13E+01	1.76E-02	-1.18E+01	40%

Eutrophication potential	7.94E+00	5.01E-03	-3.10E+00	41%

5.4.1 Alternative scenario

As already mentioned, the alternative scenario (recycled aluminum scenario) involves the use of 75% recycled aluminum during the manufacturing of the window frame. The recovery of the aluminum comes from remelting shredded, sorting and decoating of post-consumer scrap; the remaining percentage of aluminum in the final product comes from process scrap (10%) and primary ingots (15%). Compared to the base scenario, the presence of recycled aluminum is the only difference in the inventory of the SW-LSC. The results of the comparison between the base scenario and the recycling scenario is shown in Fig.51

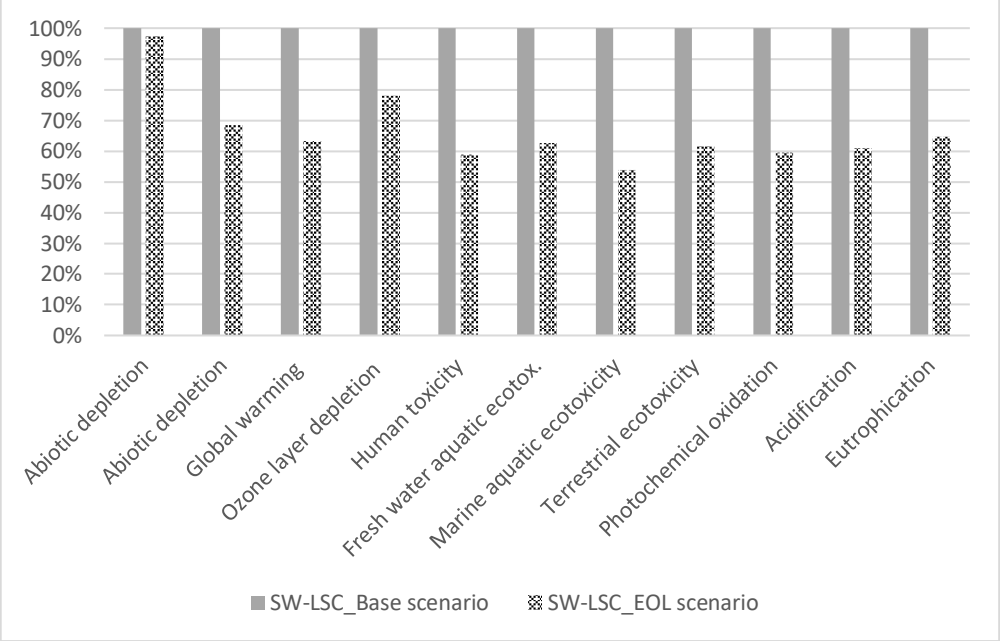

Figure 51 *– Comparison between Base scenario and Recycling (EOL) scenario for the SW-LSC*

The use of aluminum with a recycled content of 75% in the window frame allows to reduce the impacts in all categories, from 3% (ADP) to 46.% (ME). The reduction in ADP category was mainly due to aluminum; however, this reduction is attenuated due to the processes connected with recycling itself and the presence of substances such as zinc and copper, which are always present in aluminum scraps. The reduction in the ADP (fossil fuel) category is mainly due to less energy-intensive

processes than those related to the production of primary aluminum, and the consequent reduction in the use of energy carriers such as coal, gas and crude oil. The reduction for AP and EP categories is respectively related to lower emissions into air of ammonia (-16%), nitrogen oxides (-39%) and sulfur dioxide (-39%) for AP and on water emission of phosphate (-35%) and nitrate (-29%) for EP. The reduction for FE category was mainly related to lower beryllium (-21%), copper (-28%), nickel (-36%) and vanadium (-46%) emissions on water. HT and ME categories were related to the reduction of hydrogen fluoride (-49%), TE to the reduction of mercury (-42%) while for PO to the reduction of sulfur dioxide (-40%) and carbon monoxide (-46%). The reduction in ODP was mainly related to methane (-29%).

5.5 Comparisons of LCA results

5.5.1 Comparison of SW-LSC with other windows

In this section, a comparison between the impacts connected to SW-LSC with other types of windows has been made. The impacts connected with other windows were obtained from the environmental product declarations (EPDs). The results were compared on the basis of 1 m^2 of product and considering the same system boundaries (from cradle to gate with options); the disposal phase is always considered. The contribution of reuse, recovery and recycling phase was analyzed separately. According to EN-17213, indicators calculated for standard size windows can be scaled divided by their real size in order to declare environmental impacts and other parameters per 1 m^2 of product. The comparison was made using the EPD2008 method, the one used in the EPDs analyzed [153,155,156,157,158,159]. The environmental indicators were GWP, ODP, POCP, AP, EP, ADPE.

It is important to point out that the comparison made on the basis of windows size (m^2) instead of their characteristics (thermal transmittance of window (Uw) and frame (Uf)) is useful, but also limited: different results should be compared if the thermal transmittance of the window is coincident. In general, Uf is linked to the dimensions and materials constituting the frame system (and thus to their masses) with a direct consequence on the environmental loads of the production phase. Even if some quantities are fixed (for example the geometry of the element), the other variables (such as Uf, frame mass and composition) remains mutually interdependent and this cause a non-linear variation of the overall environmental loads, in particular of those relating to the production and use phases [155]. This underlines the difficulty in comparing the windows lifecycle and the need for more detailed guidelines that make it easier to analyze these aspects.

The characteristics of the windows analyzed are shown in table 43.

Table 43 *- Characteristics of SW-LSC and windows from EPDs*

Window Type	Glazing	Size	U-value (glass = g; window = w; frame =f)
W1 - wood frame and aluminum cladding	Triple-glazing	1.23 m x 1.48 m	Ug = 0.78 W/m²K

W2 - PVC frame and a transparent glass filling	Insulated double-glazing	1.23 m x 1.48 m	Uw = 1.3 W/m²K Ug = 1.1 W/m²K
W3 - PVC frame and a transparent glass filling	Insulated triple-glazing	1.23 m x 1.48 m	Uw = 0.92 W/m^{2}K Ug = 0.6 W/m^{2}K
W4 - thermal-break frame and glass-fibre-reinforcement	Double-glazing	3.0 m x 2.4 m	Uf = 3,7 W/m^{2}K
W5 - mixed frame (aluminum, multi-isolator composite material, wood)	Triple-glazing	1.23 m x 1.48 m	Uw = 0,63 W/m^{2}K
W6 - thermal break aluminum frame	Double-glazing	1.23 m x 1.48 m	Uw = between 1 and 2.1 W/m^{2}K
SW-LSC	Coated double-glazing	2.342 m x 2.252 m	Uf = 1.9W/m^{2}K; Ug = 1.1 W/m^{2}K

It should be noted that the SW-LSC prototype was analyzed in its entirety, considering the venetian blind system, the light shelf and the accessory components that allow the device to function. For the other windows, no shading system was present, and the impacts were mainly related to elements such as frame and glazing.

The results were compared for two scenarios: in scenario 1, the impacts for the product stage, construction, installation and disposal were analyzed. In scenario 2, the (negative) contribution of the potential for reuse, recycling and recovery is also considered. In particular, scenario 2 considered the following credits for the various windows:

- W1: energy from incineration and scrap metal recovered from the ashes (electricity, thermal-energy, raw materials).
- W2: energy (thermal energy and electricity) respectively the recycled material resulting from thermal and material utilization.
- W3: energy (thermal energy and electricity) respectively the recycled material resulting from thermal and material utilization.
- W4: credits deriving from the end of life scenarios; glass (50% landfilling and 50% recycling), non-glass metals (5% landfilling and 95% recycling), non-glass plastic (5% landfilling and 95% incineration with energy recovery).

- W5: energy from incineration and scrap metal recovered from the ashes (electricity, thermal-energy, raw materials).
- W6: No credits were considered.
- SW-LSC: credits deriving from the end of life scenarios; glass (62% recycling), aluminum (80% recycling), energy recovery from PMMA incineration.

The comparison results are shown in the following graphs (Fig. 52):

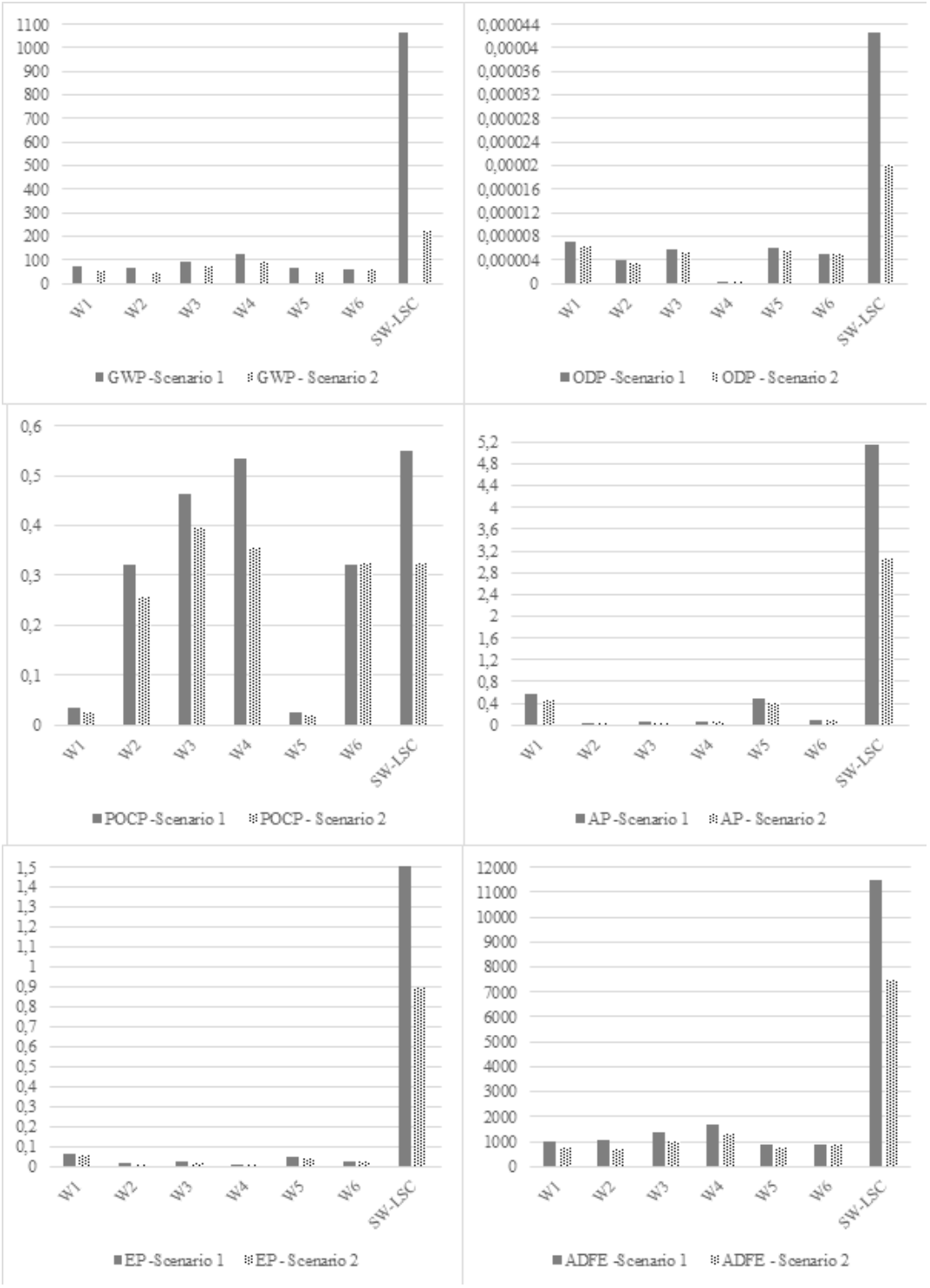

***Figure 52** - Environmental impacts of windows in scenario 1 (base) and scenario 2 (credit)*

The results showed that the impacts related to SW-LSC are higher than those of traditional windows in all categories; this is mainly due to the greater quantity of aluminum per m^2 (considering the mask, the box and the light shelf), the shading

system (Venetian blinds) and the accessory elements that allow autonomous and independent operation. As already mentioned, the SW-LSC prototype could be optimized through the use of alternative materials (such as wood) in the future. Furthermore, it must be taken into account that the analysis considered the autonomous shading system, which the other windows did not have. This aspect, not directly visible in the results, has important implications in the use phase, since the SW-LSC allows to manage the thermal loads passively and without energy consumption (since it is compensated by the energy generation LSC modules).

The recovery and recycling options allow to reduce this difference, especially for the POCP category, in which the impacts of SW-LSC resulted to be lower than W3 and W4 windows, and equal to that of W6 window.

5.5.2 Comparisons of LSC with other PV modules

In this section, the environmental impacts of the LSC modules were compared with other photovoltaic technologies on the basis of two different functional units: the m^2 of module and the kWh of electricity produced. The data relating to the other photovoltaic modules were taken from the Ecoinvent database. First, the results were compared using 1 m^2 of module surface as FU, using the CML-IA method. The choice of m^2 lies in the final application foreseen for LSC modules, which is that of integration into the building. The comparison aims to quantify the impact of LSC modules and the other modules on the market (Ribbon-Si, Multi-Si, a-Si, CIS) considering only their area production and excluding the inverter or any supporting structures for the final application. On the other hand, the analysis based on 1 kWh of energy generated as FU, considers the final purpose of the products, which is to generate electricity. In addition, all the technologies used for the comparison (single-Si, multi-Si, CdTe, a-Si, ribbon-Si) were integrated in the building (roof or façade) and the use of an inverter (200 W) was considered.

The results referring to m^2 (Fig.52) showed that LSC module had the lowest impacts in most categories (ADP, EP, HT, FAE, MAE, TE); in some categories (GWP100a, ODP and PO) LSC module resulted to be worse than a-Si and CIS technologies.

When compared with multi-Si and ribbon-Si, LSC showed a low impact in all categories.

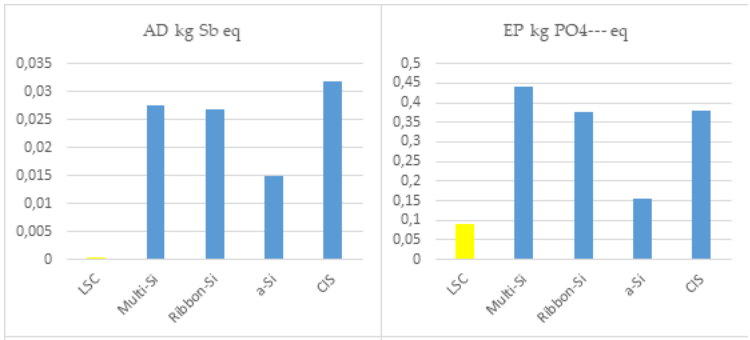
AD kg Sb eq
0,035
0,03
0,025
0,02
0,015
0,01
0,005
0
LSC
Multi-Si
Ribbon-Si
a-Si
CIS

EP kg PO4--- eq
0,5
0,45
0,4
0,35
0,3
0,25
0,2
0,15
0,1
0,05
0
LSC
Multi-Si
Ribbon-Si
a-Si
CIS

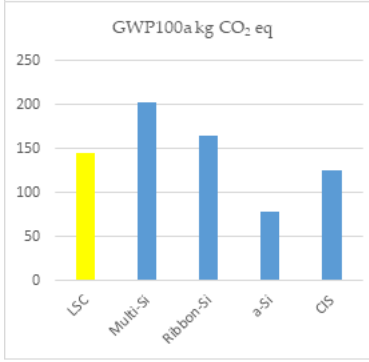
GWP100a kg CO2 eq
250
200
150
100
50
0
LSC
Multi-Si
Ribbon-Si
a-Si
CIS

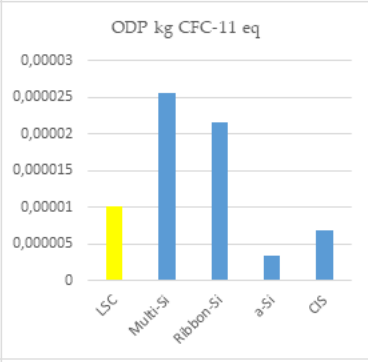
ODP kg CFC-11 eq
0,00003
0,000025
0,00002
0,000015
0,00001
0,000005
0
LSC
Multi-Si
Ribbon-Si
a-Si
CIS

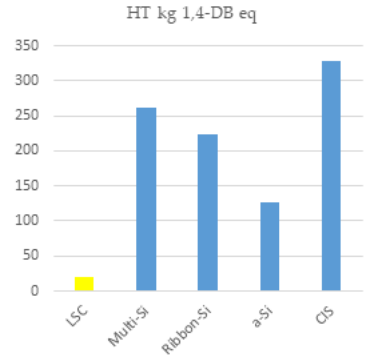
HT kg 1,4-DB eq
350
300
250
200
150
100
50
0
LSC
Multi-Si
Ribbon-Si
a-Si
CIS

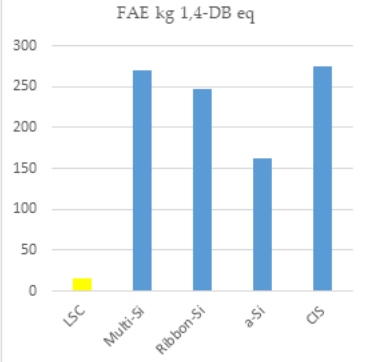
FAE kg 1,4-DB eq
300
250
200
150
100
50
0
LSC
Multi-Si
Ribbon-Si
a-Si
CIS

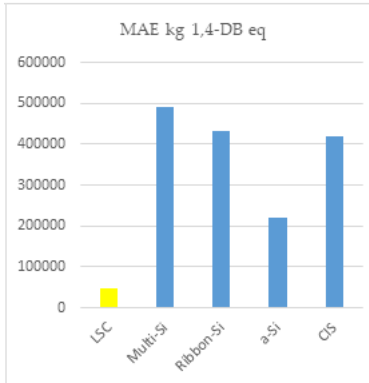
MAE kg 1,4-DB eq
600000
500000
400000
300000
200000
100000
0
LSC
Multi-Si
Ribbon-Si
a-Si
CIS

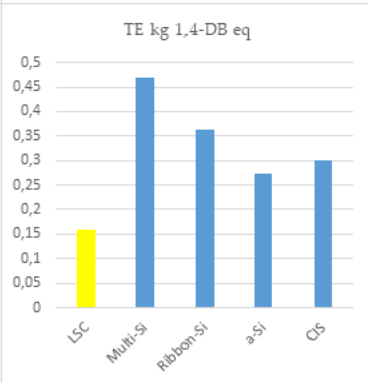
TE kg 1,4-DB eq
0,5
0,45
0,4
0,35
0,3
0,25
0,2
0,15
0,1
0,05
0
LSC
Multi-Si
Ribbon-Si
a-Si
CIS

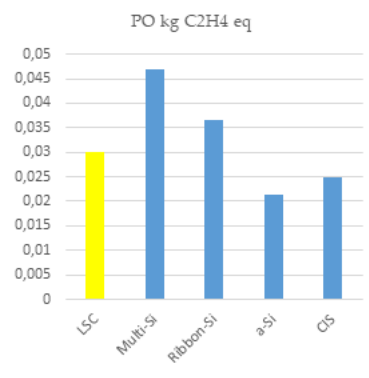
PO kg C2H4 eq
0,05
0,045
0,04
0,035
0,03
0,025
0,02
0,015
0,01
0,005
0
LSC
Multi-Si
Ribbon-Si
a-Si
CIS

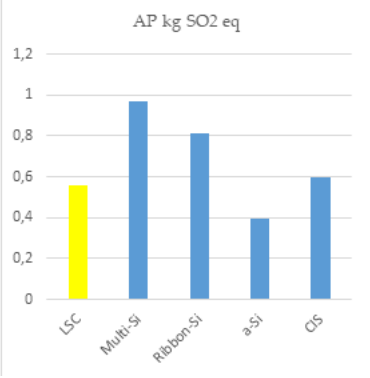
AP kg SO2 eq
1,2
1
0,8
0,6
0,4
0,2
0
LSC
Multi-Si
Ribbon-Si
a-Si
CIS

Figure 53 - Environmental impacts comparison between different PV modules (1m^2)

The results referring to the generation of 1 kWh of energy show an opposite trend, since the environmental impacts connected to the LSC modules are the highest in all categories, when compared with other photovoltaic technologies as shown in Fig. 54. Results based on electricity generation are disadvantageous for LSC models since they are closely related to LSC modules efficiency (which is much lower than that of other technologies) and to the geographical conditions in which the prototype was tested. However, the advantages of LSC modules lie in other aspects related to their versatility and to the use of lower impacts materials or low energy-intensive processes in the manufacturing phase, as shown by the results based on the m^2.

Figure 54 *- Environmental impacts comparison between different PV modules (1 kWh)*

In detail, LSC modules impacts for 1 kWh generated resulted to be more than ten times in some categories such as ADP (fossil fuel), GWP, PO, AP and EP. The smallest difference was recorded for impact categories such as ADP, HT, TE with an increase of 200%.

This result, which is mainly attributable to the low annual yield and efficiency of the LSC modules (1-1.3%), must however be interpreted on the basis of the geographical conditions (location and irradiation) and the geometry of the configuration (inclination of the modules and series/parallel connections of the cells) during data monitoring, on which the assumptions relating to the production of electricity during the useful life of the modules are based.

Since LSC modules have a lower efficiency than the analyzed photovoltaic technologies, the choice to use LSC modules lies in the advantages possessed by the technology: the possibility of application in glazed building, the possibility of integration with non-optimal angles for facades and balconies, the generation of energy also in condition of diffuse radiation. LSC modules could be a good solution for some applications, but they resulted to be a bad solution from an environmental point of view, if compared to other technologies. In conclusion, LSC technology will need improvements in efficiency and annual yield in future to compete as substitute of other PV technologies, but they could actually have niche applications thanks to some peculiar characteristics, such as transparency.

6. Conclusions

In this study, the energy and environmental performances of the SW-LSC prototype installed in Novara (Italy) were analysed. The energy performances regarded the study of optical, thermal and electrical characteristics of the device; the environmental performances study was based on the LCA methodology, using a "cradle to gate" approach but considering additional stages such as assembly, maintenance during the useful life and the recycling of some elements.

Regarding the daylighting performances, a preliminary phase allowed to obtain the illuminance level inside the rooms, where the two windows were installed, through a monitoring study. The simulation of the lighting performance started after the creation of the two rooms model and the two windows models through an illuminance map that contained the points where the real measurements were taken. After the calibration process, based on the uncertainties of some model parameters, the results of the simulations were compared with those of the measurements and the percentage error between the two values (simulated and measured) was calculated. The results show that the models created approximate with good accuracy (generally with an error of less than 10%) the characteristics of the two windows, and allow to validate the experimental procedure for obtaining and developing the data obtained. The validated models were then used to conduct simulations for a large-building and to obtain the value of daylight autonomy in the case of a threshold of 300 lux and 500 lux. Furthermore, the study made it possible to analyze the illuminance map and to compare the distribution of light in the large-building model, both for SW-LSC and for traditional window case. The results showed that the traditional window generally allows to obtain higher DA values in both cases (300 lux and 500 lux). Anyway, for the SW-LSC there were more points whose illuminance value falls in the area between 300 and 500 lux (acceptable daylight). In the case of the traditional window, the percentage of points which falls in the area of "high daylight" and "very high daylight" was average more than 6% and 8% if compared to the case of SW-LSC in the same range. In conclusion, the SW-LSC allowed a better light distribution inside the rooms, also reducing the light

intensity to acceptable values. The results showed that the traditional window generally allowed to obtain higher DA values in both cases (300 lux and 500 lux) if compared to the smart-window. For traditional window the mean DA300 for all point was 65% and DA500 was 52% while for smart-window DA300 was 51.5% and DA500 was 34%. Anyway, a deeper analysis showed that illuminance values for smart-window LSC falling in the area between 300 and 500 lux (acceptable daylight) were higher that of traditional window. Consequently, the percentage of points which falls in the area of "high daylight" and "very high day-light" is average more than 6% and 8% for the traditional window, if compared to the case of SW-LSC in the same range. These results showed that, overall, the quality and intensity of the light that filters through the LSC smart-window was more suitable for the considered environment (the office) than the traditional window.

The thermo-physical analysis based on the standard ASHRAE 90.1. The building model used refer to the small office proposed by ASHRAE Standard 2019. The analysis made it possible to obtain the daily and monthly heat balance and the heat gains and losses in two different scenarios that involved the use of traditional windows and SW-LSC, as the only change to the basic ASHRAE model of the small office. The LSC window allows significant H/C savings (+50%) if compared to traditional ones, even if a part of this saving depends on the different u-values between the two windows. Results showed that, for the traditional window scenario, the monthly heating load is al-ways higher than in the SW-LSC scenario (from 200 to 300%); the highest difference is recorded in January and it is equal to 1.723 kWh /m. In the case of the cooling load, the scenario of the traditional window shows higher values (from 10 to 67%) and the highest difference is recorded in July and is equal to 0.589 kWh/m^2. Although the results can be predictable, considering the better characteristics of the glass and the frame of the smart window, the study allowed to quantify the advantages of using the SW-LSC instead of a traditional window. The importance of these results lies in the innovation of the device and in the lack of references in the literature for this new technology; these results can be used for further investigations and for comparisons with other similar technologies suitable for the same type of application.

The analysis of electrical performance was conducted starting from the collection of generation and consumption data monitored during the experimental study. Through a statistical approach conducted on these data, the relationship between irradiation and energy generation was obtained for the SW-LSC prototype installed in the test building. Subsequently, this relationship was used on the large-building in order to determine the generation of the SW-LSCs installed in the building and exposed along the same direction as the experimental tests. Finally, a comparison was made between the consumption of internal lighting in the case of the SW-LSC and the traditional window. Results showed that the use of the traditional window involved an electrical energy saving of about 83 kWh per year for internal lighting since the perimeter areas of the building had a higher DA and this also affects electricity consumption. Anyway, the electric generation for the smart-window LSC resulted to be 59 kWh/year for the site of Novara and it can be expected that this result can be further increased in locations with an average radiation higher than that of this study. In addition, it was not considered the application of SW-LSC in west and east façade, which could further increase electricity production. As a result, the higher electricity consumption can certainly be counterbalanced by increased production thanks to LSC modules. To this end, further studies are needed to quantify the impact of the reference geographical location. Considering the mixed nature of the SW-LSC prototype, we believe that the procedure presented in this study is an effective path to evaluate the performance of this new technology, also allowing a comparison with other semitransparent PV technologies and smart glasses / smart windows, in the perspective of a real staircase of the building. Furthermore, this study provides useful information to plan energy renovation strategies for existing buildings to save on energy costs and to reduce the environmental effects of the building, involving a critical element such as windows.

LCA results showed that, considering the SW-LSC prototype, the aluminum frame was found to be the most impactful element in most of the categories (with an average contribution of about 60%). Considering the other aluminum elements that complete (the perimeter frame which protect slab edges and photovoltaic cells, the box where the storage batteries are located, and the light shelf) this contribution reaches about 80%; in particular, light shelf environmental impact ranged from 16%

to 25% in all categories, except ADP. DC motors and storage batteries were the major contributors to the abiotic depletion potential category (above 31% and 37%, respectively), but their contribution was less than 4% in the other categories. The light shelf is a controversial element in the SW-LSC, although it allows to avoid excessive lighting phenomena near the window and a better distribution of light in the rooms. In fact, it turned out to be the second contributor in most categories (about 16%); consequently, the idea of replacing it with other solutions that have a lower environmental impact or the removal of this element should be evaluated. A more in-depth analysis of this element, together with the venetian blind system, would allow to judge whether their presence can be superfluous or can represents an added value to the SW-LSC prototype.

Considering the eco-design of the final product (and for future commercialization), the use of recycled aluminum (as showed in the alternative scenario) must be confirmed, since it allows to reduce almost all impacts by about 33%. Furthermore, all results are based on the analysis of a not optimized prototype from the materials point of view; consequently the use of alternative materials such as wood or a wood-aluminum coupling could bring several benefits.

The comparison between the impacts related to the SW-LSC and other types of windows made it possible to quantify the environmental burdens related to this technology. Even if the SW-LSC environmental impacts are higher than those of traditional windows in all categories, the final application of SW-LSC inside a building, must be evaluated case by case considering the possible advantages that could derive from its operation (first of all the automated venetian blinds) and its thermal and optical characteristics. LSC modules contributed less than 5% in all impact categories. Considering that LSC modules could be used for other types of installation (integration in buildings with high glazed surfaces, skylights, etc.) it was useful to compare the environmental impacts of LSC modules with those of other photovoltaic technologies (multi-Si, ribbon Si, a-Si, CIS). The comparison was done on the basis of two different functional unit: in the first case was used 1 m^2 of modules surface; in the second case 1 kWh of energy generated was used. Results for 1 m^2 showed that LSC modules had lowest environmental impacts in some categories such as abiotic depletion potential (~2000%), eutrophication

potential (~200%), human toxicity (~1100%), fresh water aquatic ecotoxicity (~1000%), marine water aquatic ecotoxicity (~750%) and terrestrial ecotoxicity (~170%); the environmental impact of LSC modules was lower than multi-Si and ribbon Si technologies in all categories and higher than CIS and a-Si in global warming potential (~170%), photochemical oxidation potential (~130%) and ozone layer depletion potential (~150%). Results for 1 kWh of energy generated showed that LSC modules had highest impacts in all categories (from 200% to 1900%) if compared with other PV technologies, mainly due to their low efficiency. Considering these results, the application of LSC modules could be justified where a large application surface is available and the presence of transparent elements is required. In this case, the power generation could be maximized and exploited in an optimal way. On the other hand, the results showed that the impacts related to energy generation (1 kWh FU) are higher if compared to other photovoltaic technologies; consequently, future studies should focus on increasing the LSC efficiency to compete with other technologies. The use of another type of coupled photovoltaic cells (CIS or GaAs), could lead to an increase in efficiency without affecting the LSC impacts referred to m2 (since the solar cells occupy only the edges of the module, and therefore a small surface).

In conclusion, the system represents a novelty in the field of smart windows (as regards the functioning of the device) and incorporates a photovoltaic technology (luminescent solar concentrators) which is not yet fully widespread on the market. The possibility of incorporating the LSC modules inside a window, thanks to their characteristic of being semi-transparent, guarantees the production of electricity where the use of conventional PV technologies would not allow. Although the electrical performance of the LSC modules is currently not comparable with traditional PV, in terms of efficiency, this solution could still facilitate the achievement of a balanced budget between production and consumption inside buildings especially considering the thermal characteristics of SW-LSC device, equipped with a thermal break aluminum frame and a coated double glass filled with air. LSC modules also have the characteristic of producing electricity even with diffused radiation and do not require tracking systems like most solar

concentrators; in addition, LSC technology have a cost of 70$ on a prototype scale, (about 35$ after the spread of the technology, according to Eni internal experimental data) which is significantly lower than already mature technologies. The SW-LSC also allows to avoid excessive lighting phenomena near the window and a better distribution of light in the rooms, thanks to the presence of the light-shelf. In the future, this technology could find a place inside near zero energy buildings, alongside other photovoltaic and renewable technologies, contributing to the achievement good results in terms of energy generation, thermal insulation and management of solar gains. The life cycle assessment of the SW-LSC prototype allowed to quantify the environmental burdens of the device and to highlight the critical elements of the system. Although further studies regarding this technology are required, especially considering large-scale production processes and the consequent use of raw materials with greater efficiency, the device represents a promising alternative to exploit a different type of installation into building in urban contexts

References

[1] GREEN PAPER – "A 2030 framework for climate and energy policies" /* COM/2013/0169 final */

[2] T. Abergel, B. Dean and J. Dulac – "Towards a zero-emission, efficient, and resilient buildings and construction sector". GLOBAL STATUS REPORT 2017.

[3] S. Bilgen, "Structure and environmental impact of global energy consumption" Renew. Sustain. Energy Rev., vol. 38, pp. 890–902, 2014, doi: 10.1016/j.rser.2014.07.004.

[4] Petter, B., Hynd, A., Gustavsen, A., Arasteh, D., Goudey, H., & Hart, R. (2012). Solar Energy Materials & Solar Cells Fenestration of today and tomorrow: A state-of-the-art review and future research opportunities. 96(7465), 1–28. https://doi.org/10.1016/j.solmat.2011.08.010

[5] A. Hermelink, S. Schimschar, T. Boermans, L. Pagliano, P. Zangheri, R. Armani, K. Voss, E. Musall - "Towards nearly zero-energy buildings Definition of common principles under the EPBD". February 2013.

[6] Liu, Z., Zhou, Q., Tian, Z., He, B. jie, & Jin, G. (2019). A comprehensive analysis on definitions, development, and policies of nearly zero energy buildings in China. Renewable and Sustainable Energy Reviews, 114(August 2019), 109314. https://doi.org/10.1016/j.rser.2019.109314

[7] Karlessi, T., Kampelis, N., Kolokotsa, D., Santamouris, M., Standardi, L., Isidori, D., & Cristalli, C. (2017). The Concept of Smart and NZEB Buildings and the Integrated Design Approach. Procedia Engineering, 180, 1316–1325. https://doi.org/10.1016/j.proeng.2017.04.294

[8] Magrini, A., Lentini, G., Cuman, S., Bodrato, A., & Marenco, L. (2020). From nearly zero energy buildings (NZEB) to positive energy buildings (PEB): The next challenge - The most recent European trends with some notes on the energy analysis of a forerunner PEB example. Developments in the Built Environment, 3(March), 100019. https://doi.org/10.1016/j.dibe.2020.100019

[9] Kim, J. H., Kim, H. R., & Kim, J. T. (2015). Analysis of photovoltaic applications in zero energy building cases of IEA SHC/EBC Task 40/Annex 52. Sustainability (Switzerland), 7(7), 8782–8800. https://doi.org/10.3390/su7078782

[10] Debije, M. G., & Verbunt, P. P. C. (2012). Thirty Years of Luminescent Solar Concentrator Research : Solar Energy for the Built Environment. 12–35. https://doi.org/10.1002/aenm.201100554

[11] Weber, W. H. and Lambe, J. Appl. Opt. 15(10), 2299-2300 (1976).

[12] Batchelder, J. S., Zewail, A. H., and Cole, T. Appl. Opt. 20(21), 3733-3754 (1981)

[13] Batchelder, J. S., Zewail, A. H., and Cole, T. Appl. Opt. 18(18), 3090-3110 (1979)

[14] Tsoi, S. "Structured Luminescent Solar Energy a New Route Towards Inexpensive Photovoltaic Energy" (2012). https://doi.org/10.6100/IR724488

[15] van Sark, W. G. J. H. M. Luminescent solar concentrators - A low cost photovoltaics alternative. Renewable Energy, 49, 207–210. (2013). https://doi.org/10.1016/j.renene.2012.01.030

[16] R. Tällberg, B. Petter, R. Loonen, T. Gao, and M. Hamdy, "Comparison of the energy saving potential of adaptive and controllable smart windows : A state-of-the-art review and simulation studies of thermochromic, photochromic and electrochromic technologies" Sol. Energy Mater. Sol. Cells, vol. 200, no. February, p. 109828, 2019, doi: 10.1016/j.solmat.2019.02.041.

[17] D. H. W. Li, "A review of daylight illuminance determinations and energy implications" Appl. Energy, vol. 87, no. 7, pp. 2109–2118, 2010, doi: 10.1016/j.apenergy.2010.03.004.

[18] A. Das and S. K. Paul, "Artificial illumination during daytime in residential buildings: Factors, energy implications and future predictions" Appl. Energy, vol. 158, pp. 65–85, 2015, doi: 10.1016/j.apenergy.2015.08.006.

[19] Muteri, V., Cellura, M., Curto, D., Franzitta, V., Longo, S., Mistretta, M., & Parisi, M. L. (2020). Review on life cycle assessment of solar photovoltaic panels. Energies, 13(1). https://doi.org/10.3390/en13010252

[20] Sørensen, B. Renewable Energy: Physics, Engineering, Environmental Impacts, Economics and Planning, 5th ed.; Academic Press: Cambridge, MA, USA, 2017.

[21] Hossam-Eldin, A.; Rafaey, M.; Farghly, A. A Review on Photovoltaic Solar Energy Technology and Its Efficiency. In Proceedings of the Conference: 17th International Middle-East Power System Conference (MEPCON'15), Mansoura, Egypt, 15–17 December 2015

[22] Green, M.A. Third Generation Photovoltaics: Advanced Solar Energy Conversion. Springer Series in Photonics (12);Springer: Berlin/Heidelberg, Germany, 2006. [CrossRef]

[23] Green, M.A.; Hishikawa, Y.; Dunlop, E.; Levi, D.; Hohl-Ebinger, J.; Toshita, M.; Ho-Baillie, A.W.Y. Solar cell efficiency tables (version 53). Prog. Photovolt. Res. Appl. 2018, 27. [CrossRef]

[24] Fukurozaki, S.H.; Zilles, R.; Sauer, I.L. Energy Payback Time and CO2 Emissions of 1.2kWp Photovoltaic Roof-Top System in Brazil. Int. J. Smart Grid Clear Energy 2012, 164–1699. [CrossRef]

[25] Kim, B.J.; Lee, J.Y.; Kim, K.H.; Hur, T. Evaluation of the environmental performance of sc-Si and mc-Si PV systems in Korea. Sol. Energy 2014, 99, 100–114. [CrossRef]

[26] Stylos, N.; Koroneos, C. Carbon footprint of polycrystalline photovoltaic systems. J. Clean. Prod. 2014, 64, 639–645. [CrossRef]

[27] Fu, Y.; Liu, X.; Yuan, Z. Life-cycle assessment of multi-crystalline photovoltaic (PV) systems in China. J. Clean. Prod. 2015, 86, 180–190

[28] Yang, D.; Liu, J.; Yang, J.; Ding, N. Life-cycle assessment of China's multi-crystalline silicon photovoltaic modules considering international trade. J. Clean. Prod. 2015, 94, 35–45.

[29] Hong, J.; Chen,W.; Qi, C.; Ye, L.; Xu, C. Life cycle assessment of multi-crystalline silicon photovoltaic cell production in China. Sol. Energy 2016, 133, 283–293.

[30] Latunussa, C.E.L.; Ardente, F.; Blengini, G.A.; Mancini, L. Life Cycle Assessment of an innovative recycling process for crystalline silicon photovoltaic panels. Sol. Energy Mater. Sol. Cells 2016, 156,

[31] Hou, G.; Sun, H.; Jiang, Z.; Pan, Z.; Wang, Y.; Zhang, X.; Zhao, Y.; Yao, Q. Life cycle assessment of grid-connected photovoltaic power generation from crystalline silicon solar modules in China. Appl. Energy 2016, 164, 882–890.

[32] Akinyele, D.O.; Rayudu, R.K.; Nair, N.K.C. Life cycle impact assessment of photovoltaic power generation from crystalline silicon-based solar modules in Nigeria. Renew. Energy 2017, 101, 537–549

[33] Huang, B.; Zhao, J.; Chai, J.; Xue, B.; Zhao, F.; Wang, X. Environmental influence assessment of China's multi-crystalline silicon (multi-Si) photovoltaic modules considering recycling process. Sol. Energy 2017, 143, 132–141. [CrossRef]

[34] Luo, W.; Khoo, Y.S.; Kumar, A.; Low, J.S.C.; Li, Y.; Tan, Y.S.; Wang, Y.; Aberle, A.G.; Ramakrishna, S. A comparative life-cycle assessment of photovoltaic electricity generation in Singapore by multicrystalline silicon technologies. Sol. Energy Mater. Sol. Cells 2018, 174, 157–162.

[35] Mohr, N.; Meijer, A.; Huijbregts, M.A.J.; Reijnders, L. Environmental impact of thin-film GaInP/GaAs and multicrystalline silicon solar modules produced with solar electricity. Int. J. Life Cycle Assess. 2009, 14, 225–235.

[36] van der Meulen, R.; Anselma, E. Life-cycle greenhouse gas e_ects of introducing nano-crystalline materials in thin-film silicon solar cells. Prog. Photovolt. Res. Appl. 2010, 19, 453–463

[37] Held, M.; Ilg, R. Update of environmental indicators and energy payback time of CdTe PV systems in Europe. Prog. Photovolt. Res. Appl. 2011, 19, 614–626.

[38] Kim, H.C.; Fthenakis, V.M. Comparative life-cycle energy payback analysis of multi-junction a-SiGe and nanocrystalline/a-Si modules. Prog. Photovolt. Res. Appl. 2011, 19, 228–239.

[39] Mohr, N.J.; Maijer, A.; Huijbregts, M.A.J.; Reijnders, L. Environmental life cycle assessment of roof-integrated flexible amorphous silicon/nanocrystalline silicon solar cell laminate. Prog. Photovolt. Res. Appl. 2012, 21, 802–815

[40] Kreiger, M.A.; Shonnard, D.R.; Pearce, J.M. Life cycle analysis of silane recycling in amorphous silicon-based solar photovoltaic manufacturing. Resour. Conserv. Recycl. 2013, 70, 44–92.

[41] Collier, J.; Wu, S.; Apul, D. Life cycle environmental impacts from CZTS (copper zinc tin sulfide) and Zn3P2 (zinc phosphide) thin film PV (photovoltaic) cells. Energy 2014, 74, 314–321.

[42] Bergesen, J.D.; Heath, G.A.; Gibon, T.; Suh, S. Thin-film photovoltaic power generation o_ers decreasing greenhouse gas emissions and increasing environmental co-benefits in the long term. Environ. Sci. Technol. 2014, 48, 9834–9843.

[43] Lunardi, M.M.; Moore, S.; Alvarez-Gaitan, J.P.; Yan, C.; Hao, X.; Corkish, R. A comparative life cycle assessment of chalcogenide/Si tandem solar modules. Energy 2018, 145, 700–709.

[44] Rajput, P.; Singh, Y.K.; Tiwari, G.N.; Sastry, O.S.; Dubey, S.; Pandey, K. Life cycle assessment of the 3.2kW cadmium telluride (CdTe) photovoltaic system in composite climate of India. Sol. Energy. 2018, 159, 415–422. [CrossRef]

[45] Valverde, G.R.; Cherni, J.A.; Urbina, A. Life cycle analysis of organic photovoltaic technologies. Prog. Photovolt. Res. Appl. 2010, 18, 535–538. [CrossRef]

[46] Anctil, A.; Babbitt, C.; Landi, B.; Raffaelle, R.P. Life-cycle assessment of organic solar cell technologies. In Proceedings of the 2010 35th IEEE Photovoltaic Specialists Conference, Honolulu, HI, USA, 20–25 June 2010; pp. 742–74747

[47] Sengül, H.; Theis, T.L. An environmental impact assessment of quantum dot photovoltaics (QDPV) from raw material acquisition through use. J. Clean. Prod. 2011, 19, 21–31.

[48] Espinosa, N.; García-Valverde, R.; Urbina, A.; Krebs, F.C. A life cycle analysis of polymer solar cell modules prepared using roll-to-roll methods under ambient conditions. Sol. Energy Mater. Sol. Cells 2011, 95, 1293–1302. [CrossRef]

[49] Espinosa, N.; García-Valverde, R.; Urbina, A.; Lenzmann, F.; Manceau, M.; Angmo, D.; Krebs, F.C. Life cycle assessment of ITO-free flexible polymer solar cells prepared by roll-to-roll coating and printing. Sol. Energy Mater. Sol. Cells 2012, 97, 3–13.

[50] Anctil, A.; Fthenakis, V. Life Cycle Assessment of Organic Photovoltaics. Third Gener. Photovolt. 2012, 91–110. [CrossRef]

[51] Parisi, M.L.; Maranghi, S.; Sinicropi, A.; Basosi, R. Development of dye sensitized solar cells: A life cycle perspective for the environmental and market potential assessment of a renewable energy technology. Int. J. Heat Technol. 2013, 31, 143–148

[52] Azzopardi, B.; Mutale, J. Life cycle analysis for future photovoltaic systems using hybrid solar cells. Renew. Sustain. Energy Rev. 2010, 14, 1130–1134

[53] Espinosa, N.; Krebs, F.C. Life cycle analysis of organic tandem solar cells: When are they warranted? Sol. Energy Mater. Sol Cells 2014, 120, 692–700.

[54] Parisi, M.L.; Maranghi, S.; Basosi, R. The evolution of the dye sensitized solar cells from Grätzel prototype to up-scaled solar applications: A life cycle assessment approach. Renew. Sustain. Energy Rev

[55] Parisi, M.L.; Basosi, R. Environmental Life Cycle Analysis of Non Conventional Thin-Film Photovoltaics: The case of Dye-Sensitized solar devices. Energy Secur. Dev. 2015, 193–210.

[56] Tsang, M.P.; Sonnemann, G.W.; Bassani, D.M. Life-cycle assessment of cradle-to-grave opportunities and environmental impacts of organic photovoltaic

solar panels compared to conventional technologies. Sol. Energy Mater. Sol. Cells 2016, 156, 37–48.

[57] Celik, I.; Song, Z.; Cimaroli, A.J.; Yan, Y.; Heben, M.J.; Apul, D. Life Cycle Assessment (LCA) of perovskite PV cells projected from lab to fab. Sol. Energy Mater. Sol. Cells 2016, 156, 157–169.

[58] Hengevoss, D.; Baumgartner, C.; Nisato, G.; Hugi, C. Life Cycle Assessment and eco-effciency of prospective, flexible, tandem organic photovoltaic module. Sol. Energy 2016, 137, 317–327.

[59] Zhang, J.; Gao, X.; Deng, Y.; Zha, Y.; Yuan, C. Comparison of life cycle environmental impacts of different perovskite solar cell systems. Sol. Energy Mater. Sol. Cells 2017, 166, 9–17.

[60] Lunardi, M.M.; Wing, Y.; Ho-Baillie, A.; Alvarez-Gaitan, J.P.; Moore, S.; Corkish, R. A life cycle assessment of perovskite/silicon tandem solar cells. Prog. Photovolt. Res. Appl. 2017, 25, 679–695.

[61] Maranghi, S.; Parisi, M.L.; Basosi, R.; Sinicropi, A. Environmental Profile of the Manufacturing Process of Perovskite Photovoltaics: Harmonization of Life Cycle Assessment Studies

[62] Shukla, A. K., Sudhakar, K., & Baredar, P. (2017). Recent advancement in BIPV product technologies: A review. Energy and Buildings, 140, 188–195. https://doi.org/https://doi.org/10.1016/j.enbuild.2017.02.015

[63] Hudişteanu, S. V., Popovici, C. G., Mateescu, T. D., & Cherecheş, N. C. “Efficiency Analysis of BIPV Systems for Different Locations in Romania.” EnergyProcedia (2017). https://doi.org/10.1016/j.egypro.2017.03.1089

[64] Biyik, E., Araz, M., Hepbasli, A., Shahrestani, M., Yao, R., Shao, L., Essah, E., Oliveira, A. C., del Caño, T., Rico, E., Lechón, J. L., Andrade, L., Mendes, A., & Atlı, Y. B. (2017). A key review of building integrated photovoltaic (BIPV) systems. Engineering Science and Technology, an International Journal, 20(3), 833–858. https://doi.org/10.1016/j.jestch.2017.01.009

[65] S.A. Omer, R. Wilson, S.B. Riffat, Monitoring results of two examples of building integrated PV (BIPV) systems in the UK, Renewable Energy 28 (2003) 1387–1399, http://dx.doi.org/10.1016/S0960-1481(02)00257-4.

[66] H. Yang, G. Zheng, C. Lou, D. An, J. Burnett, Grid-connected buildingintegrated photovoltaics: A Hong Kong case study, Sol. Energy 76 (2004) 55–59, http://dx.doi.org/10.1016/j.solener.2003.09.007.

[67] T.K. Mallick, P.C. Eames, B. Norton, Non-concentrating and asymmetric compound parabolic concentrating building fa??ade integrated photovoltaics: An experimental comparison, Sol. Energy 80 (2006) 834– 849, http://dx.doi.org/10.1016/j.solener.2005.05.011.

[68] J. Urbanetz, C.D. Zomer, R. Rüther, Compromises between form and function in grid-connected, building-integrated photovoltaics (BIPV) at low-latitude sites, Build. Environ. 46 (2011) 2107–2113, http://dx.doi.org/10.1016/j.buildenv.2011.04.024.

[69] J.H. Yoon, J. Song, S.J. Lee, Practical application of building integrated photovoltaic (BIPV) system using transparent amorphous silicon thin-film PV module, Sol. Energy 85 (2011) 723–733, http://dx.doi.org/10.1016/j.solener.2010.12.026.

[70] Ritzen, M. J. (2017). Environmental impact assessment of building integrated photovoltaics: numerical and experimental carrying capacity based approach. 2017, 217.

[71] Cerón, I., Caamaño-Martín, E., & Neila, F. J. (2013). “State-of-the-art” of building integrated photovoltaic products. Renewable Energy, 58, 127–133. https://doi.org/10.1016/j.renene.2013.02.013

[72] Lamnatou, C., Baig, H., Chemisana, D., & Mallick, T. K. (2016). Environmental assessment of a building-integrated linear dielectric-based concentrating photovoltaic according to multiple life-cycle indicators. Journal of Cleaner Production, 131, 773–784. https://doi.org/10.1016/j.jclepro.2016.04.094

[73] Menoufi, K., Chemisana, D., & Rosell, J. I. (2013). Life Cycle Assessment of a Building Integrated Concentrated Photovoltaic scheme. Applied Energy, 111, 505–514. https://doi.org/10.1016/j.apenergy.2013.05.037

[74] Perez, M. J. R., & Fthenakis, V. (2011). A lifecycle assessment of façade BIPV in New York. Conference Record of the IEEE Photovoltaic Specialists Conference, 003271–003276. https://doi.org/10.1109/PVSC.2011.6186636

[75] Baumann, A. E., Hill, R., & Hynes, K. M. (1997). Environmental impacts of PV systems - ground-based vs BIPV. Conference Record of the IEEE Photovoltaic Specialists Conference, 1361–1364. https://doi.org/10.1109/PVSC.1997.654343

[76] Hammond, G. P., Harajli, H. A., Jones, C. I., & Winnett, A. B. (2009). Integrated appraisal of a building integrated photovoltaic (BIPV) system. 1st International Conference on Sustainable Power Generation and Supply, SUPERGEN '09, 1–9. https://doi.org/10.1109/SUPERGEN.2009.5348173

[77] Jayathissa, P., Jansen, M., Heeren, N., Nagy, Z., & Schlueter, A. (2016). Life cycle assessment of dynamic building integrated photovoltaics. Solar Energy Materials and Solar Cells, 156, 75–82. https://doi.org/10.1016/j.solmat.2016.04.017

[78] Tripathy, M., Joshi, H., & Panda, S. K. (2017). Energy payback time and life-cycle cost analysis of building integrated photovoltaic thermal system influenced by adverse effect of shadow. Applied Energy, 208(September), 376–389. https://doi.org/10.1016/j.apenergy.2017.10.025

[79] Lu, L., & Yang, H. X. (2010). Environmental payback time analysis of a roof-mounted building-integrated photovoltaic (BIPV) system in Hong Kong. Applied Energy, 87(12), 3625–3631. https://doi.org/10.1016/j.apenergy.2010.06.011

[80] Keoleian, G. A., & Lewis, G. M. D. (2003). Modeling the life cycle energy and environmental performance of amorphous silicon BIPV roofing in the US. Renewable Energy, 28(2), 271–293. https://doi.org/10.1016/S0960-1481(02)00022-8

[81] Oliver, M., & Jackson, T. (2001). Energy and economic evaluation of building-integrated photovoltaics. Energy, 26(4), 431–439. https://doi.org/10.1016/s0360-5442(01)00009-3

[82] Y. Sun, K. Shanks, H. Baig, W. Zhang, X. Hao, Y. Li, B. He, R. Wilson, H. Liu, S. Sundaram, J. Zhang, L. Xie, T. Mallic and Y. Wu, "Integrated CdTe PV glazing into windows: energy and daylight Integrated CdTe PV glazing into windows : energy daylight performance for different window-to-wall ratio performance for different window-to-wall ratio" pp. 1–6, 2019, doi:10.1016/j.egypro.2019.01.976.

[83] Martellotta, F., Cannavale, A., & Ayr, U. (2017). Comparing energy performance of different semi-transparent, building-integrated photovoltaic cells applied to "reference" buildings. Energy Procedia, 126, 219–226. https://doi.org/10.1016/j.egypro.2017.08.143

[84] K. Kapsis and A. K. Athienitis, "A study of the potential benefits of semi-transparent photovoltaics in commercial buildings," Sol. Energy, vol. 115, pp. 120–132, 2015, doi: 10.1016/j.solener.2015.02.016.

[85] S. Lok, M. Shin, J. Baltazar, and J. Kim, "Energy benefits from semi-transparent BIPV window and daylight- dimming systems for IECC code-compliance residential buildings in hot and humid climates" Sol. Energy, vol. 155, pp. 291–303, 2017, doi: 10.1016/j.solener.2017.06.039.

[86] Y. Tae, J. Kim, H. Park, and B. Shin, "Building energy performance evaluation of building integrated photovoltaic (BIPV) window with semi-transparent solar cells" Appl. Energy, vol. 129, pp. 217–227, 2014, doi: 10.1016/j.apenergy.2014.04.106.

[87] M. Wang, J. Peng, N. Li, L. Lu, T. Ma, and H. Yang, "Assessment of energy performance of semitransparent PV insulating glass units using a validated simulation model" Energy, vol. 112, pp. 538–548, 2016, doi: 10.1016/j.energy.2016.06.120.

[88] F. J. Moralejo, F. Olivieri, and F. J. Neila-gonzalez, “Energy saving potential of semi-transparent photovoltaic elements for building integration” vol. 76, pp. 572–583, 2014, doi: 10.1016/j.energy.2014.08.054.

[89] Xu, S., Liao, W., Huang, J., & Kang, J. (2014). Optimal PV cell coverage ratio for semi-transparent photovoltaics on office building façades in central China. Energy and Buildings, 77, 130–138. https://doi.org/10.1016/j.enbuild.2014.03.052

[90] Karthick, A., Kalidasa Murugavel, K., & Kalaivani, L. (2018). Performance analysis of semitransparent photovoltaic module for skylights. Energy, 162, 798–812. https://doi.org/10.1016/j.energy.2018.08.043

[91] Cheng, Y., Gao, M., Dong, J., Jia, J., Zhao, X., & Li, G. (2018). Investigation on the daylight and overall energy performance of semi-transparent photovoltaic facades in cold climatic regions of China. Applied Energy, 232(May), 517–526. https://doi.org/10.1016/j.apenergy.2018.10.006

[92] Ng, P. K., & Mithraratne, N. (2014). Lifetime performance of semi-transparent building-integrated photovoltaic (BIPV) glazing systems in the tropics. Renewable and Sustainable Energy Reviews, 31, 736–745. https://doi.org/10.1016/j.rser.2013.12.044

[93] Ng, P. K., Mithraratne, N., & Kua, H. W. (2013). Energy analysis of semi-transparent BIPV in Singapore buildings. Energy and Buildings, 66, 274–281. https://doi.org/10.1016/j.enbuild.2013.07.029

[94] Khai, N. P., Mithraratne, N., & Wittkopf, S. (2012). Semi-transparent building-integrated photovoltaic windows: Potential energy savings of office buildings in tropical Singapore. Proceedings - 28th International PLEA Conference on Sustainable Architecture + Urban Design: Opportunities, Limits and Needs - Towards an Environmentally Responsible Architecture, PLEA 2012, November.

[95] Torres-Pierna, H., Ruiz, D.-M., & Roscini, C. (2020). Highly Transparent Photochromic Films with Tunable and Fast Solution-like Response. Materials Horizons, 7. https://doi.org/10.1039/D0MH01073A

[96] Casini, M. (2015). Smart windows for energy efficiency of buildings. International Journal of Civil and Structural Engineering - IJCSE, May.

[97] L. Y. L. Wu, Q. Zhao, H. Huang, and R. J. Lim, “Sol-gel based photochromic coating for solar responsive smart window” Surf. Coatings Technol., vol. 320, pp. 601–607, 2017, doi: 10.1016/j.surfcoat.2016.10.074.

[98] M. Hočevar and U. Opara Krašovec, “A photochromic single glass pane” Sol. Energy Mater. Sol. Cells, vol. 186, no. May, pp. 111–114, 2018, doi: 10.1016/j.solmat.2018.06.035.

[99] Wang, Y., Runnerstom, E., & Milliron, D. (2016). Switchable Materials for Smart Windows. Annual Review of Chemical and Biomolecular Engineering, 7. https://doi.org/10.1146/annurev-chembioeng-080615-034647

[100] M. E. A. Warwick, I. Ridley, and R. Binions, “The effect of variation in the transition hysteresis width and gradient in thermochromic glazing systems” Sol. Energy Mater. Sol. Cells, vol. 140, pp. 253–265, 2015, doi: 10.1016/j.solmat.2015.04.022.

[101] Aburas, M., Soebarto, V., Williamson, T., & Liang, R. (2019). Thermochromic smart window technologies for building application : A review. 255(April).

[102] X. U. Xiaojie, W. U. Xi, Z. Chao, W. Jiangxiang, and G. E. Xiaotong, “Simulation and improvement of energy consumption on intelligent glasses in typical cities of China” vol. 55, no. 7, pp. 1999–2005, 2012, doi: 10.1007/s11431-012-4854-1.

[103] H. Ye, L. Long, H. Zhang, Y. Gao, L. Kang and Z. Chen, “The demonstration and simulation of the application performance of the vanadium dioxide single glazing” Sol. Energy Mater. Sol. Cells, vol. 117, pp. 168–173, 2013, doi: 10.1016/j.solmat.2013.05.061.

[104] J. Yang, Z. Xu, H. Ye, X. Xu, X. Wu, and J. Wang, “Performance analyses of building energy on phase transition processes of VO2 windows with an improved model” vol. 159, pp. 502–508, 2015, doi: 10.1016/j.apenergy.2015.08.130.

[105] G. Kokogiannakis, J. Darkwa, and C. Aloisio, “Simulating thermochromic and heat mirror glazing systems in hot and cold climates” Energy Procedia, vol. 62, pp. 22–31, 2014, doi: 10.1016/j.egypro.2014.12.363.

[106] V. Costanzo, G. Evola, and L. Marletta, “Thermal and visual performance of real and theoretical thermochromic glazing solutions for office buildings” Sol. Energy Mater. Sol. Cells, vol. 149, pp. 110–120, 2016, doi: 10.1016/j.solmat.2016.01.008.

[107] Piccolo, A., & Simone, F. (2015). Performance requirements for electrochromic smart window. Journal of Building Engineering, 3, 94–103. https://doi.org/10.1016/j.jobe.2015.07.002

[108] Hoon Lee, J., Jeong, J., & Tae Chae, Y. (2020). Optimal control parameter for electrochromic glazing operation in commercial buildings under different climatic conditions. Applied Energy, 260(July 2019), 114338. https://doi.org/10.1016/j.apenergy.2019.114338

[109] R. Tällberg, B. Petter, R. Loonen, T. Gao, and M. Hamdy, “Comparison of the energy saving potential of adaptive and controllable smart windows : A state-of-the-art review and simulation studies of thermochromic , photochromic and electrochromic technologies” Sol. Energy Mater. Sol. Cells, vol. 200, no. February, p. 109828, 2019, doi: 10.1016/j.solmat.2019.02.041.

[110] Makitalo - Simulating control strategies of electrochromic windows. (2013). November.

[111] Reynisson, H. E. (2015). Energy Performance of Dynamic Windows in Different Climates. June.

[112] Y. Ajaji and P. André, “Thermal comfort and visual comfort in an office building equipped with smart electrochromic glazing : an experimental study” Energy Procedia, vol. 78, pp. 2464–2469, 2015, doi: 10.1016/j.egypro.2015.11.230.

[113] Gugliermetti, F., & Bisegna, F. (2003). Visual and energy management of electrochromic windows in Mediterranean climate. Building and Environment, 38(3), 479–492.

[114] Aldawoud, A. (2013). Conventional fixed shading devices in comparison to an electrochromic glazing system in hot, dry climate. Energy and Buildings, 59, 104–110. https://doi.org/10.1016/j.enbuild.2012.12.031

[115] L. L. Fernandes, E. S. Lee, and G. Ward, "Lighting energy savings potential of split-pane electrochromic windows controlled for daylighting with visual comfort" Energy Build., vol. 61, pp. 8–20, 2013, doi: 10.1016/j.enbuild.2012.10.057.

[116] A. Frattolillo, G. Loddo, C. C. Mastino, and R. Baccoli, "Heating and cooling loads with electrochromic glazing in Mediterranean climate" Energy Build., vol. 201, pp. 174–182, 2019, doi: 10.1016/j.enbuild.2019.06.042.

[117] Kim, J.-H., Yang, K.-W., Park, Y.-J., Lee, K.-H., Yeo, M.-S., & Kim, K.-W. (2007). An experimental study for the evaluation of the environmental performance by the application of the automated venetian blind. Proceedings of Clima, February, 1678–1685.

[118] Carletti, C., Sciurpi, F., Pierangioli, L., Asdrubali, F., Pisello, A. L., Bianchi, F., Sambuco, S., & Guattari, C. (2016). Thermal and lighting effects of an external venetian blind: Experimental analysis in a full scale test room. Building and Environment, 106, 45–56. https://doi.org/10.1016/j.buildenv.2016.06.017

[119] Lee, E. S., DiBartolomeo, D. L., Vine, E. L., & Selkowitz, S. E. (1998). Integrated performance of an automated venetian blind/electric lighting system in a full-scale private office. Thermal Performance of the Exterior Envelopes of Whole Buildings.

[120] N. Aste. M. Buzzetti, C. Del Pero, F. Leonforte "Progettazione definitiva e redazione del piano di industrializzazione di una Smart Window integrata con componenti LSC (Concentratori Solari Luminescenti) Secondo Rapporto Intermedio," 2017.

[121] N. Aste, M. Buzzetti, C. Del Pero, R. Fusco, D. Testa, and F. Leonforte, "Visual Performance of Yellow, Orange and Red LSCs Integrated in a Smart Window" Energy Procedia, vol. 105, pp. 967–972, 2017, doi: https://doi.org/10.1016/j.egypro.2017.03.427

[122] N. Aste. M. Buzzetti, C. Del Pero, F. Leonforte “Progettazione definitiva e redazione del piano di industrializzazione di una Smart Window integrata con componenti LSC (Concentratori Solari Luminescenti) Primo Rapporto Intermedio” 2017.

[123] N. Aste. M. Buzzetti, C. Del Pero, F. Leonforte “Sviluppo tecnologico di componenti LSC destinati all’ integrazione edilizia e attività di supporto allo sviluppo industriale Secondo rapporto intermedio” pp. 1–105, 2016.

[124] N. Aste, M. Buzzetti, C. Del Pero, R. Fusco, F. Leonforte, and D. Testa, “Triggering a large scale luminescent solar concentrators market: The smart window project” J. Clean. Prod., vol. 219, pp. 35–45, 2019, doi: 10.1016/j.jclepro.2019.02.089.

[125] Dijkstra, J. “Life Cycle Assessment Study on Luminescent Solar Concentrators”. University of Utrecht, Netherlands. Faculty of Geosciences Theses. (Master thesis) July 24, 2015

[126] N. Aste. M. Buzzetti, C. Del Pero, F. Leonforte “Sviluppo tecnologico di componenti LSC destinati all’integrazione edilizia e attività di supporto allo sviluppo industriale” 2015.

[127] N. Aste. M. Buzzetti, C. Del Pero, F. Leonforte “Progettazione definitiva e redazione del piano di industrializzazione di una Smart Window integrata con componenti LSC (Concentratori Solari Luminescenti) Rapporto Finale,” 2017.

[128] N. Aste. M. Buzzetti, C. Del Pero, F. Leonforte "Progettazione definitiva e redazione del piano di industrializzazione di una Smart Window integrata con componenti LSC (Concentratori Solari Luminescenti)" Rapporto Finale 2018.

[129] N. Aste. M. Buzzetti, C. Del Pero, F. Leonforte “Supporto alla pre-commercializzazione di componenti LSC (Concentratori Solari Luminescenti) destinati all’integrazione edilizia Rapporto definitivo,” 2019

[130] N. Aste. M. Buzzetti, C. Del Pero, F. Leonforte “Sviluppo tecnologico di componenti LSC destinati all’integrazione edilizia e attività di supporto allo sviluppo industriale Rapporto finale,” 2016.

[131] Aste, N., Tagliabue, L. C., Pero, C. Del, Testa, D., & Fusco, R. (2015). Performance analysis of a large-area luminescent solar concentrator module. Renewable Energy, 76, 330–337. https://doi.org/10.1016/j.renene.2014.11.026

[132] Kottek, M., Grieser, J., Beck, C., Rudolf, B., & Rubel, F. (2006). World map of the Köppen-Geiger climate classification updated. Meteorologische Zeitschrift, 15(3), 259–263.

[133] Tumminia, G.Towards sustainable Net Zero Energy Buildings: life cycle energy performances and environmental impacts of a prefabricated building module.

[134] Crawley, D. B., Lawrie, L. K., Pedersen, C. O., & Winkelmann, F. C. (2000). Energy plus: energy simulation program. ASHRAE Journal, 42(4), 49–56.

[135] Curcija, Dragan Charlie, Zhu, Ling, Czarnecki, Stephen, Mitchell, Robin D., Kohler, Christian, Vidanovic, Simon V., Huizenga, Charlie, and USDOE. Berkeley Lab WINDOW. Computer software. https://www.osti.gov//servlets/purl/1232115. USDOE. 6 Mar. 2015. Web. doi:10.11578/dc.20210416.62.

[136] UNI EN 12464-1 "Illuminazione dei Luoghi di Lavoro”

[137] S. Attia, M. Hamdy, S. Carlucci, L. Pagliano, S. Bucking, and A. Hasan, “Building performance optimization of net zero-energy buildings” Modeling, Design, and Optimization of Net- Zero EnergyBuildings. pp. 175–206, Feb. 04, 2015, doi: https://doi.org/10.1002/9783433604625.ch05.

[138] T. Kesik, “Solar Design Days: A Tool for Passive Solar House Design” ASHRAE Trans., vol. 120, Jan. 2014

[139] ISO 14040:2006 Environmental management — Life cycle assessment — Principles and framework

[140] ISO 14044:2006 Environmental management — Life cycle assessment — Requirements and guidelines

[141] Sala, S., Reale, F., Cristóbal-García, J., Marelli, L., & Rana, P. (2016). Life cycle assessment for the impact assessment of policies. Life thinking and assessment in the European policies and for evaluating policy options. In Joint Research Centre (Vol. 28380). https://doi.org/10.2788/318544

[142] UNI EN 15804:2019 - Sostenibilità delle costruzioni - Dichiarazioni ambientali di prodotto - Regole quadro di sviluppo per categoria di prodotto

[143] Tarantini, M., Loprieno, A.D. and Porta, P.L. (2011). A life cycle approach to green public procurement of building materials and elements: a case study on windows, Energy,36(5):2473 – 2482.

[144] Stachowiak-Wencek, A., Pradzynski, W., & Deska, T. (2013). Environmental impact analysis of windows made from wood and PVC using LCA. Annals of Warsaw University of Life Sciences - SGGW. Forestry and Wood Technology, 84, 293–299.

[145] Citherlet, S., Di Guglielmo, F., & Gay, J. B. (2000). Window and advanced glazing systems life cycle assessment. Energy and Buildings, 32(3), 225–234. https://doi.org/10.1016/S0378-7788(98)00073-5

[146] M. Baitz, J. Kreißig, E. Byrne, C. Makishi, T. Kupfer, N. Frees, N. Bey, M.S. Hansen, A. Hansen, T. Bosch, V. Borghi, J. Watson, M. Miranda "Life Cycle Assessment of PVC and of principal competing materials". Commissioned by the European Commission, July 2004

[147] Wernet, G., Bauer, C., Steubing, B., Reinhard, J., Moreno-Ruiz, E., and Weidema, B., 2016. The ecoinvent database version 3 (part I): overview and methodology. The International Journal of Life Cycle Assessment, [online] 21(9), pp.1218–1230.

[148] Richa, K., Babbitt, C. W., Nenadic, N. G., & Gaustad, G. (2017). Environmental trade-offs across cascading lithium-ion battery life cycles.

International Journal of Life Cycle Assessment, 22(1), 66–81. https://doi.org/10.1007/s11367-015-0942-3

[149] Ny, R. - Supplementary Material.

[150] Smart, E. I. (2019). Environmental Product Declaration Era Inn Smart S; Era Mat MA Gear motor for blinds and shutter automation.

[151] Kikuchi, Y., Hirao, M., Sugiyama, H., Papadokonstantakis, S., Hungerbühler, K., Ookubo, T., & Sasaki, A. (2014). Design of recycling system for poly(methyl methacrylate) (PMMA). Part 2: Process hazards and material flow analysis. International Journal of Life Cycle Assessment, 19(2), 307–319. https://doi.org/10.1007/s11367-013-0625-x

[152] Kikuchi, Y., Hirao, M., Ookubo, T., & Sasaki, A. (2014). Design of recycling system for poly(methyl methacrylate) (PMMA). Part 1: Recycling scenario analysis. International Journal of Life Cycle Assessment, 19(1), 120–129. https://doi.org/10.1007/s11367-013-0624-y

[153] ENVIRONMENTAL PRODUCT DECLARATION - ISO 14025 and EN 15804. “PVC-U plastic windows with the dimensions 1.23 x 1.48 m and insolated double-glazing”. QKE e.V.EPPA ivzw

[154] Economy, C. (2019). Aluminium windows contribute to the circular economy Fact sheet Aluminium is a perfect fit for the Circular Economy - March, 1–4.

[155] ENVIRONMENTAL PRODUCT DECLARATION – ISO 14025 and EN 15804. “PVC-U plastic windows with the dimensions 1.23 x 1.48 m and insolated triple-glazing” QKE e.V.EPPA ivzw

[156] ENVIRONMENTAL PRODUCT DECLARATION - As, N. K. (2020). Opening Window with aluminium cladding. 1–9.

[157] ENVIRONMENTAL PRODUCT DECLARATION Operator, P., Number, D., Number, R., & Date, I. (2018). Metra spa. environmental product declaration.

[158] ENVIRONMENTAL PRODUCT DECLARATION - The Danish Technological Institue. (2013). Environmental Product Declaration: Kerto-LVL. 8.

[159] ENVIRONMENTAL PRODUCT DECLARATION - Aluminium Window System. (2017). February.

[160] Expo, M. (2010). Confronto tra serramenti in PVC, Alluminio e Legno mediante l'Analisi del Ciclo di Vita (LCA) (inclusi gli avvolgibili).

[161] PlasticsEurope: Eco-profiles and environmental declarations – LCI methodology and PCR for uncompounded polymer resins and reactive polymer precursor (version 2.0, April 2011) [PLASTICSEUROPE 2011].

La borsa di dottorato è stata cofinanziata con risorse del
Programma Operativo Nazionale Ricerca e Innovazione 2014-2020 (CCI 2014IT16M2OP005),
Fondo Sociale Europeo, Azione I.1 "Dottorati Innovativi con caratterizzazione Industriale"

UNIONE EUROPEA
Fondo Sociale Europeo